

Mammalian Cell Surface Imaging with Nitrile-Functionalized Nanoprobes: Biophysical Characterization of Aggregation and Polarization Anisotropy in SERS Imaging

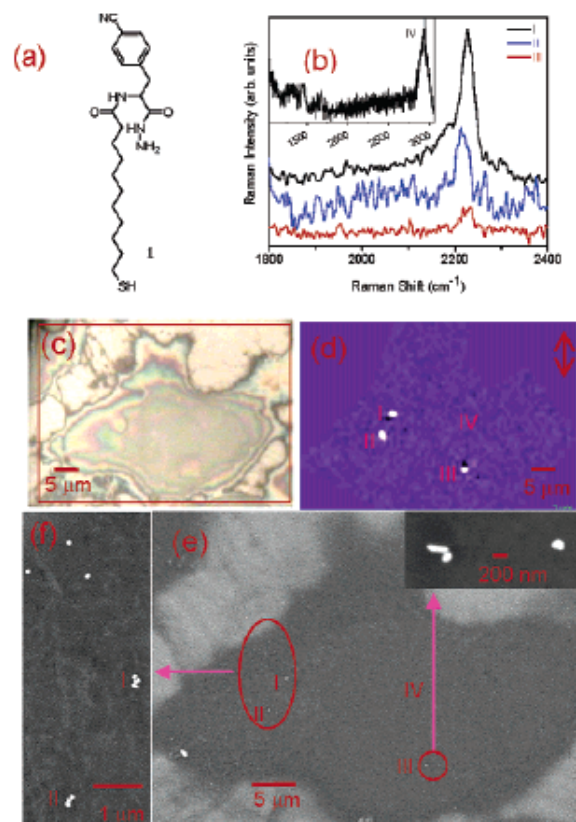


Figure 1. (a) The chemical structure of Raman reporter I; (b) Raman spectra of the CN vibration mode extracted from positions I, II, and III of the cell shown in the optical image (c). Inset of (b) is a cellular Raman spectrum taken from spot IV of the same cell. (d) Raman intensity map of the C=N band of the same cell, and (e) the corresponding SEM image. Inset in (e) showed the NPs in the lower right circle. (f) The group of NPs as shown in the large oval of (e).

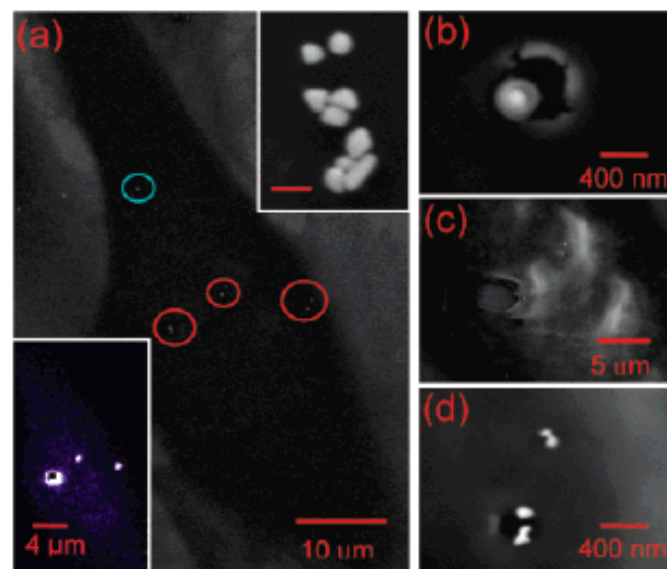
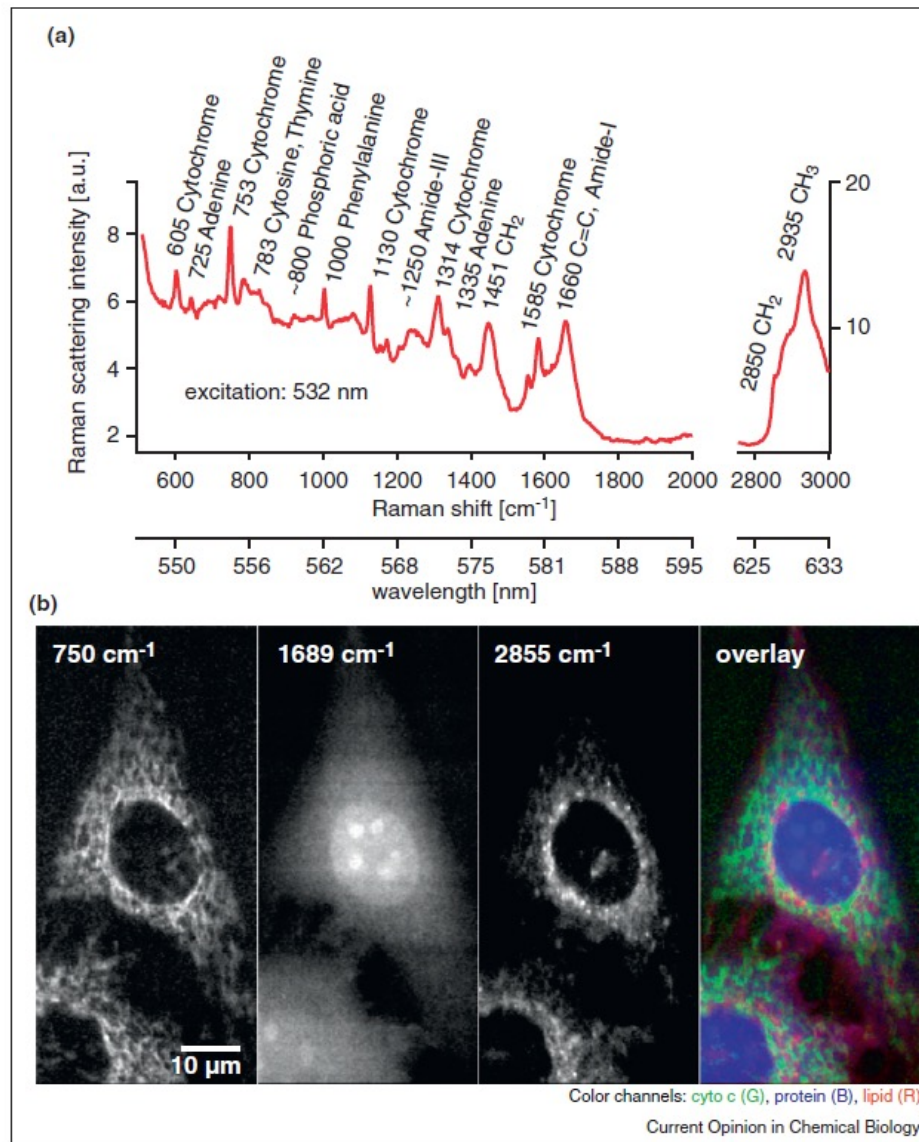


Figure 2. (a) SEM image of a cell. Upper right inset: magnification of a group of aggregated NPs. The scale bar is 200 nm. Lower left inset: the corresponding Raman intensity image of the same cell obtained with a power density of 10^3 W/cm². Laser-induced damage to the cell is shown in (b) the monomer (blue circle in a), (c) the aggregates, and (d) a pair of dimers.

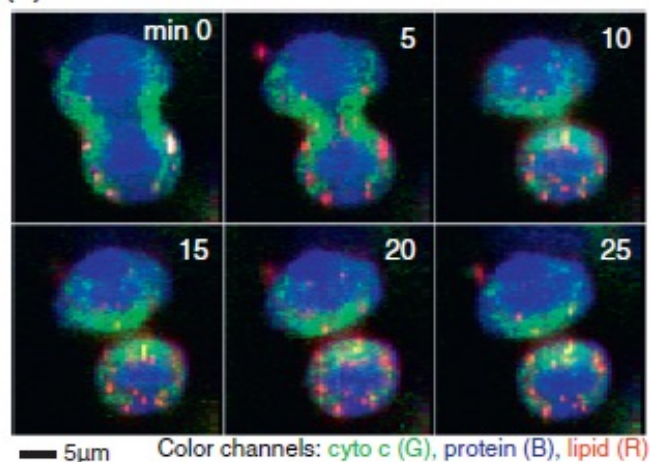
Molecular imaging of live cells by Raman microscopy

Almar F Palonpon^{1,2}, Mikiko Sodeoka^{2,3} and Katsumasa Fujita^{1,2}

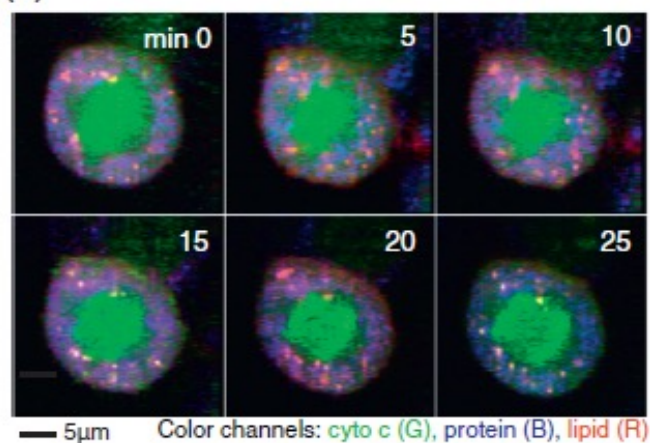
Current Opinion in Chemical Biology 2013, 17:708–715



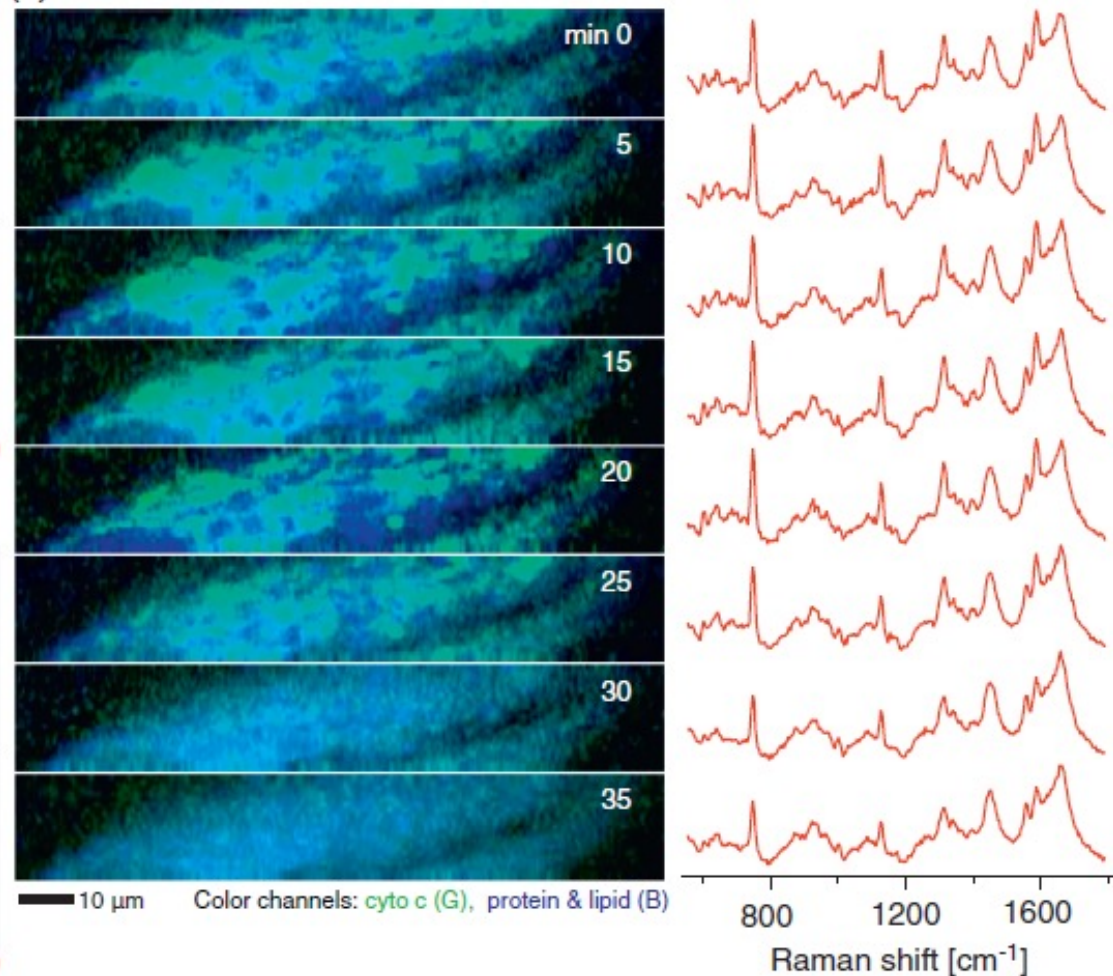
(a)

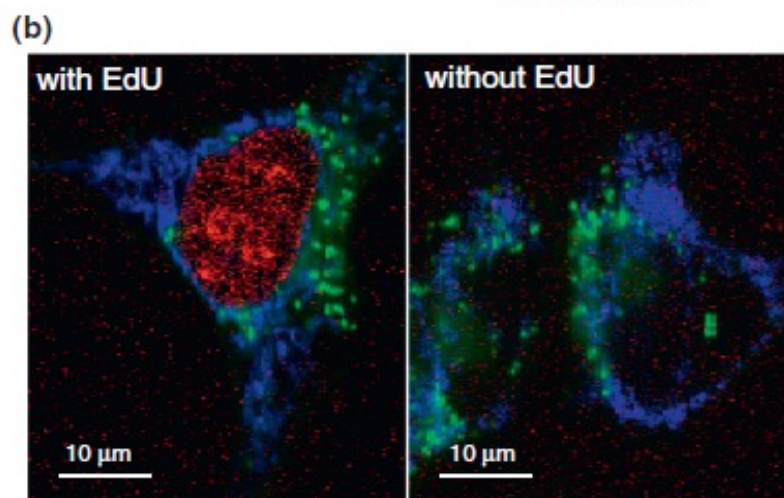
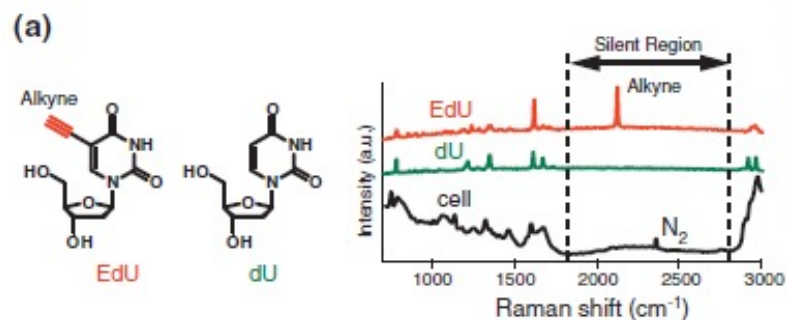


(b)

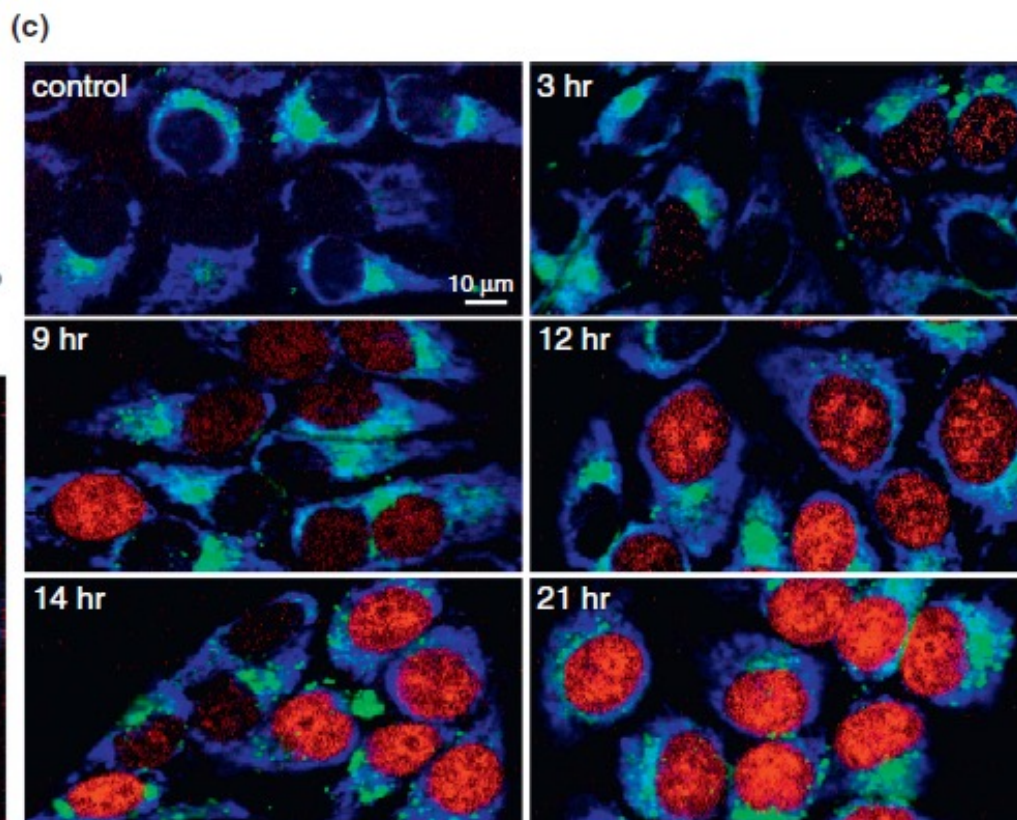


(c)

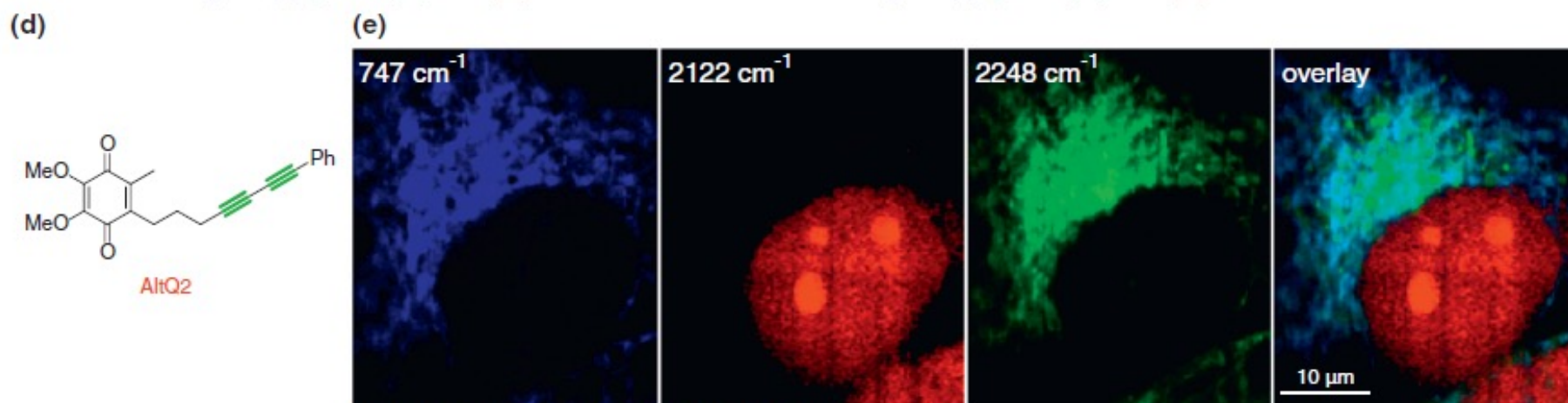




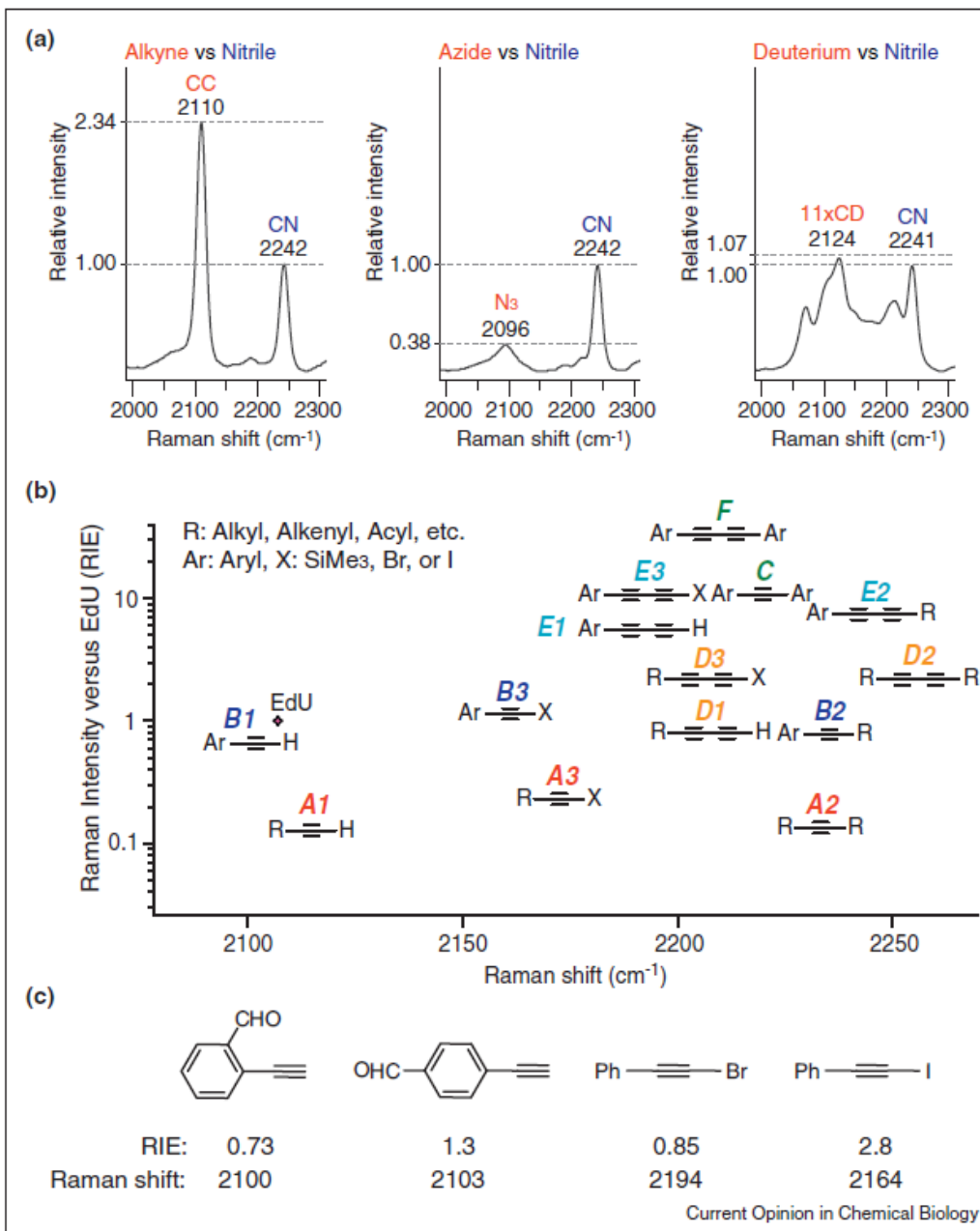
Color channels: cyto c (B), protein (G), EdU (R)



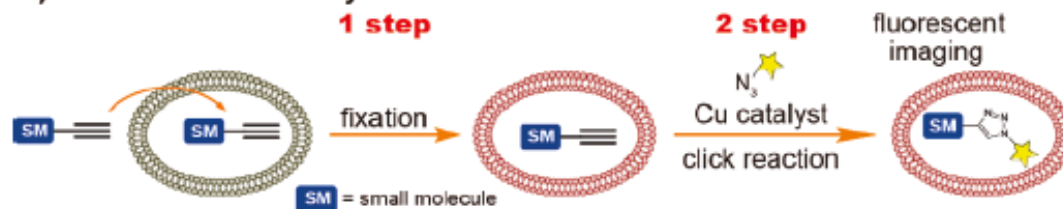
Color channels: cyto c (B), protein (G), EdU (R)



Color channels: cyto c (B), EdU (R), AltQ2 (G)



A) General click chemistry



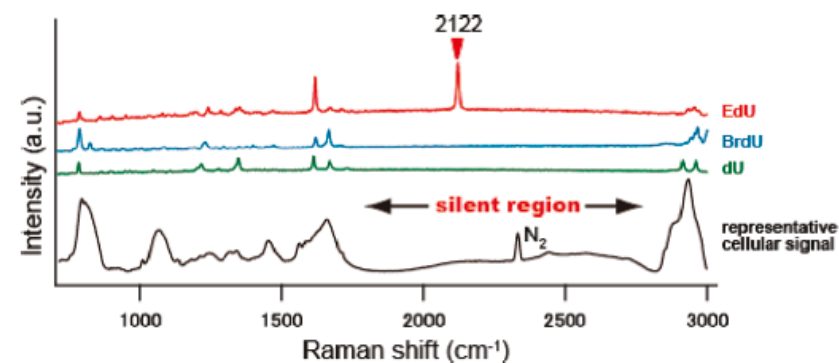
B) Cu-free click chemistry



C) This time (Click-free)



Figure 1. Concept of click-free imaging.



alkyne tag

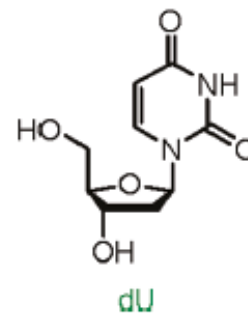
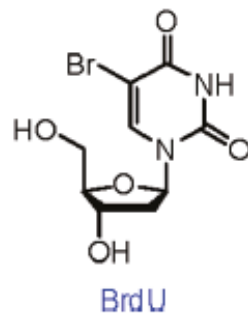
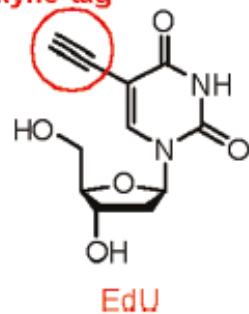
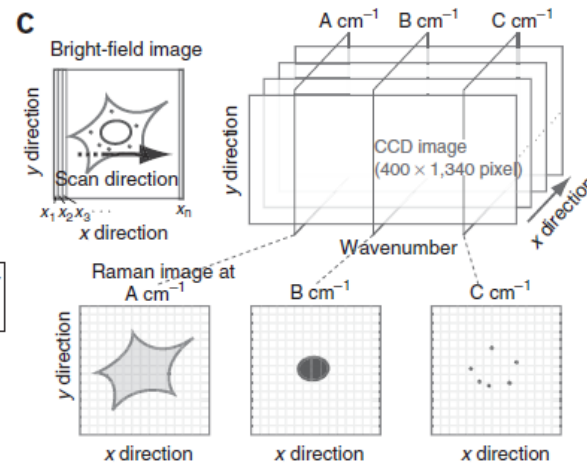
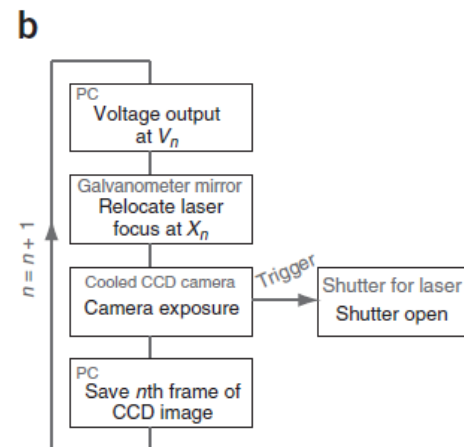
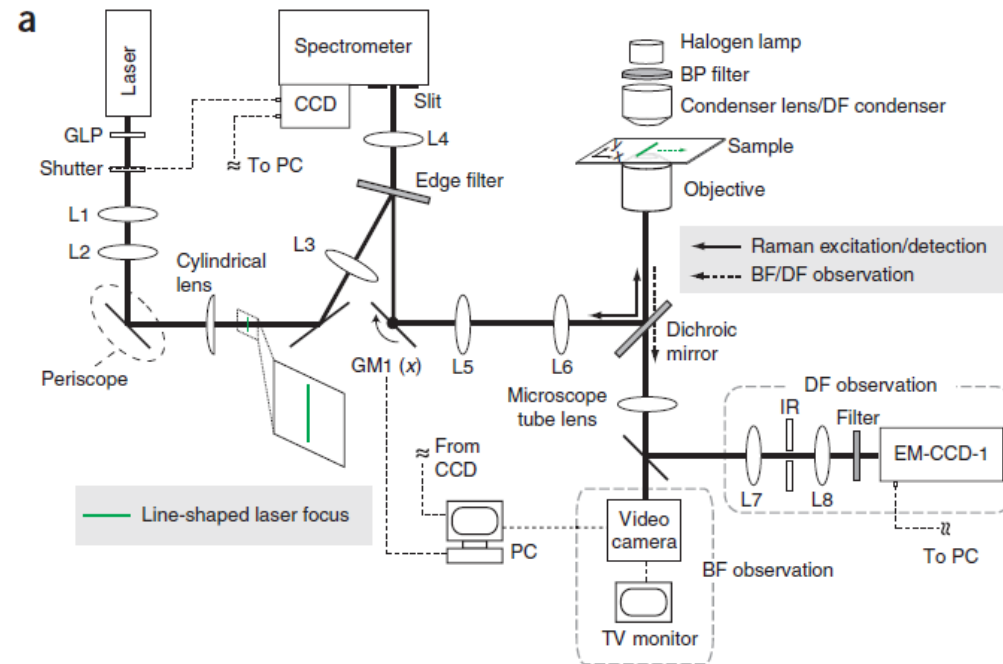
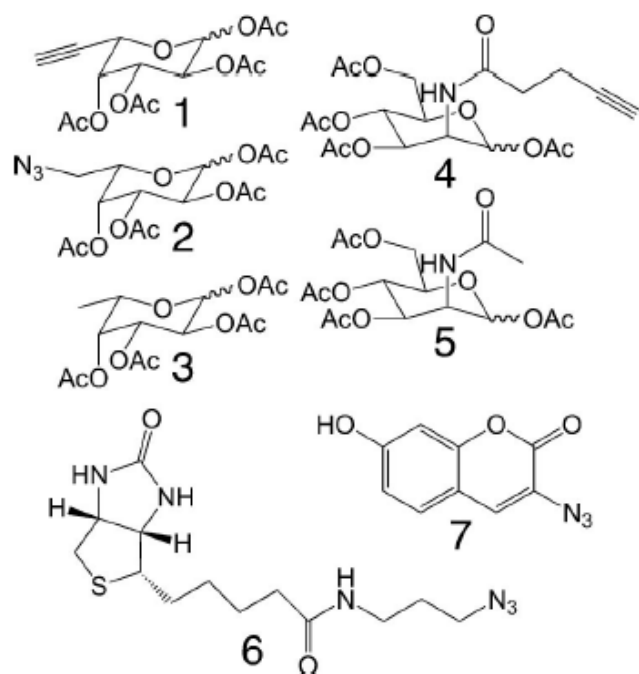


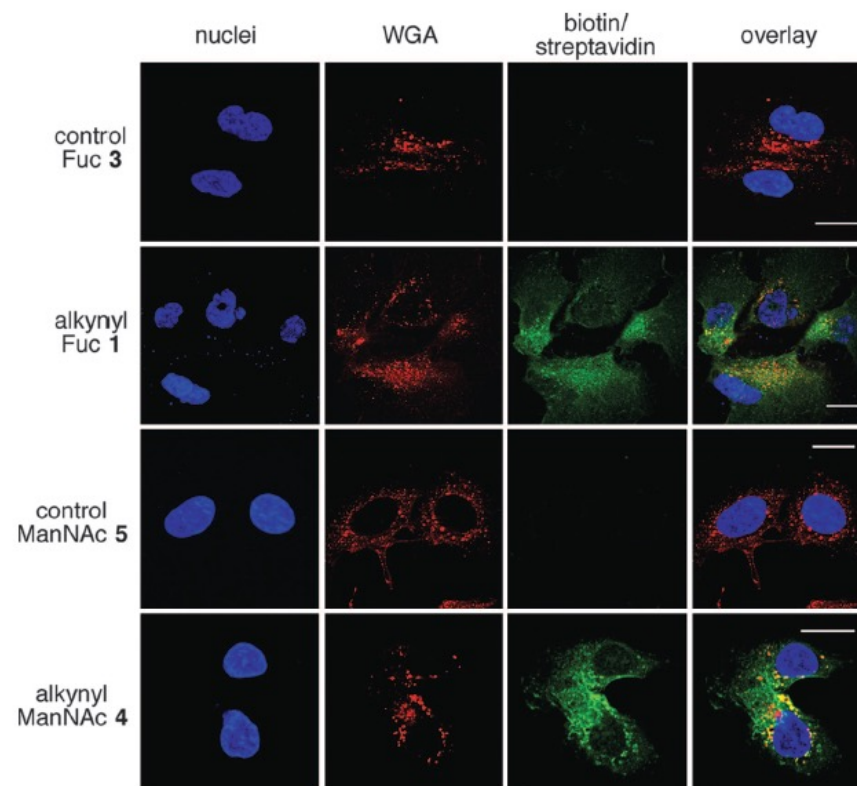
Figure 2. Structures of thymidine analogues.



Alkynyl sugar analogs for the labeling and visualization of glycoconjugates in cells



Scheme 1. Modified sugar analogs and probes used in this study.



Cell-permeable probe for identification and imaging of sialidases

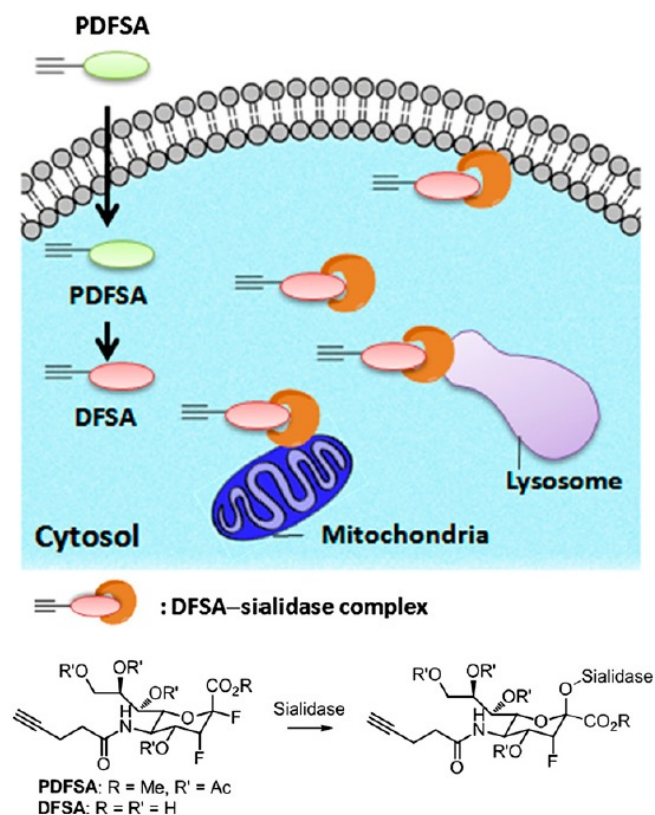
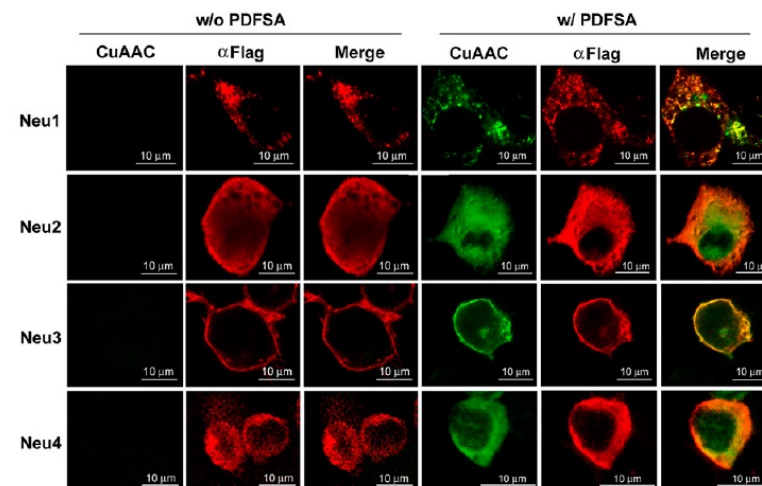
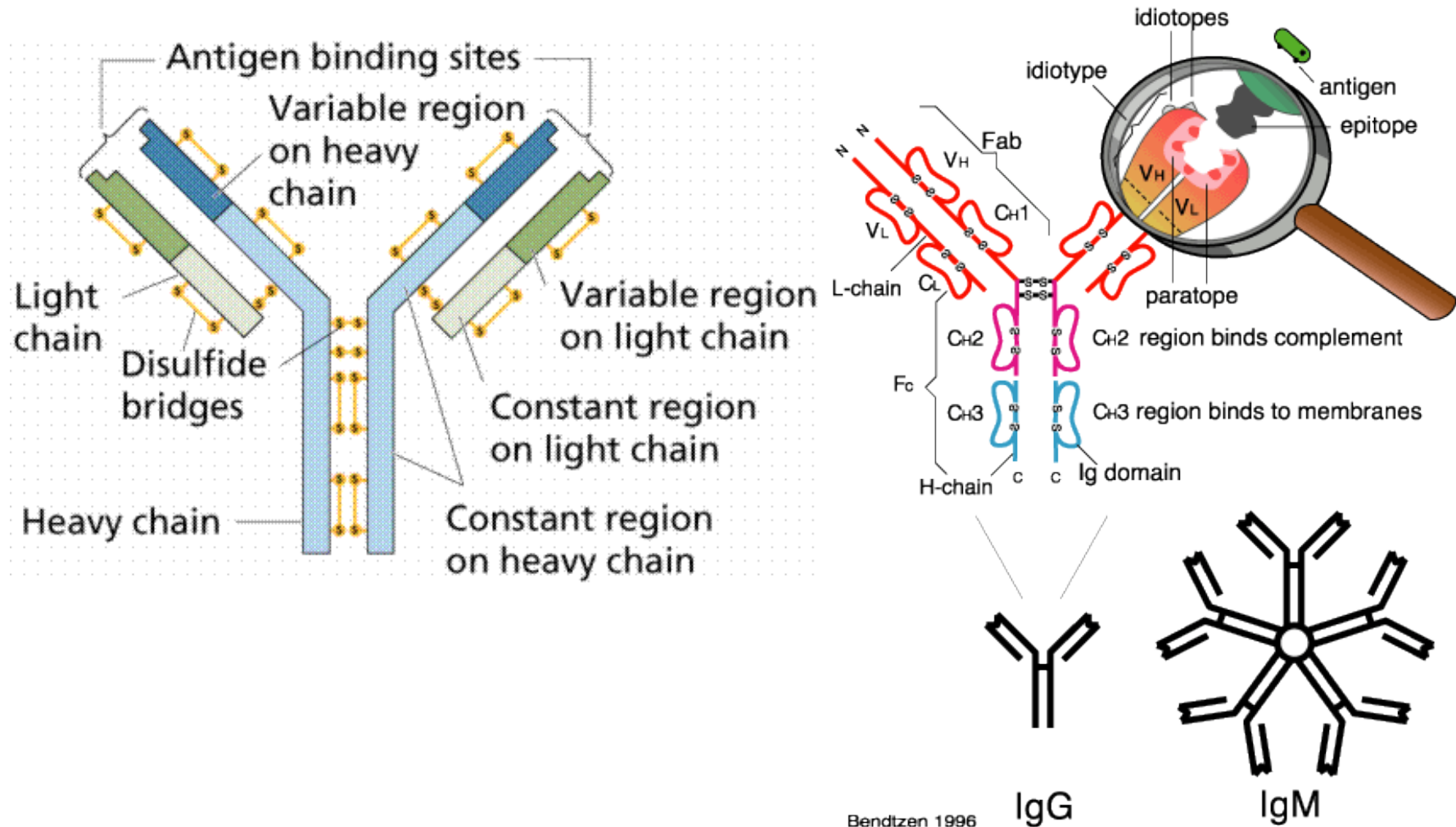


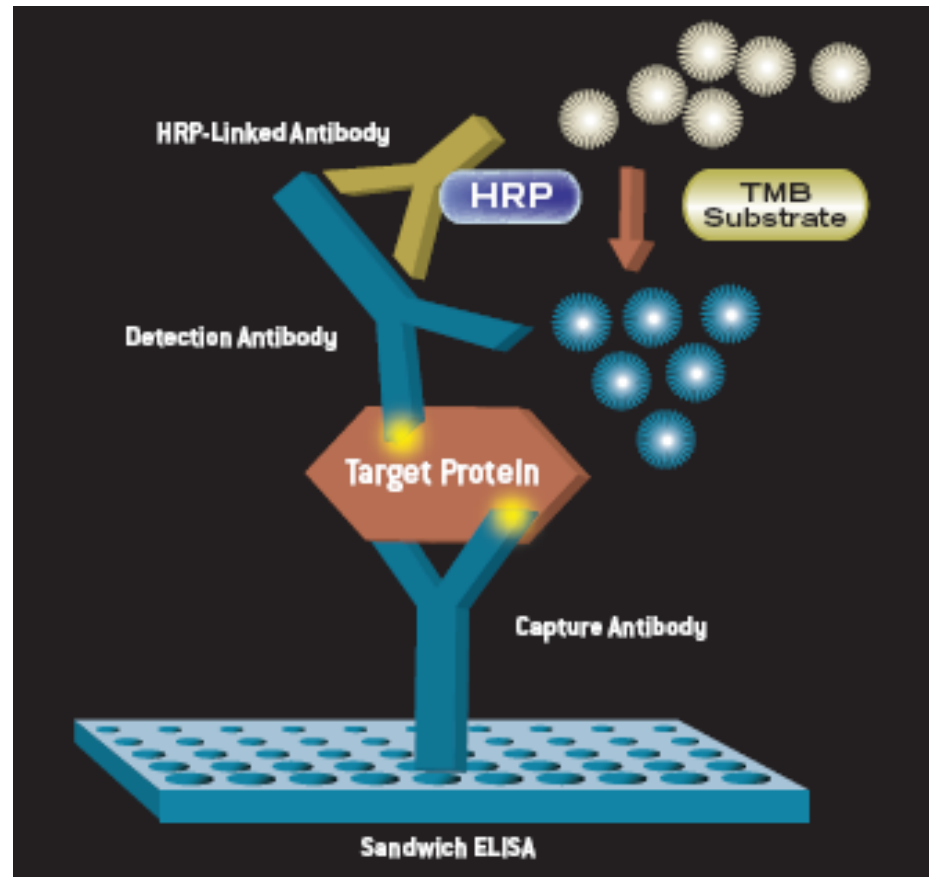
Fig. 1. Identification and imaging of sialidase with activity changes using these activity-based sialidase probes.



Antibody and Antigen



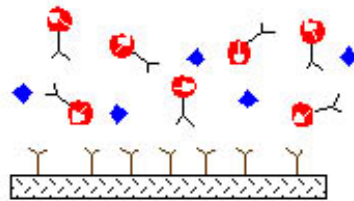
Enzyme-Linked ImmunoSorbent Assay (ELISA)



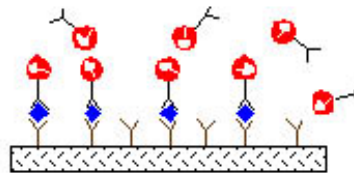
Labeling
BSA/PEG

Microarray

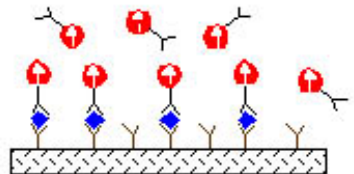
◆ Biomolecules of interest Y Capture antibody ▨ Solid support ● Magnetically labeled antibody



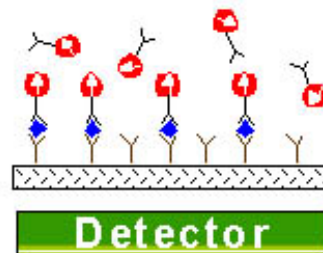
Add biomolecules of interest and magnetically labeled detect antibodies to well coated with capture antibody.



Immobilized immune complexes form on solid support.

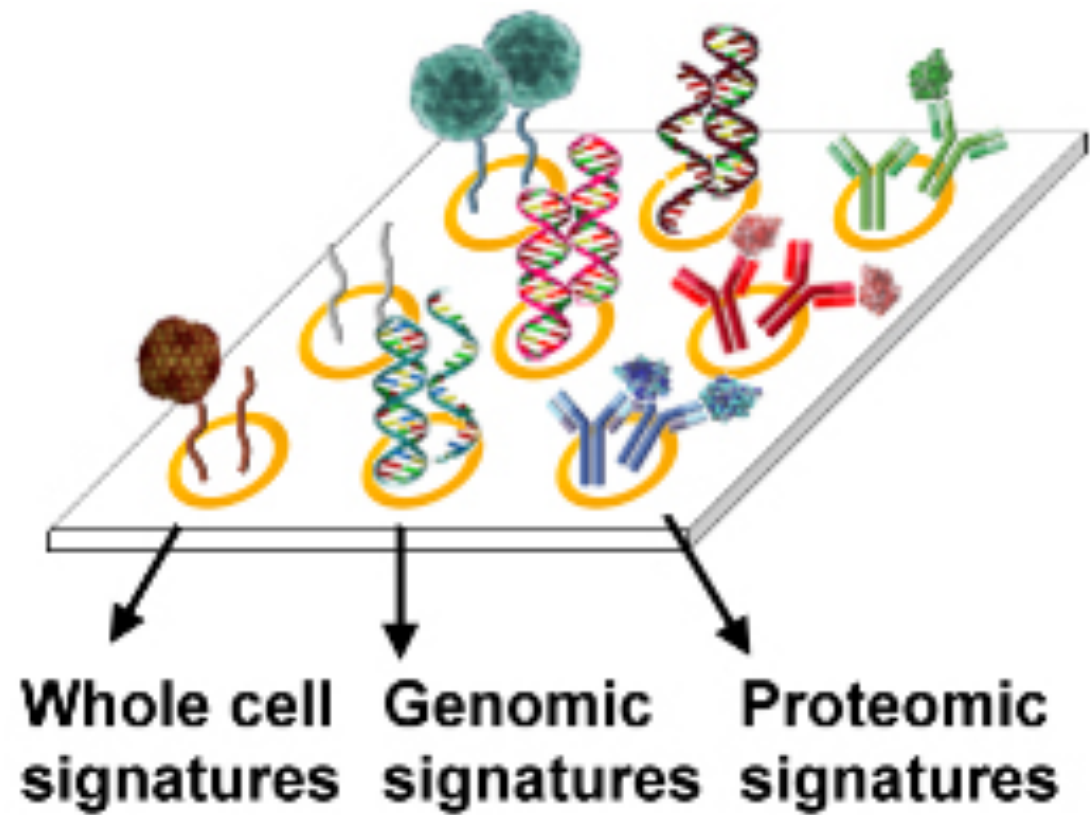


Apply external magnetic field, magnetic dipoles align.



Remove field, measure net magnetization due to bound antibody labels. Unbound labels randomize quickly and contribute no net signal.

Microarray



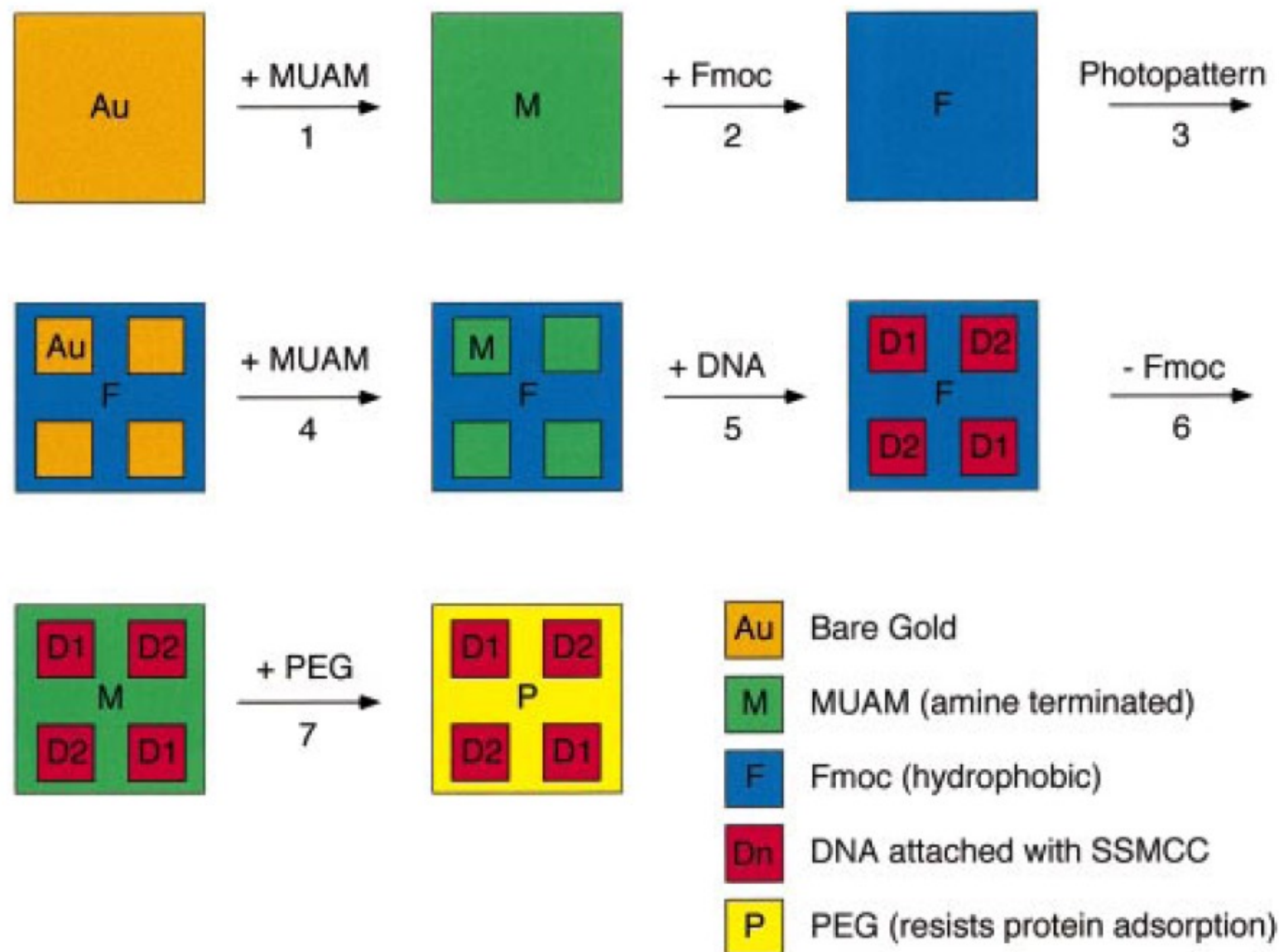


Figure 1. Fabrication scheme for the construction of multi-element DNA arrays. A clean gold surface is reacted with the amine-terminated alkanethiol MUAM, and subsequently reacted with Fmoc-NHS to create a hydrophobic surface. This surface is then exposed to UV radiation through a quartz mask and rinsed with solvent to remove the MUAM+Fmoc from specific areas of the surface, leaving bare gold pads. These bare gold areas on the sample surface are filled in with MUAM, resulting in an array of MUAM pads surrounded by a hydrophobic Fmoc background. Solutions of DNA are then delivered by pipet onto the specific array locations and are covalently bound to the surface via the bifunctional linker SSMCC. In the final two steps, the Fmoc-terminal groups on the array background are removed and replaced by PEG groups which prohibit the nonspecific binding of analyte proteins to the background.

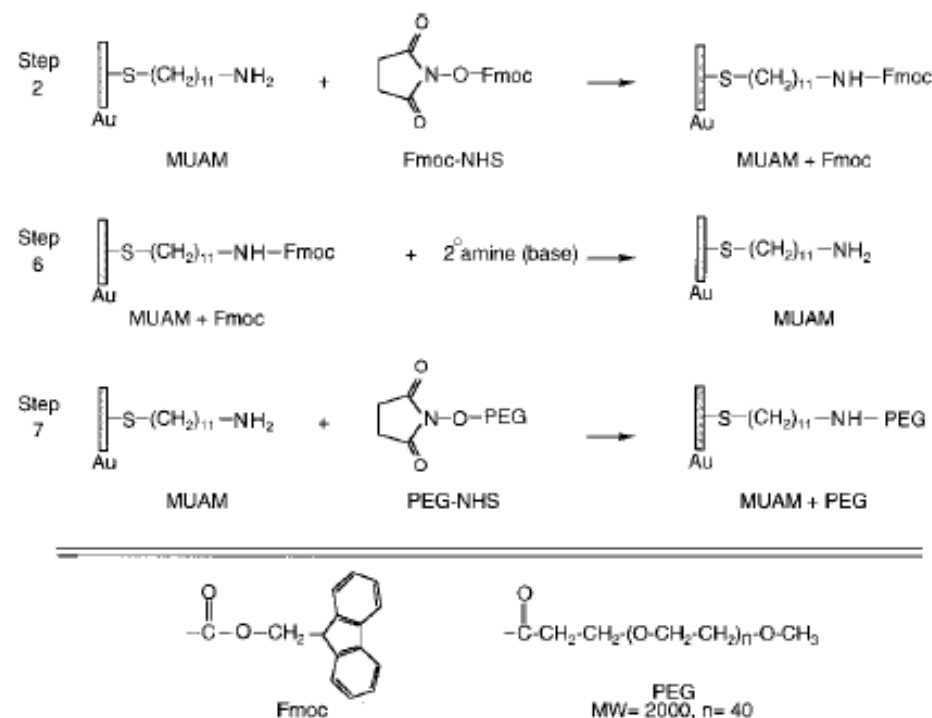


Figure 2. Surface reaction scheme showing the steps involved in the reversible modification of the array background. (Step 2) The starting amine-terminated alkanethiol surface (MUAM) is reacted with the Fmoc-NHS protecting group to form a carbamate linkage thus creating a hydrophobic Fmoc-terminated surface. (Step 6) After DNA immobilization (see Figure 3), the hydrophobic Fmoc group is removed from the surface with a basic secondary amine, resulting in the return of the original MUAM surface. (Step 7) In the final array fabrication step, the deprotected MUAM is reacted with PEG-NHS to form an amide bond that covalently attaches PEG to the array surface.

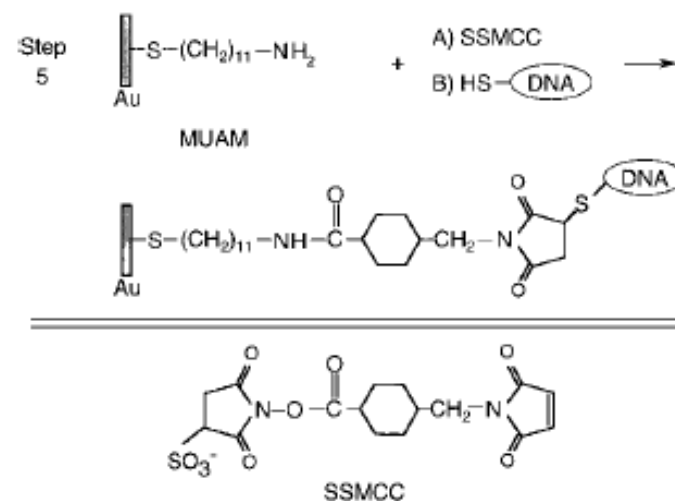
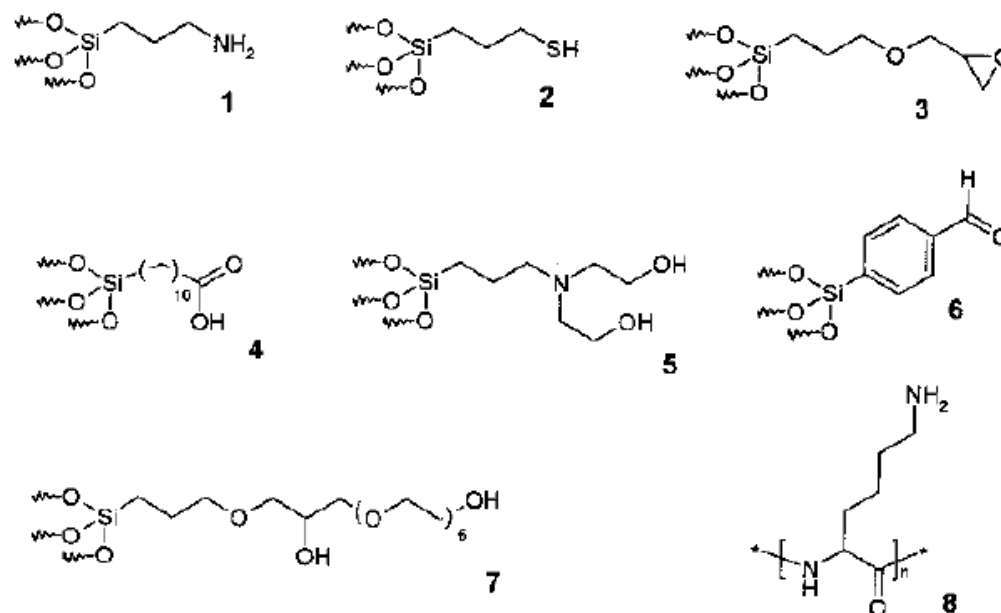
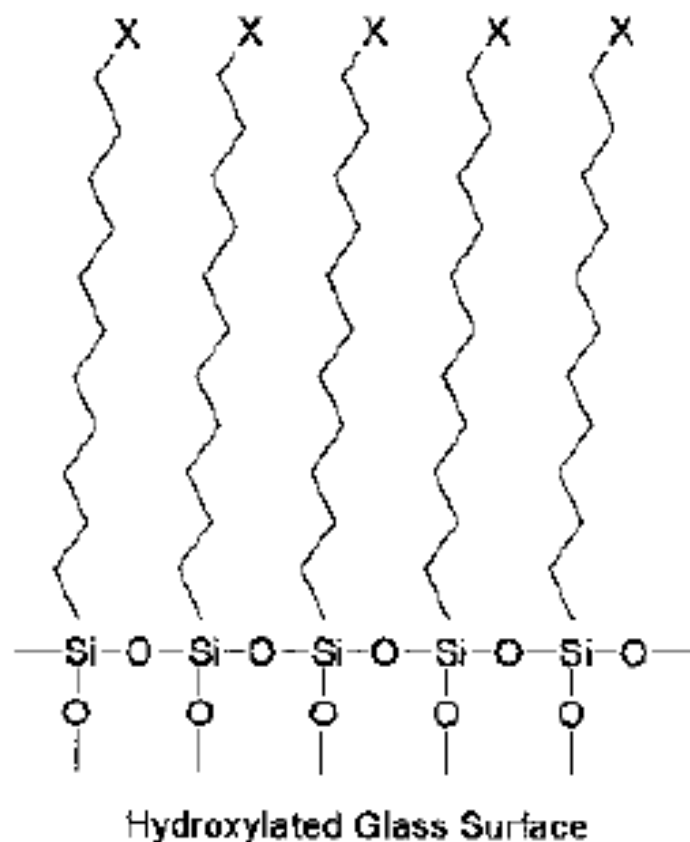


Figure 3. Surface reaction scheme showing the immobilization of thiol-terminated DNA to the array surface. In Step 5 of the DNA array fabrication, the heterobifunctional linker SSMCC is used to attach 5'-thiol modified oligonucleotide sequences to reactive pads of MUAM. This linker contains an NHSS ester functionality (reactive toward amines) and a maleimide functionality (reactive toward thiols). The surface is first exposed to a solution of the linker, whereby the NHSS ester end of the molecule reacts with the MUAM surface. Excess linker is rinsed away and the array surface is then spotted with 5'-thiol-modified DNA that reacts with the maleimide groups forming a covalent bond to the surface monolayer.

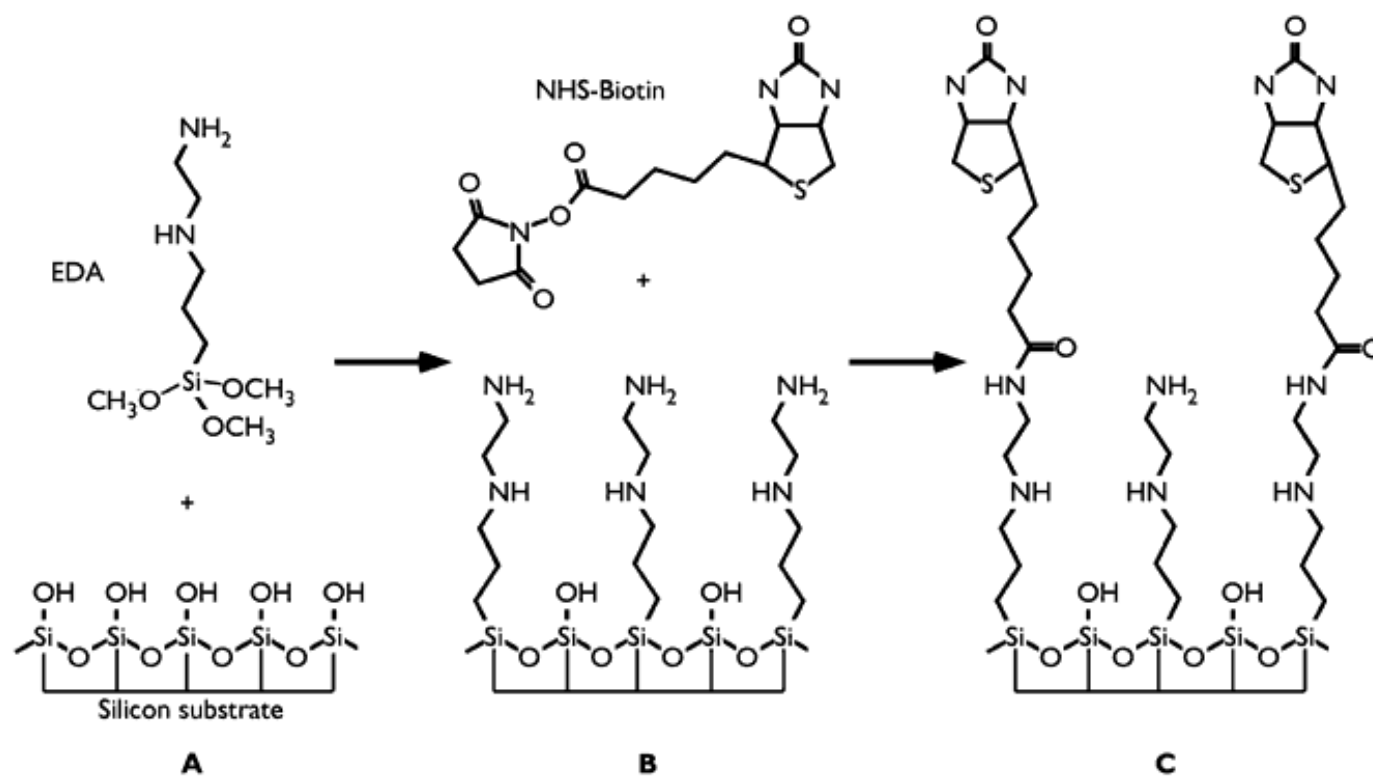
Glass Surface Modification



Scheme 2.2 Reagents for derivatization of glass surfaces. 1 APTES = aminopropyltriethoxysilane; 2 MPTS = 3-mercaptopropyltrimethoxysilane; 3 GPTS = glycidoxypropyltrimethoxysilane; 4 TETU = triethoxysilane undecanoic acid;

5 HE-APTS = bis(hydroxyethyl)aminopropyltriethoxysilane; 6 4-trimethoxysilylbenzaldehyde; 7 GPTS/HEG = glycidoxypropyltrimethoxysilane-hexaethylene glycol; 8 poly(lysine).

Scheme 2.1 2D schematic description of a polysiloxane monolayer on a glass surface (X = terminal functional)



Biotin-Streptavidin

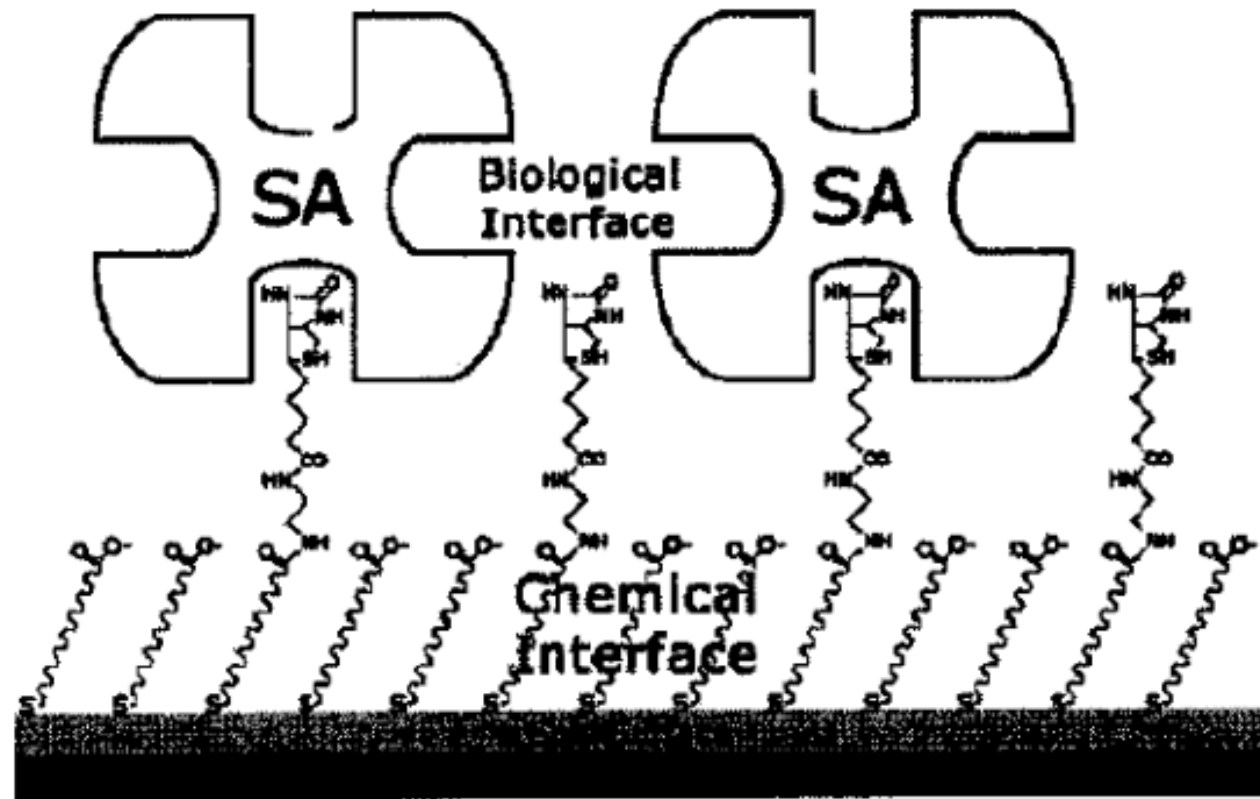
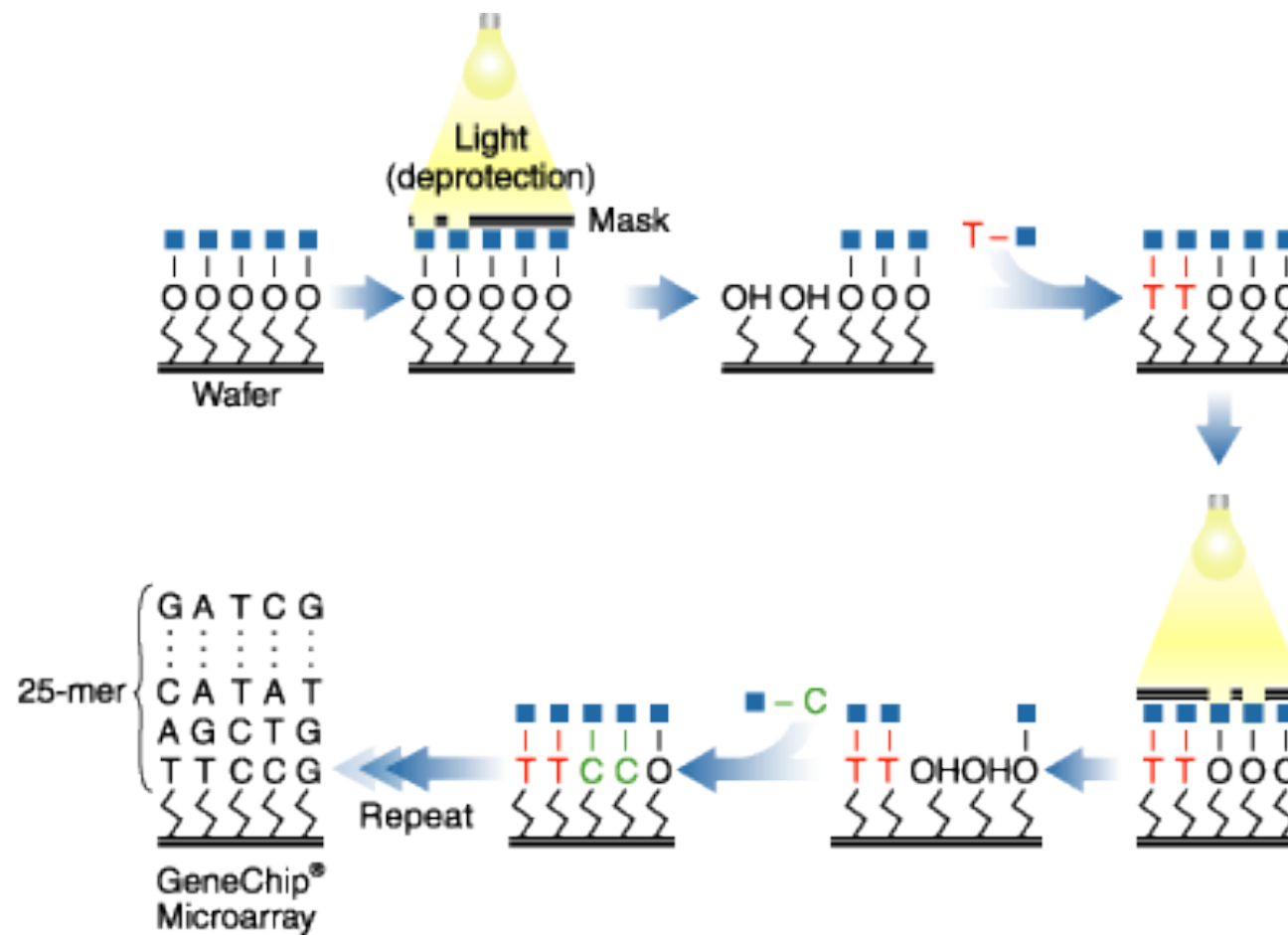
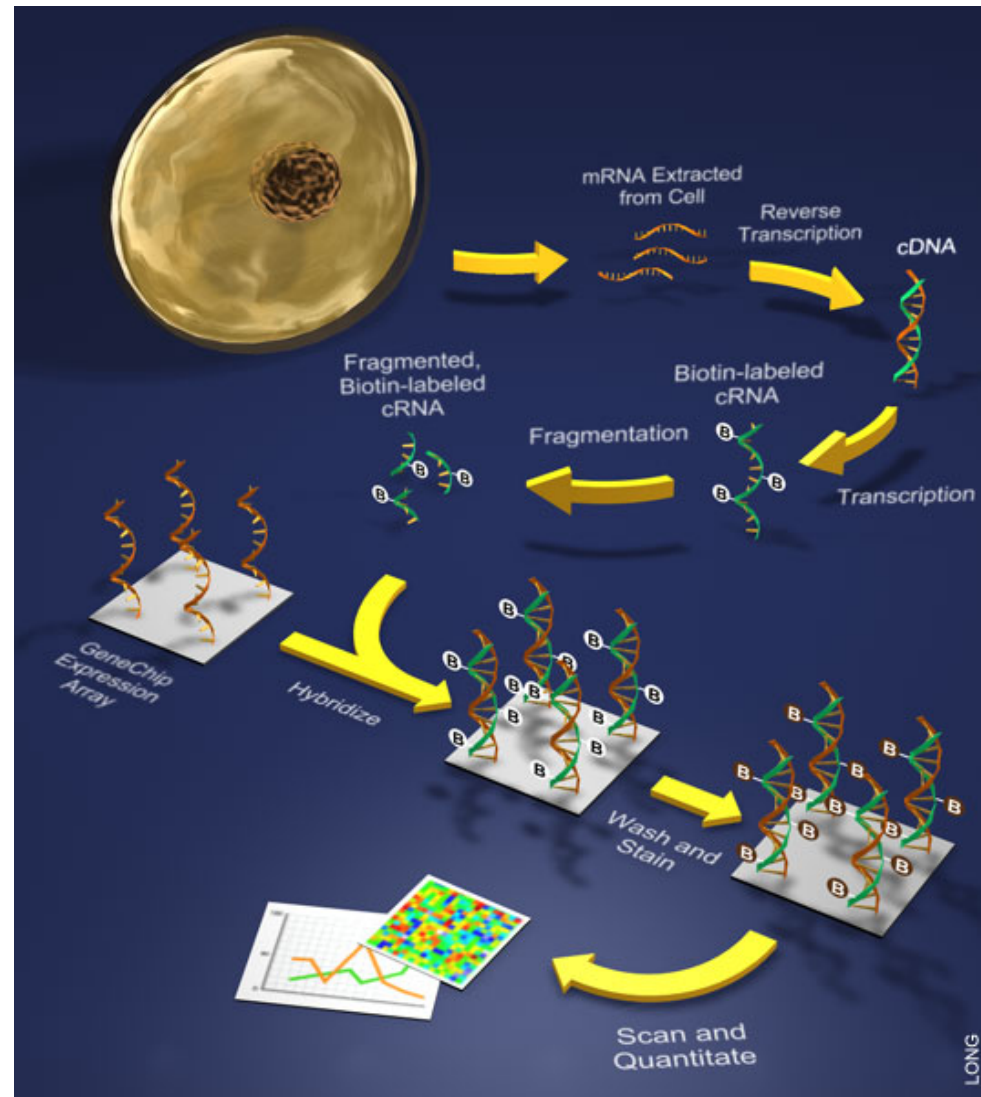


Figure 2.3 Schematic representation of a streptavidin sensor surface assembled on a reaction-controlled biotinylated SAM [28].

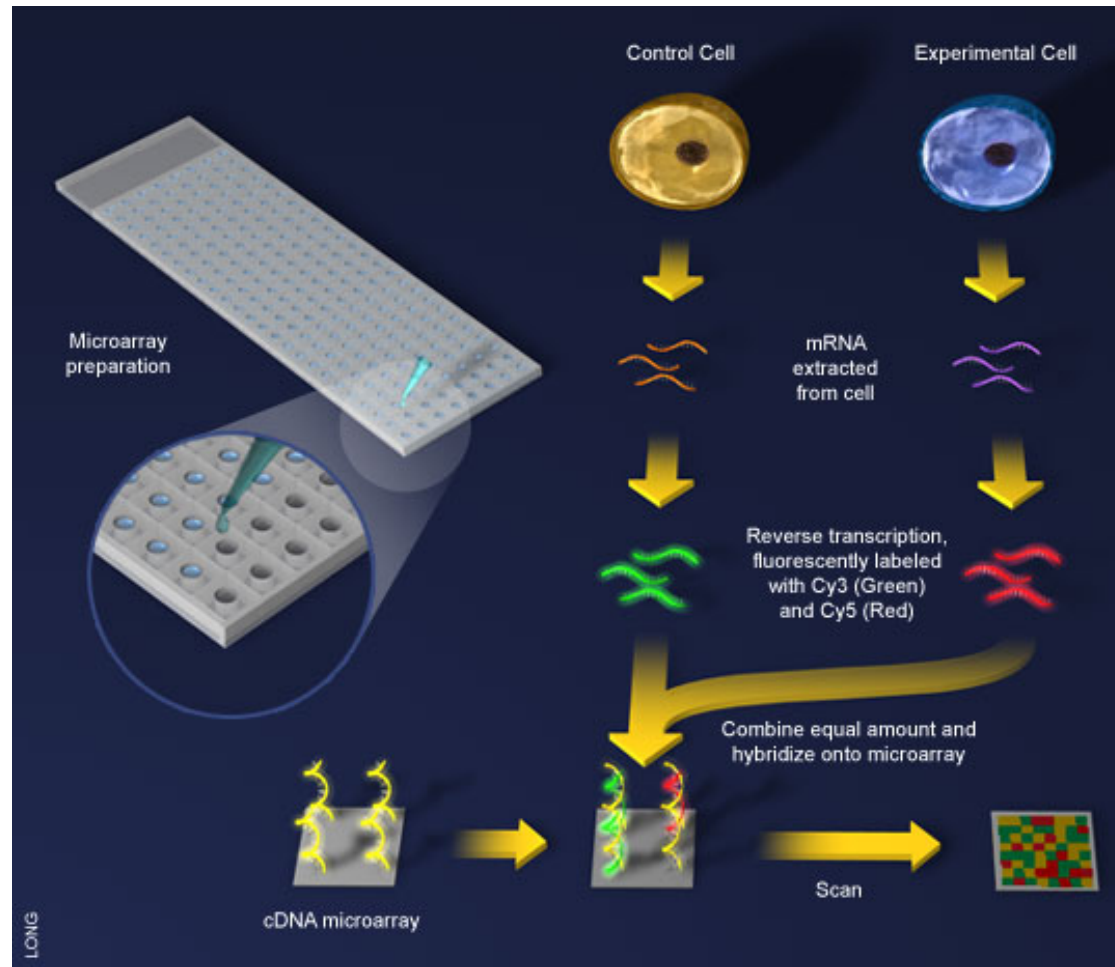
GeneChip



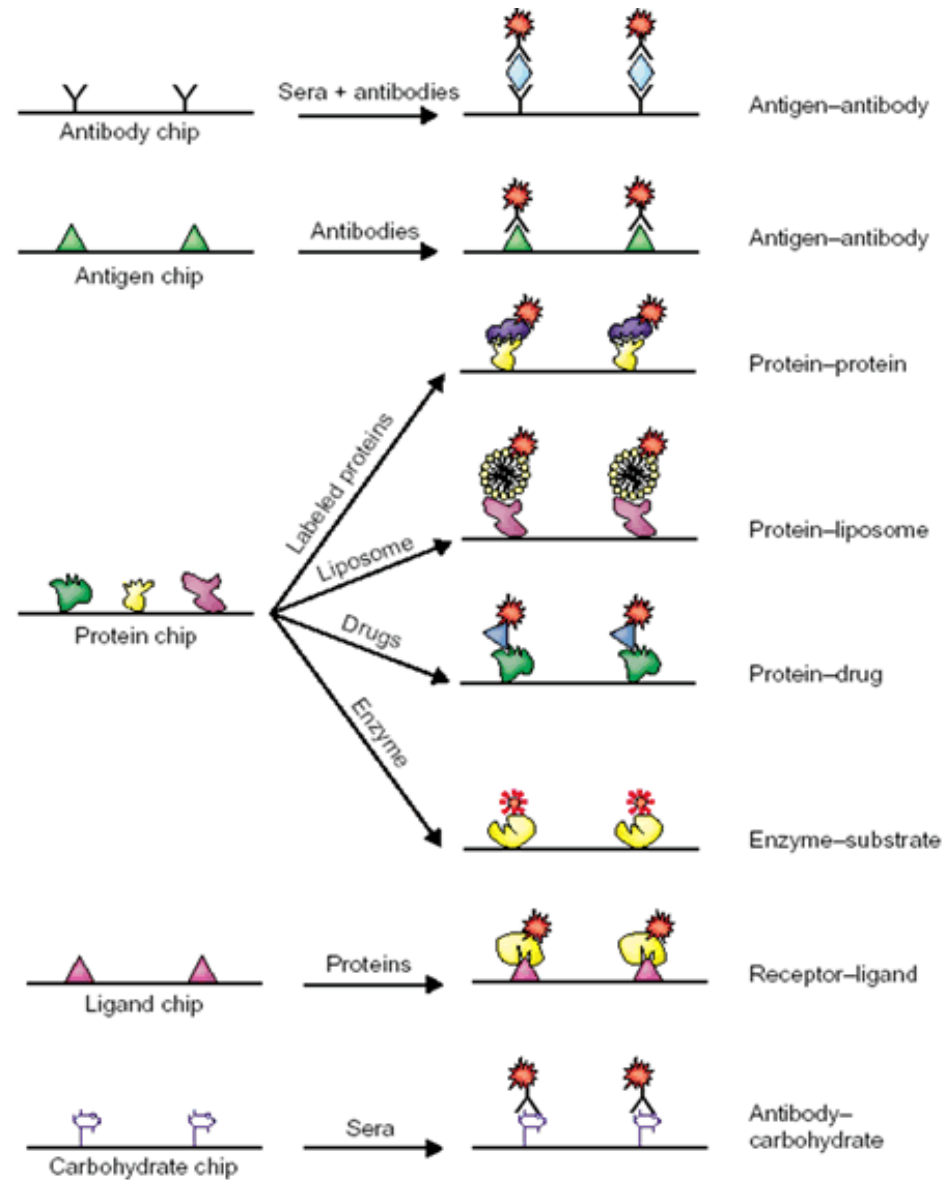
Scheme



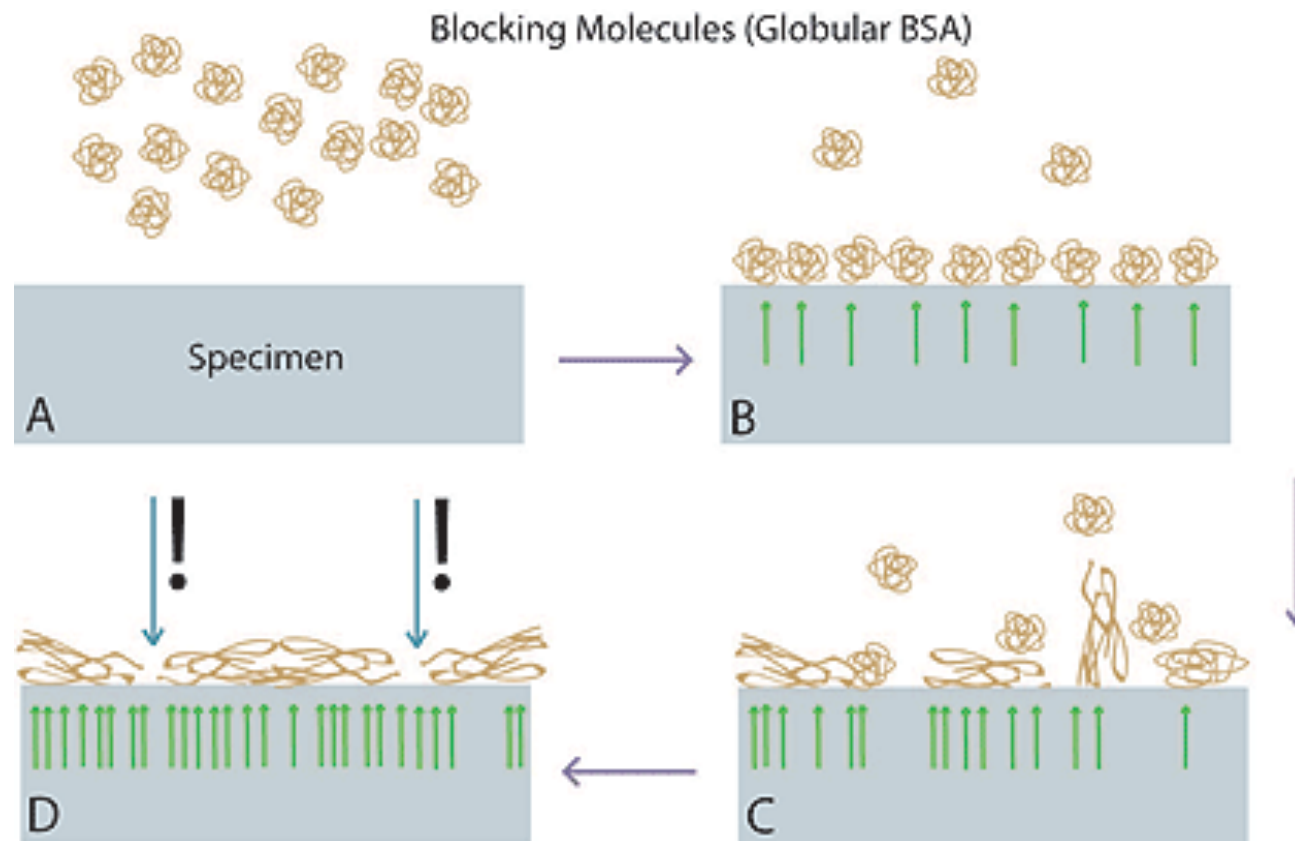
cDNA Microarray



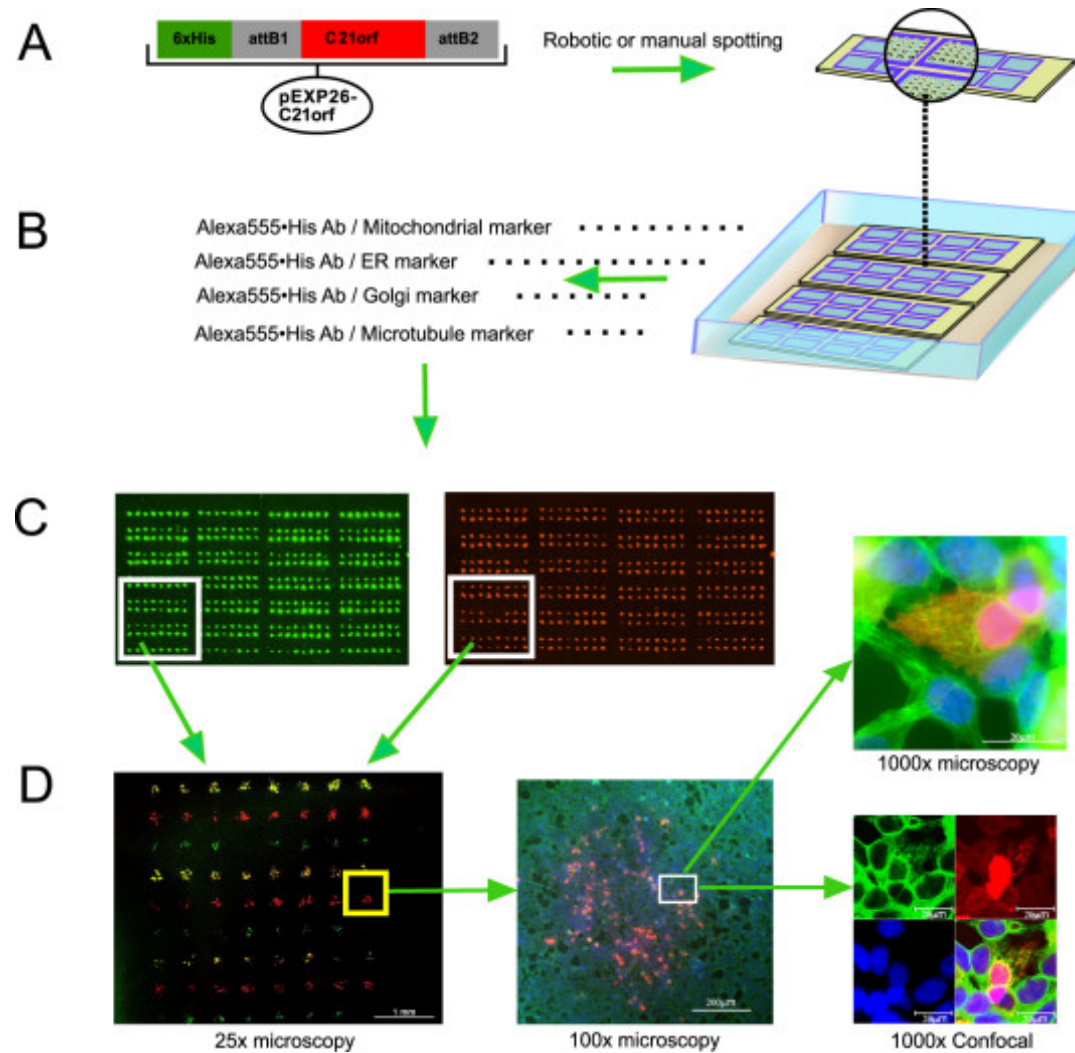
Protein Array



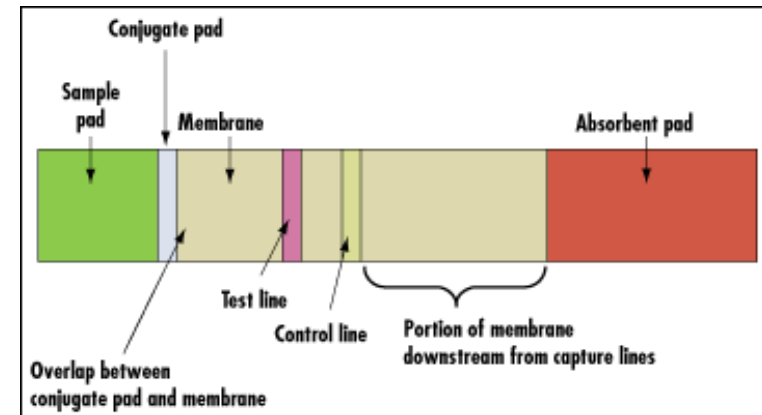
BSA Blocking



Cell Array

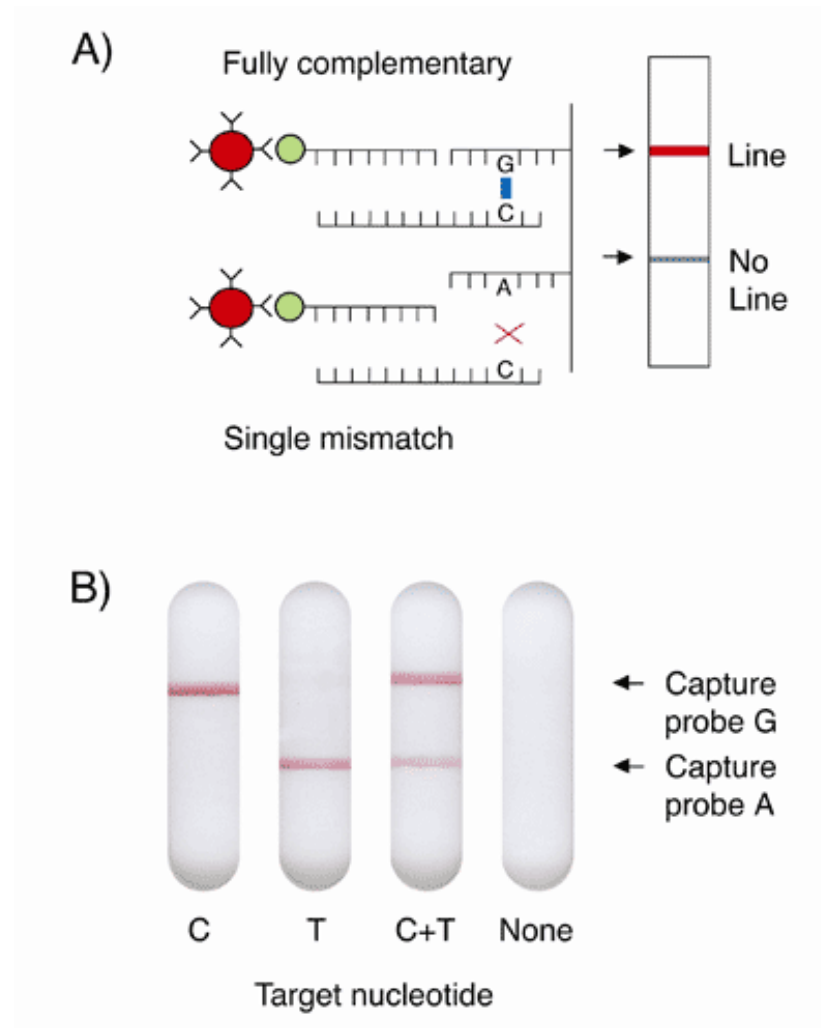


hCG immunoassay



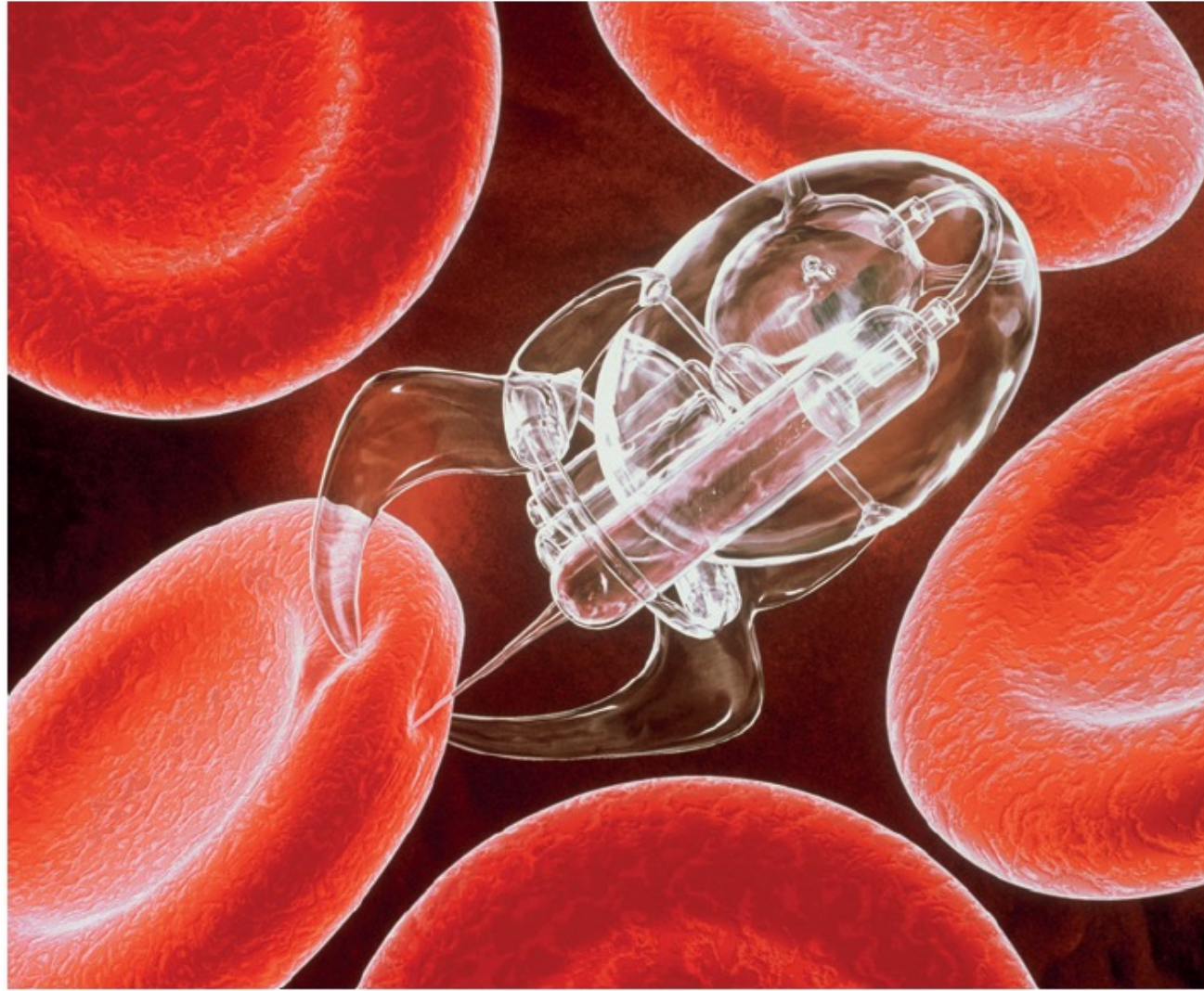
human chorionic gonadotropin (hCG)

Nucleotide Sensor



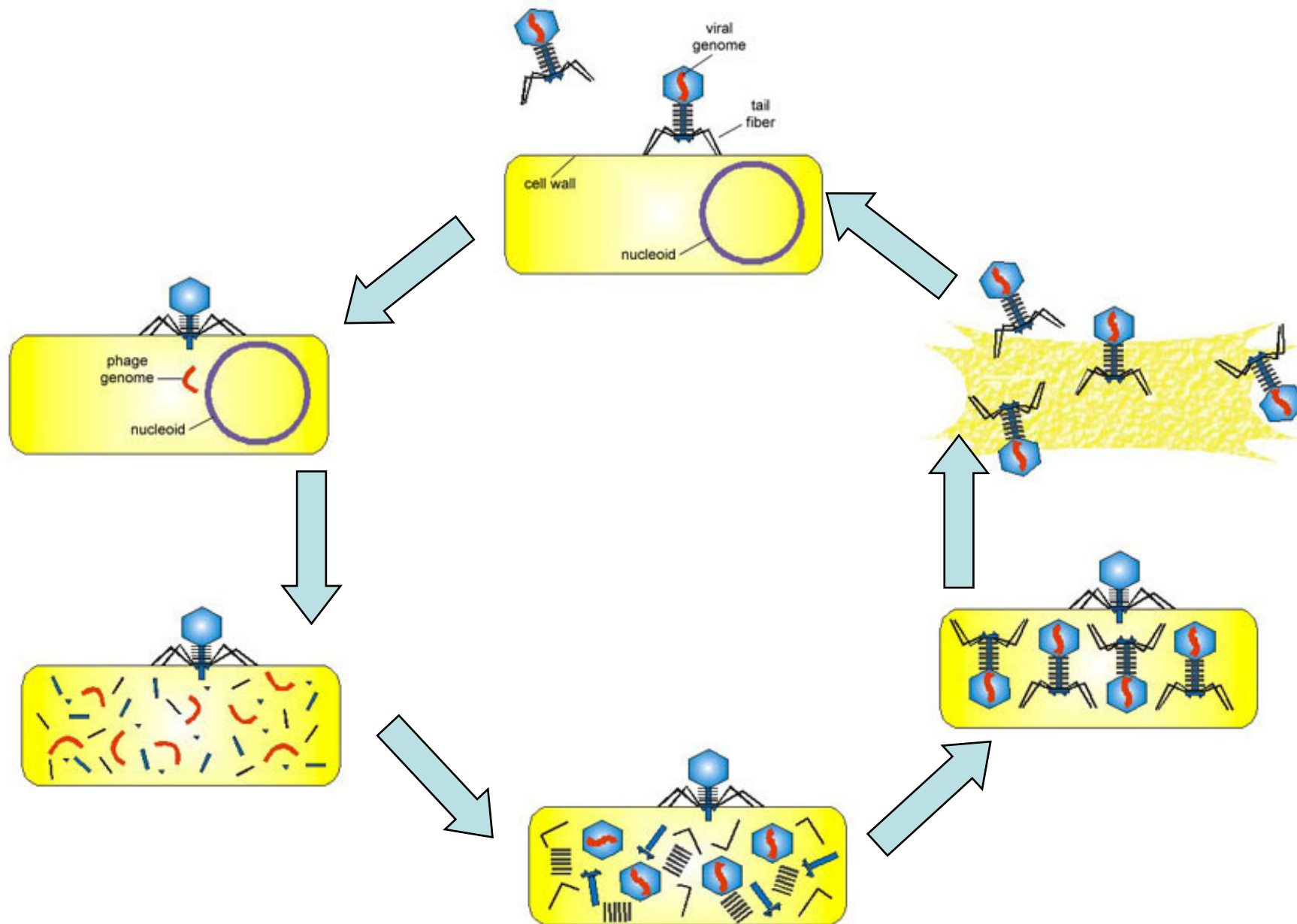
Nanomedicine

Nanobots

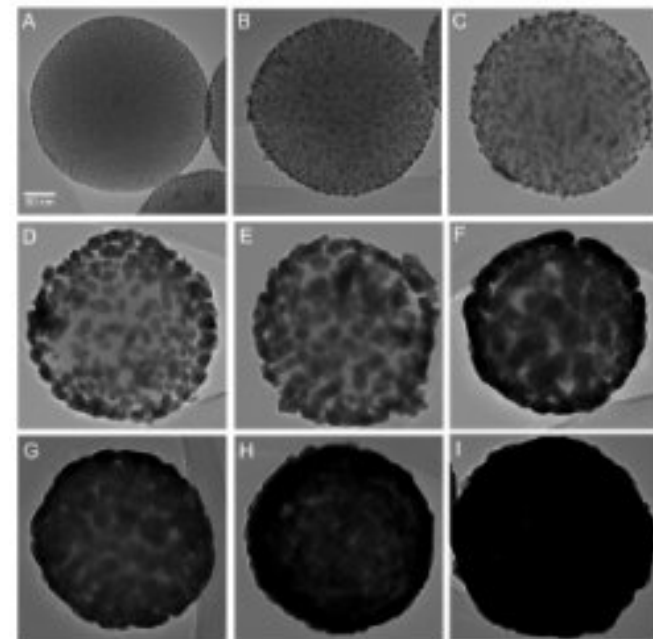
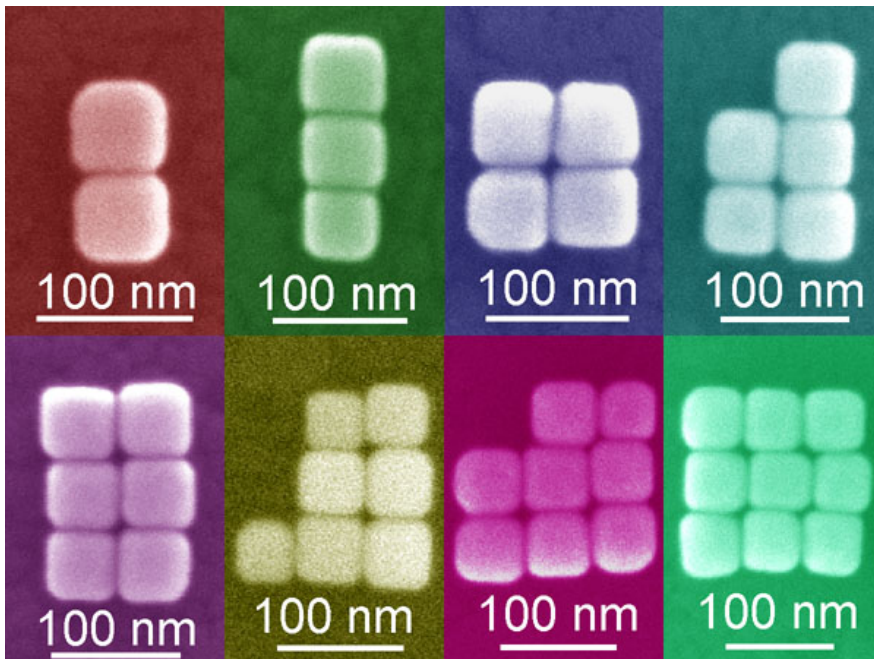
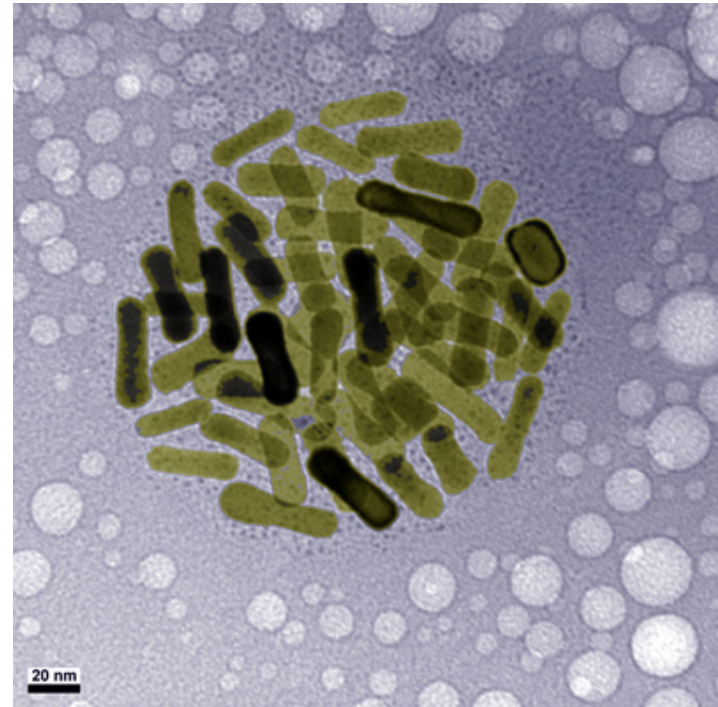
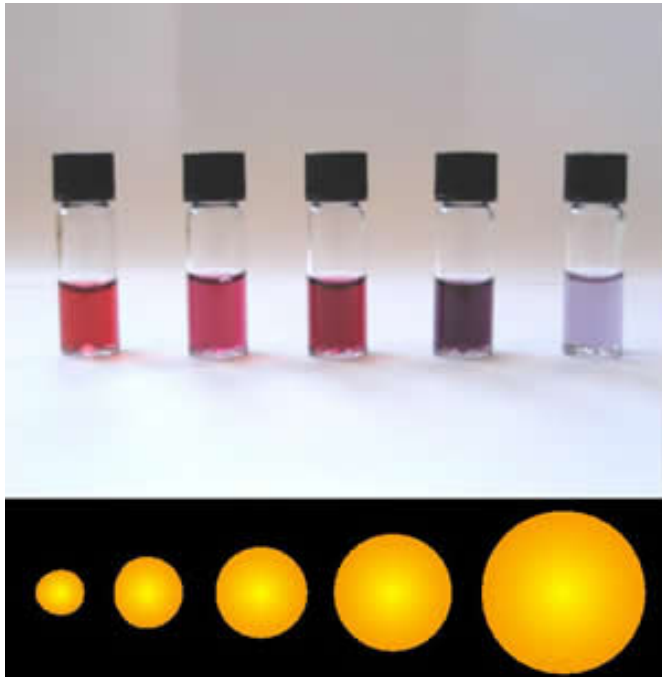


© CONEY L JAY / GETTY IMAGES

Virus Infection



Gold



Nanorods

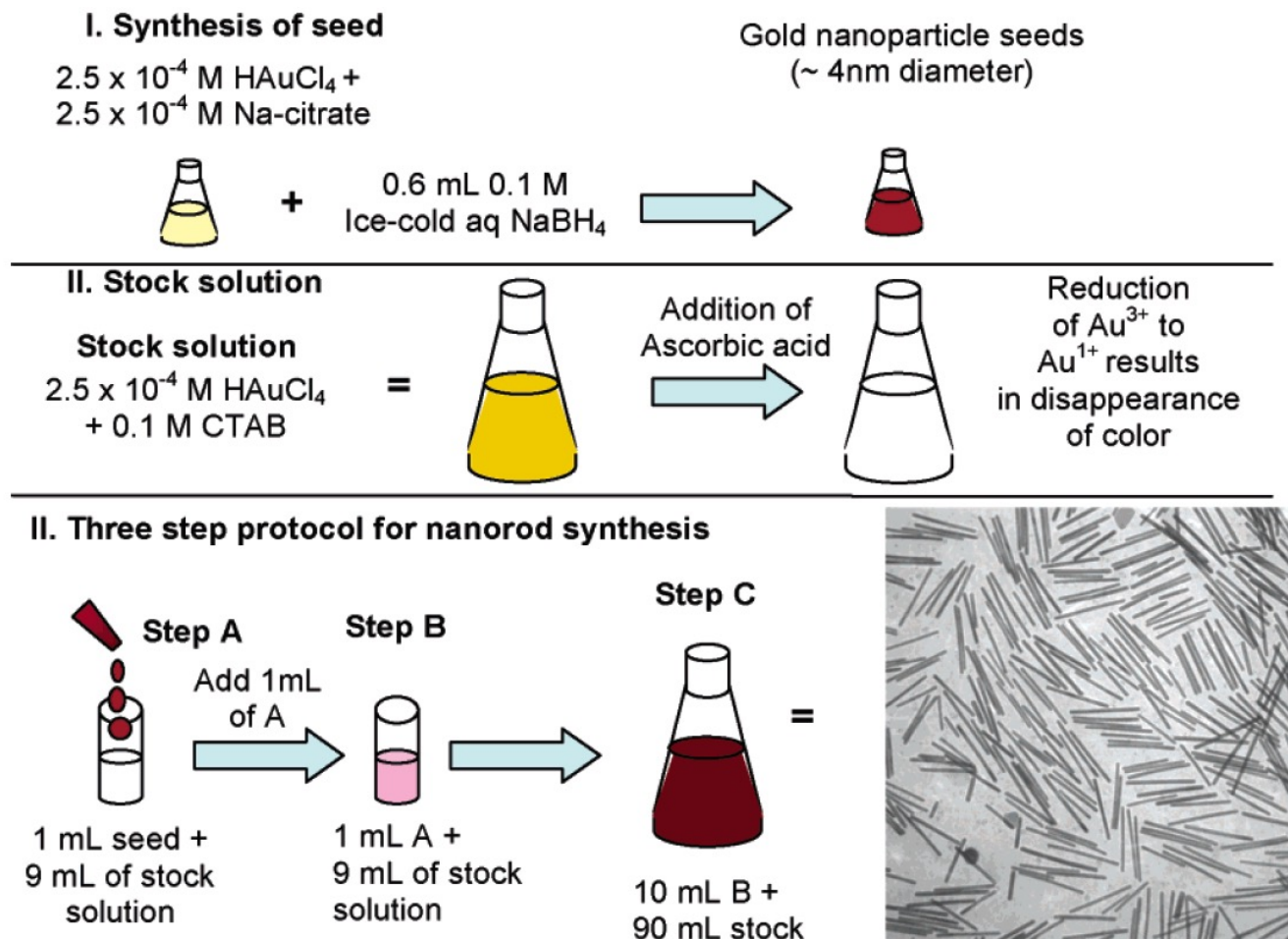
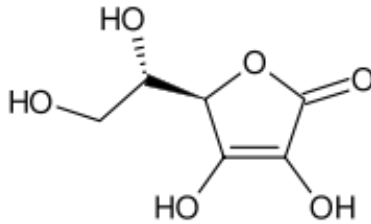
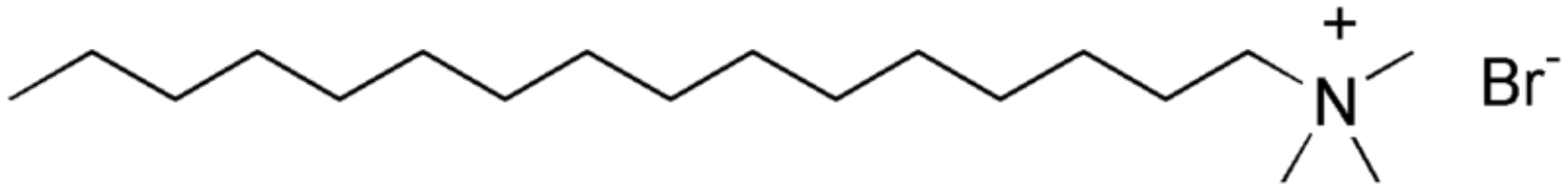


Figure 2. Seed-mediated growth approach to making gold and silver nanorods of controlled aspect ratio. The specific conditions shown here, for 20 mL volume of seed solution, lead to high-aspect ratio gold nanorods. (bottom right) Transmission electron micrograph of gold nanorods that are an average of 500 nm long.

Directional Growth

Cetrimonium bromide ($(\text{C}_{16}\text{H}_{33})\text{N}(\text{CH}_3)_3\text{Br}$) (CTAB)



Ascorbic acid

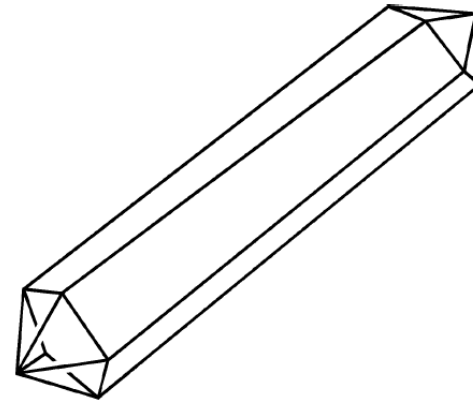


Figure 5. Cartoon of the crystallography of gold nanorods. The direction of elongation is $[110]$. The cross-sectional view is a pentagon; each end of the rod is capped with five triangular faces that are $\text{Au}\{111\}$. The sides of the rods are not as well-defined; either $\text{Au}\{100\}$ or $\text{Au}\{110\}$ faces, or both.

STEP 1: SYMMETRY BREAKING IN FCC METALS



STEP 2: PREFERENTIAL SURFACTANT BINDING TO SPECIFIC CRYSTAL FACES

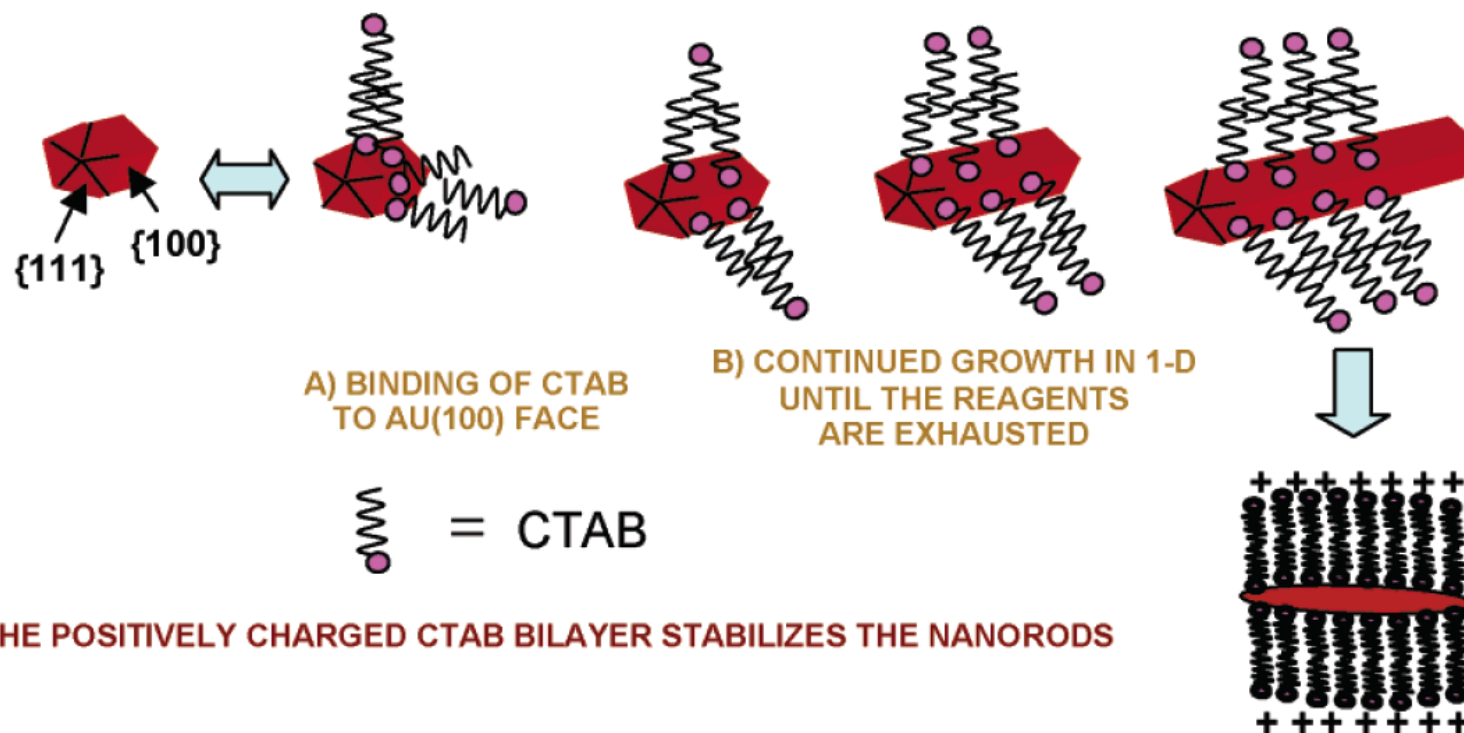


Figure 8. Proposed mechanism of surfactant-directed metal nanorod growth. The single crystalline seed particles have facets that are differentially blocked by surfactant (or an initial halide layer that then electrostatically attracts the cationic surfactant). Subsequent addition of metal ions and weak reducing agent lead to metallic growth at the exposed particle faces. In this example, the pentatetrahedral twin formation leads to Au {111} faces that are on the ends of the nanorods, leaving less stable faces of gold as the side faces, which are bound by the surfactant bilayer.

Nanorods

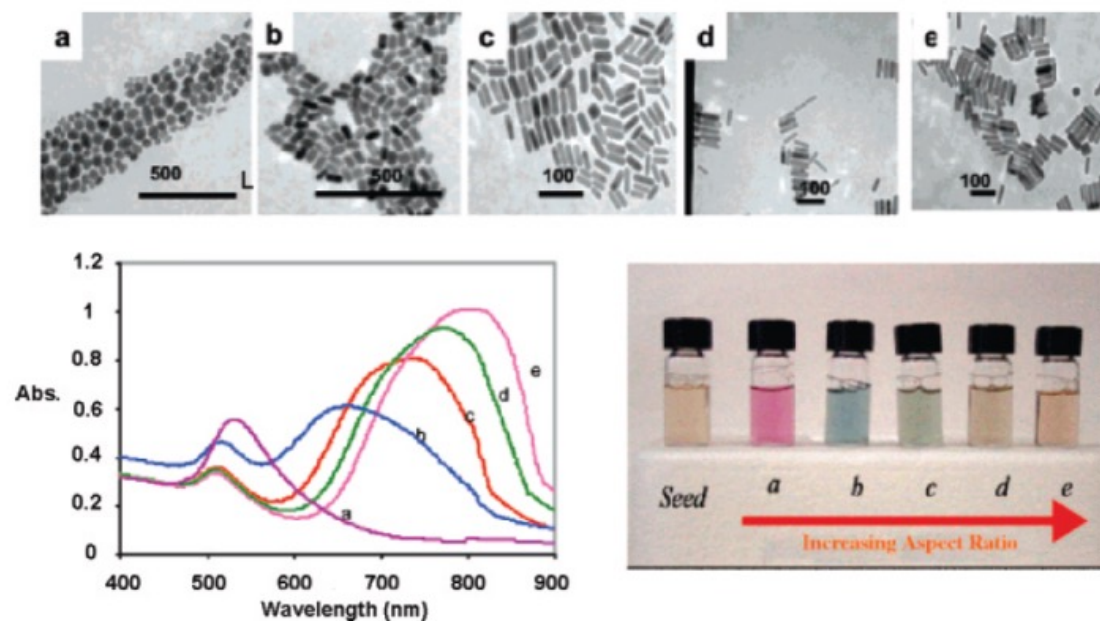
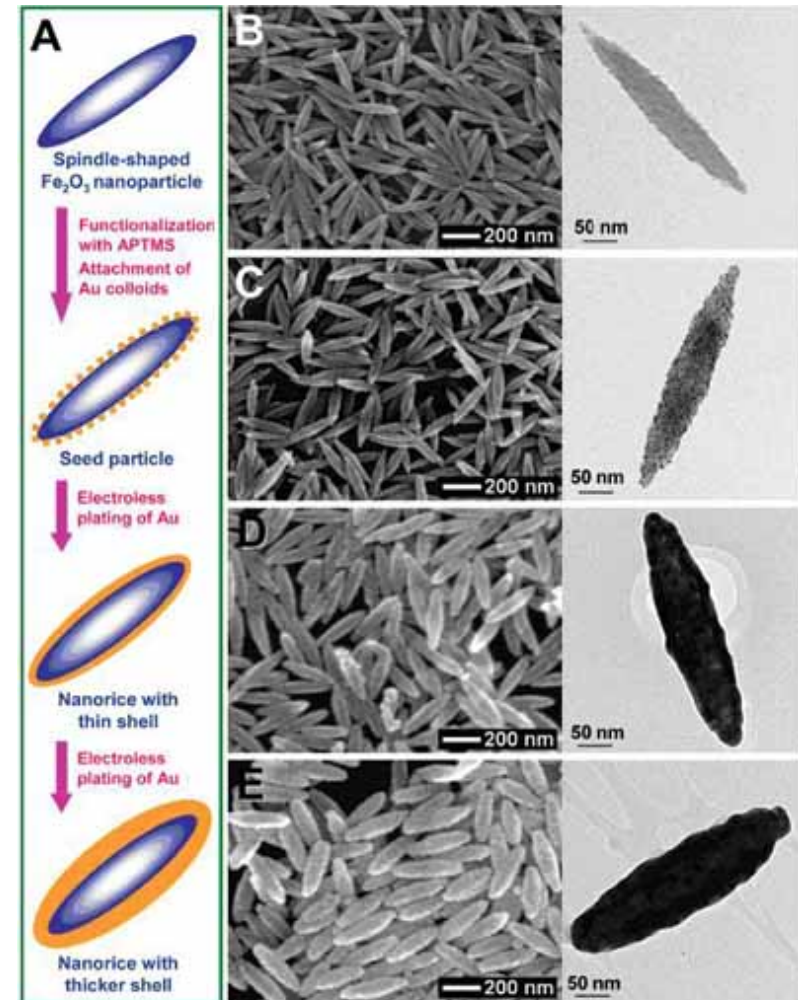
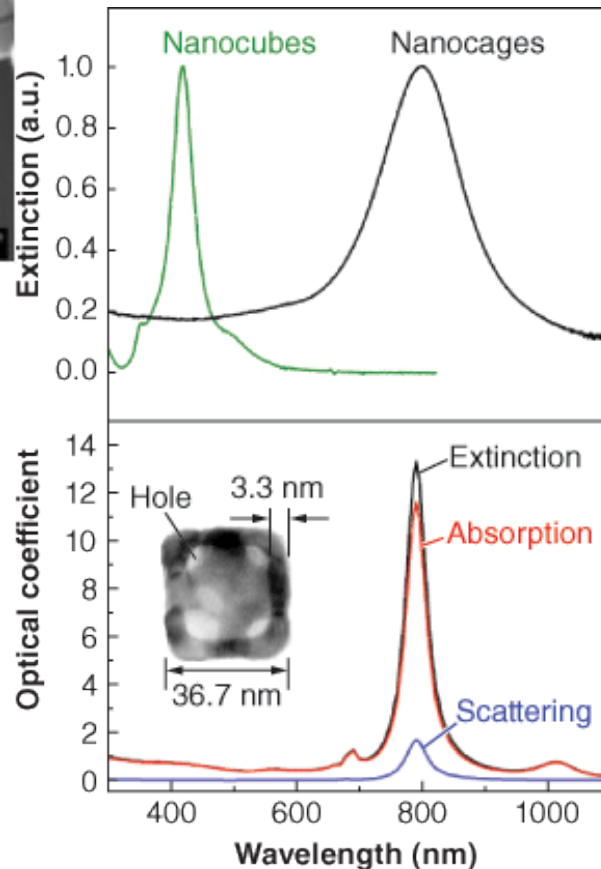
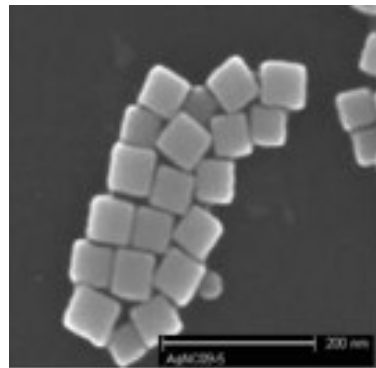


Figure 3. Transmission electron micrographs (top), optical spectra (left), and photographs (right) of aqueous solutions of Au nanorods of various aspect ratios. The seed sample has an aspect ratio of 1. Samples a, b, c, d, and e have aspect ratios of 1.35 ± 0.32 , 1.95 ± 0.34 , 3.06 ± 0.28 , 3.50 ± 0.29 , and 4.42 ± 0.23 , respectively. Scale bars: 500 nm for a and b, 100 nm for c–e. Reprinted with permission from ref 16. Copyright 2005 American Chemical Society.

Nanocube and Nanorice



The graphic above depicts various magnitudes of nanorice, which is a rice-shaped nanoparticle with a non-conducting core made of iron oxide and covered by a metallic shell made of gold. Scientists plan to attach the nanorice to scanning probe microscopes to obtain very clear image quality that surpasses today's technology. For the Air Force, this technology could be used as a tool to develop new high-speed optoelectronic materials and to monitor chemical reactions. (Graphic provided by Prof. Naomi Halas)

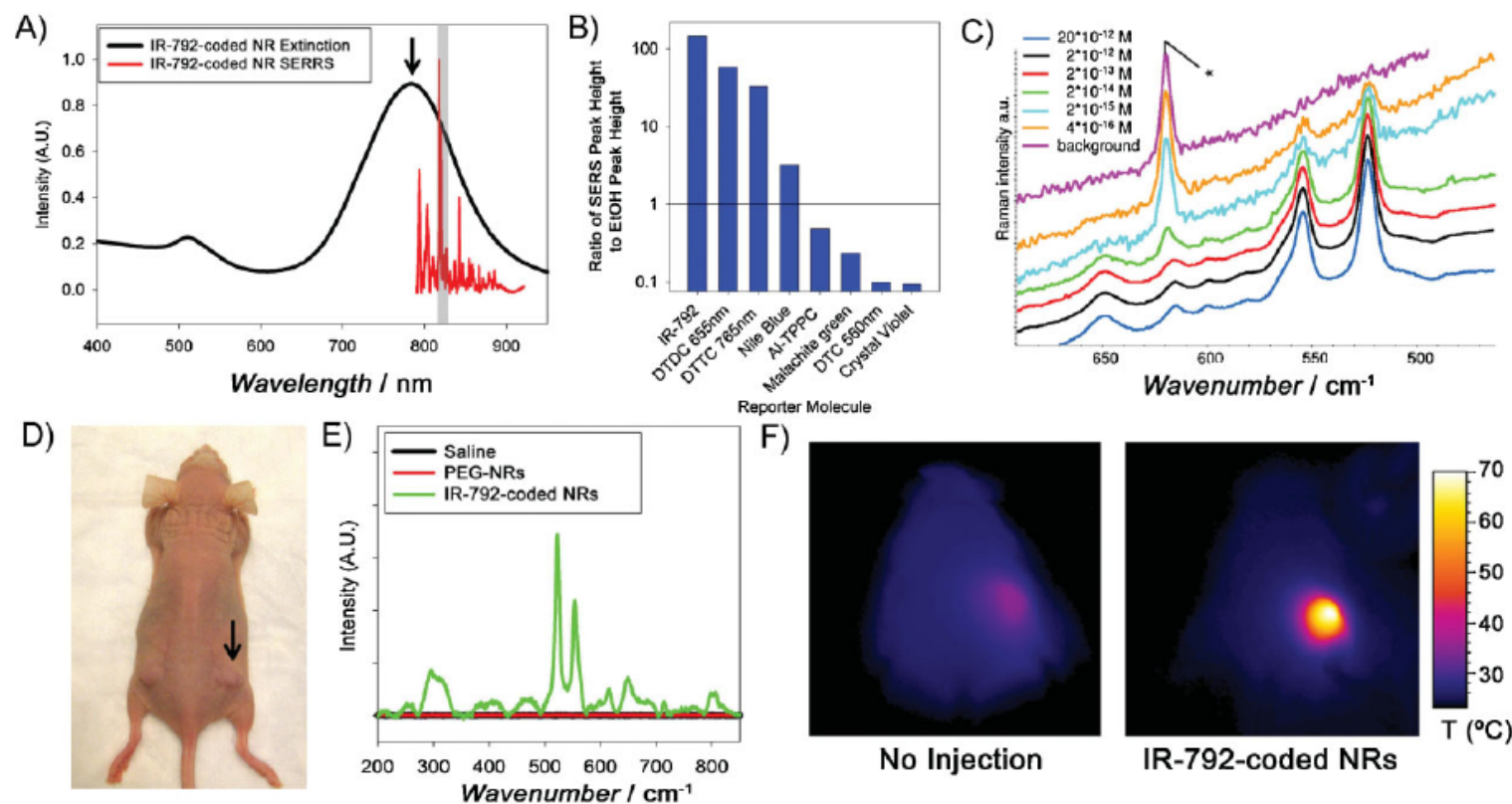

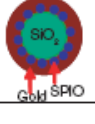

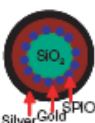








Figure 2. SERS-coded PEG-NRs for ultra-sensitive near-infrared detection and photothermal heating. A) Overlay of NIR absorption and emission of SERS-coded NRs. The arrow indicates the NIR Raman exciting-line and the gray column represents the wavelength of the diode laser source utilized for photothermal heating. B) Peak height ratios of the most intense SERS peak of each molecule with respect to the internal ethanol standard vibration at 879 cm^{-1} . C) SERS spectra of homogenous solutions of IR-792-coded NRs at various concentrations to explore the limit of detection. Spectra are displayed at full scale and offset for clarity to accommodate the intensity differences of several orders of magnitude. The relative intensity of the polystyrene multiwell plate line (*) increases with respect to the SERS spectra at low concentrations. D) Athymic (nu/nu) mice bearing bilateral human MDA-MB-435 tumors were injected intratumorally with either SERS-coded NRs, PEG-NRs, or saline (arrow) to evaluate potential for in vivo detection and photothermal heating. E) In vivo Raman spectra of IR-792-coded NRs, PEG-NRs and saline solution; 10 acquisitions of 4 s each were acquired for each spectrum. F) Infrared thermographic maps of mouse surface temperature 3 min after onset of irradiation with diode laser (810 nm , 2 W cm^2).

Table II: Summary of Gold-Shelled Magnetic Nanoparticles.

Structure	Characteristics	<i>In vitro</i>	<i>In vivo</i>	Ref
	Size: ~120 nm Surface: PEG and anti-HER2/neu Absorbance: 700–900 nm (broad) Magnetic: $r_2 = 251 \text{ nM}^{-1} \text{ s}^{-1}$	T_2 -weighted MRI showed darker images with nanoparticle with anti-HER2/neu. Lower laser power (20 mW) was needed to kill cells for HER2-positive cells (SKBr3) than HER2-negative cells (H520 at 60 mW).	None	8
	Size: >200 nm Surface: 3' and 5' -thiol modified DNA Absorbance: 600–900 nm (broad) Magnetic: Movement of nanoparticle with a bar of magnet	None	None	10
	Size: >200 nm Surface: None Absorbance: Can be tuned from visible to near infrared Magnetic: Reversible hysteresis loop and movement of nanoparticle with a bar of magnet.	None	None	11
	Size: ~170 nm Surface: None Absorbance: ~480–1000 nm (broad) Magnetic: Reversible hysteresis loop. Irradiation with 808 nm laser had temperature increase with increasing nanoparticle concentration.	None	None	12
	Size: $273 \pm 17.9 \text{ nm}$ Surface: None Absorbance: 600–900 nm (broad) Magnetic: Reversible hysteresis loop and movement of sample with a bar of magnet	None	None	14
	Size: Longitudinal = $340 \pm 20 \text{ nm}$; transverse = $54 \pm 4 \text{ nm}$ Surface: None Absorbance: 860 nm and 1160	None	None	13
	Size: $82.2 \pm 9.7 \text{ nm}$ Surface: Poly(ethylene glycol) (PEG) Absorbance: 600–900 nm (broad) Magnetic: Reversible hysteresis loop and movement of nanoparticles with a bar of magnet	None	None	17
	Size: ~80 nm Shape: Spherical Surface: PEG Absorbance: 600–900 nm (broad) Magnetic: $r_2 = 369 \text{ nM}^{-1} \text{ s}^{-1}$	Darkening of agar embedded with nanoparticle. Photothermal ablation using 808 nm laser showed increase in temperature of 40°C . Temperature increase is linearly related to laser power and nanoparticle concentration.	Darkening of the tumor in mice after injection of nanoparticle in T_2 -weighted MRI and increase in temperature of $\sim 60^\circ\text{C}$ in MRTI.	29
	Size: $30.4 \pm 4.4 \text{ nm}$ Shape: Spherical Surface: C225 monoclonal antibody Absorbance: 808 nm (narrow)	Selective binding of C225-HGN was observed with A431 cells. Only the cells treated with C225-HGN and 808 nm laser died after PTT but not the controls (no laser, nontargeting nanoparticle).	More C225-HGN localized into the tumor than the nontargeting nanoparticle.	3
	Size: $43.5 \pm 2.3 \text{ nm}$ Shape: Spherical Surface: Melanocyte stimulating hormone (MSH) peptide Absorbance: 808 nm (narrow)	Selective binding of MSH-HGN was observed in B16/F10 melanoma cells. Only the cells treated with MSH-HGN and 808 nm laser died after photothermal ablation but not the controls (nanoparticle alone, laser alone, nontargeting nanoparticle + laser).	More MSH-HGN localized into B16/F10 tumor than the nontargeting nanoparticle. Destruction of tumors with MSH-HGN-treated tumors correlated with histology.	49

SPIO, superparamagnetic iron oxide; PTT, photothermal ablation therapy; r_2 , relaxivity measure of the ability of the material to change the relaxation time of the surrounding water protons; MRTI, magnetic resonance temperature imaging; HGN, hollow gold nanoshell. None = no available information provided in publication.



Scheme 1. Synthesis of SPIO@silica-Au nanoshells.¹⁷ Silica-coated superparamagnetic iron oxide ($\gamma\text{-Fe}_2\text{O}_3$) nanoparticles were synthesized using the Stober process. After the surface of the silica shell (white) was functionalized with 3-aminopropyltrimethoxysilane (APTMS), 2–3 nm gold nanocrystal seeds (blue) were attached to the amino groups on the silica sphere by reducing chloroauric acid (HAuCl_4) with tetraakis(hydroxymethyl) phosphonium chloride (THPC). Finally, the attached gold nanoseeds were used to nucleate the growth of a gold overlay on the silica surface to form a gold nanoshell. NH_4OH and K_2CO_3 are weak bases to keep the pH high enough for the reaction. TEOS, tetraethyl orthosilicate.

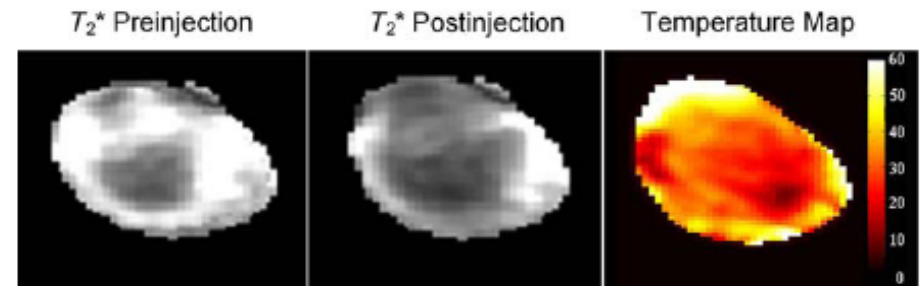


Figure 1. T_2 magnetic resonance imaging (MRI) and the magnetic resonance temperature (MRTI) map of a subcutaneous A431 tumor injected with SPIO@silica-Au nanoparticles in the tumor at a dose of 1×10^{11} particles/site. Note the darkening of the tumor in T_2 -weighted MRI after the injection of the SPIO@silica-Au and the increase in temperature by as much as 60°C , as shown in MRTI. This indicates the potential use of SPIO@silica-Au for the simultaneous use in MRI and photothermal therapy.

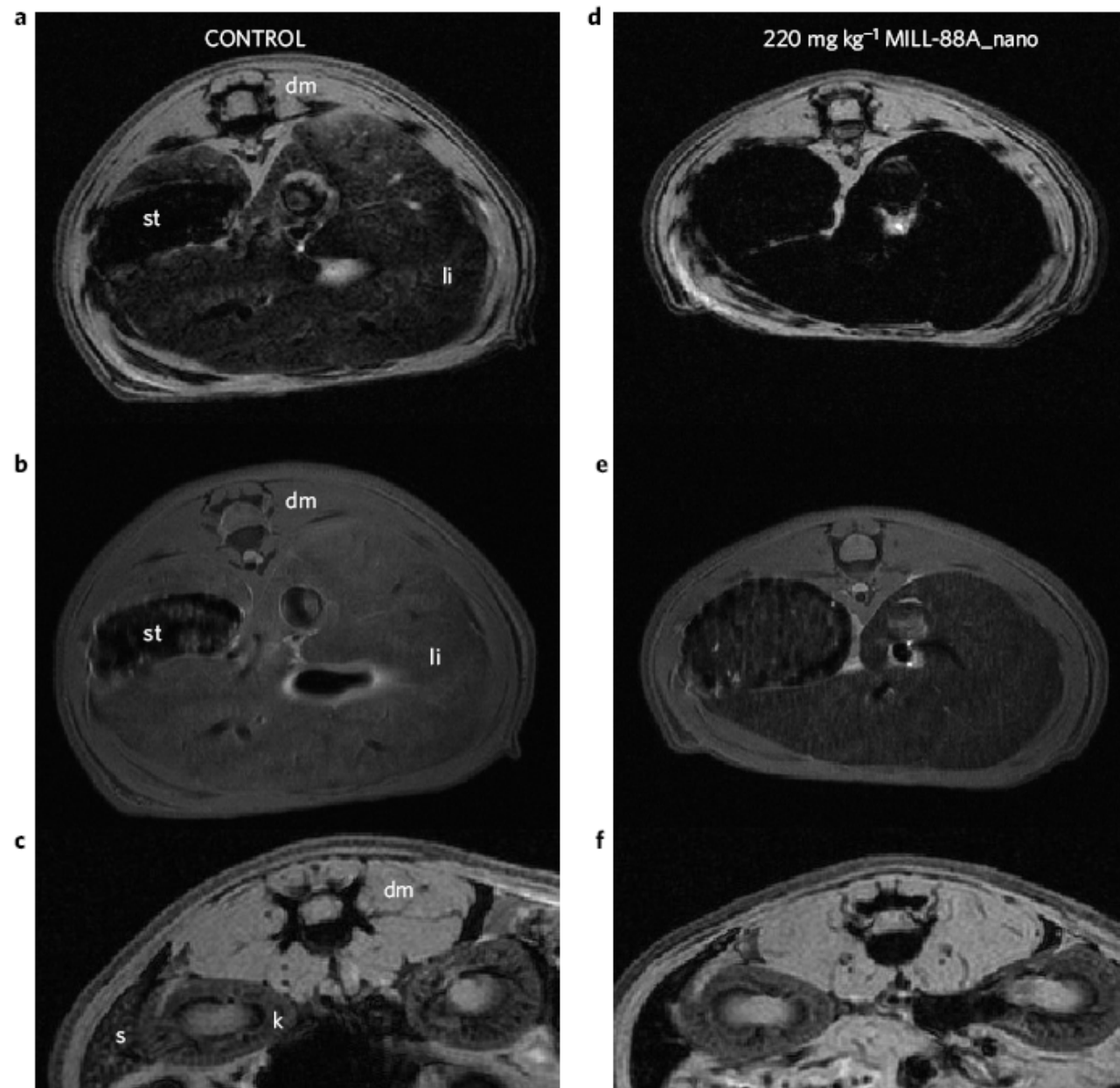
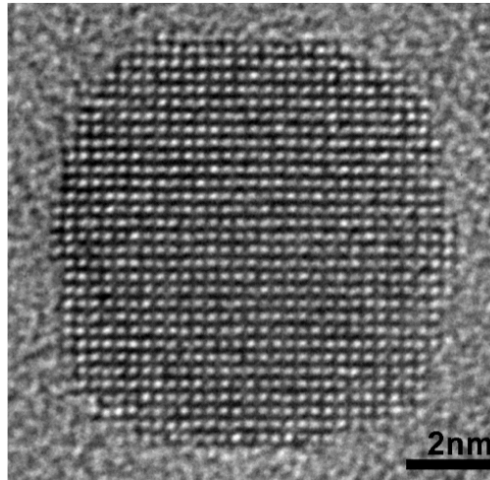
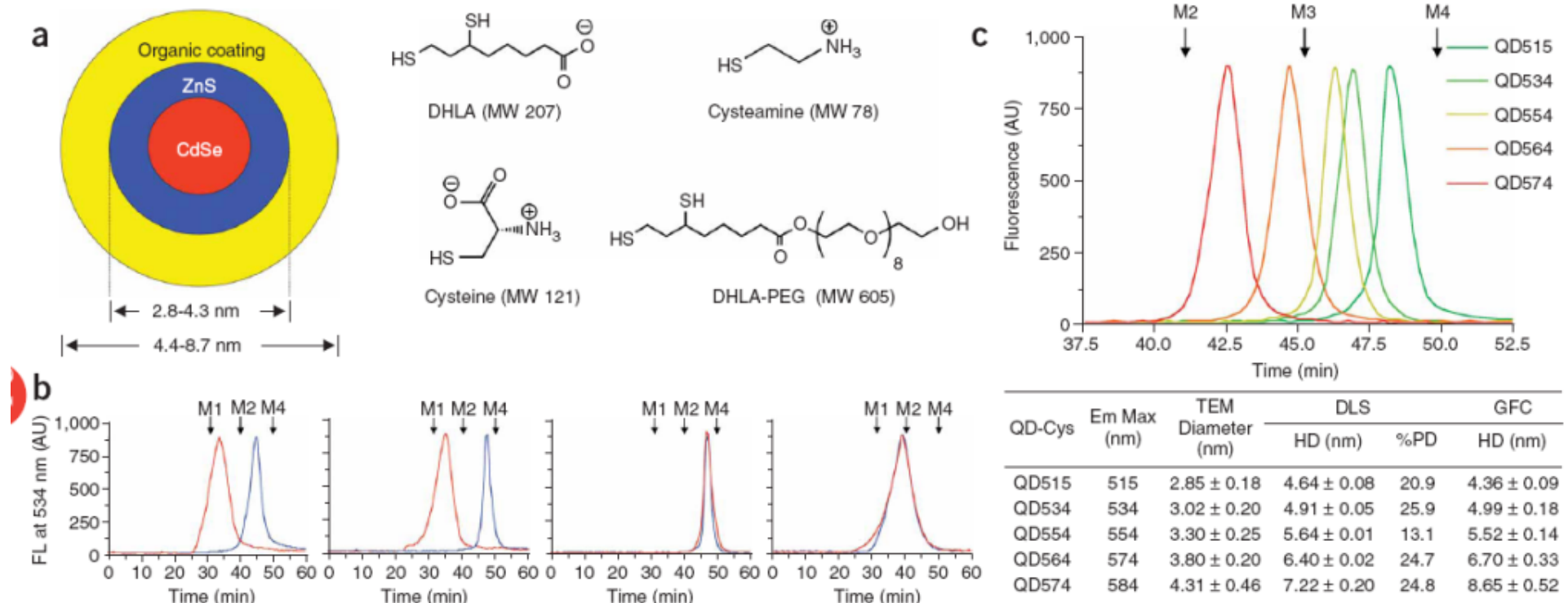


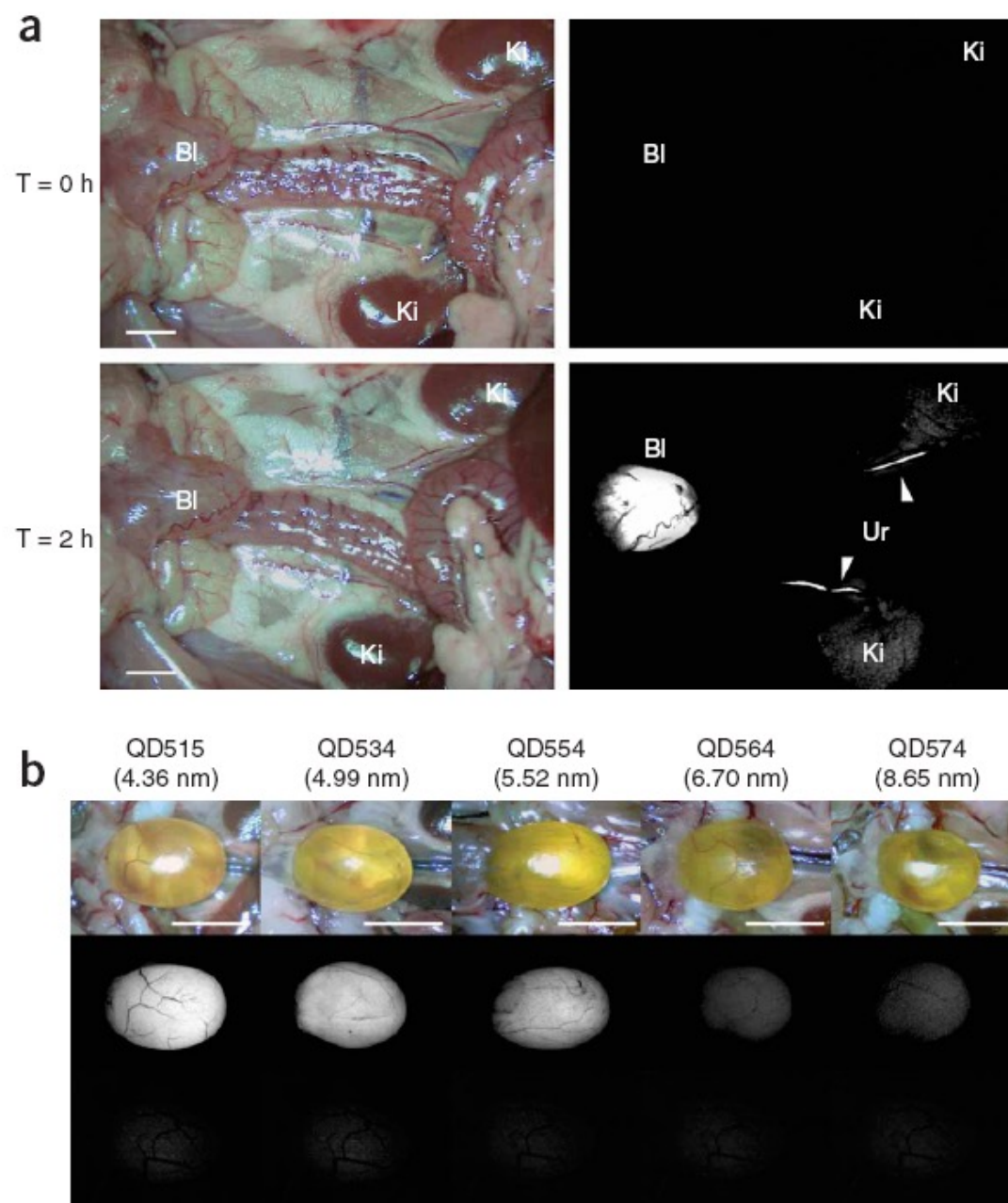
Figure 4 | Magnetic resonance images. The images were acquired with gradient echo (**a**, **c**, **d**, **f**) or spin echo (**b**, **e**) sequence of control rats (left; **a-c**) and rats injected with 220 mg kg^{-1} MIL-88A (right; **d-f**), in liver (**a**, **b**, **d**, **e**) and spleen (**c**, **f**) regions. 30 min after injection, product effect is observable on the liver and spleen. (dm, dorsal muscle; k, kidney; li, liver; s, spleen; st, stomach.)

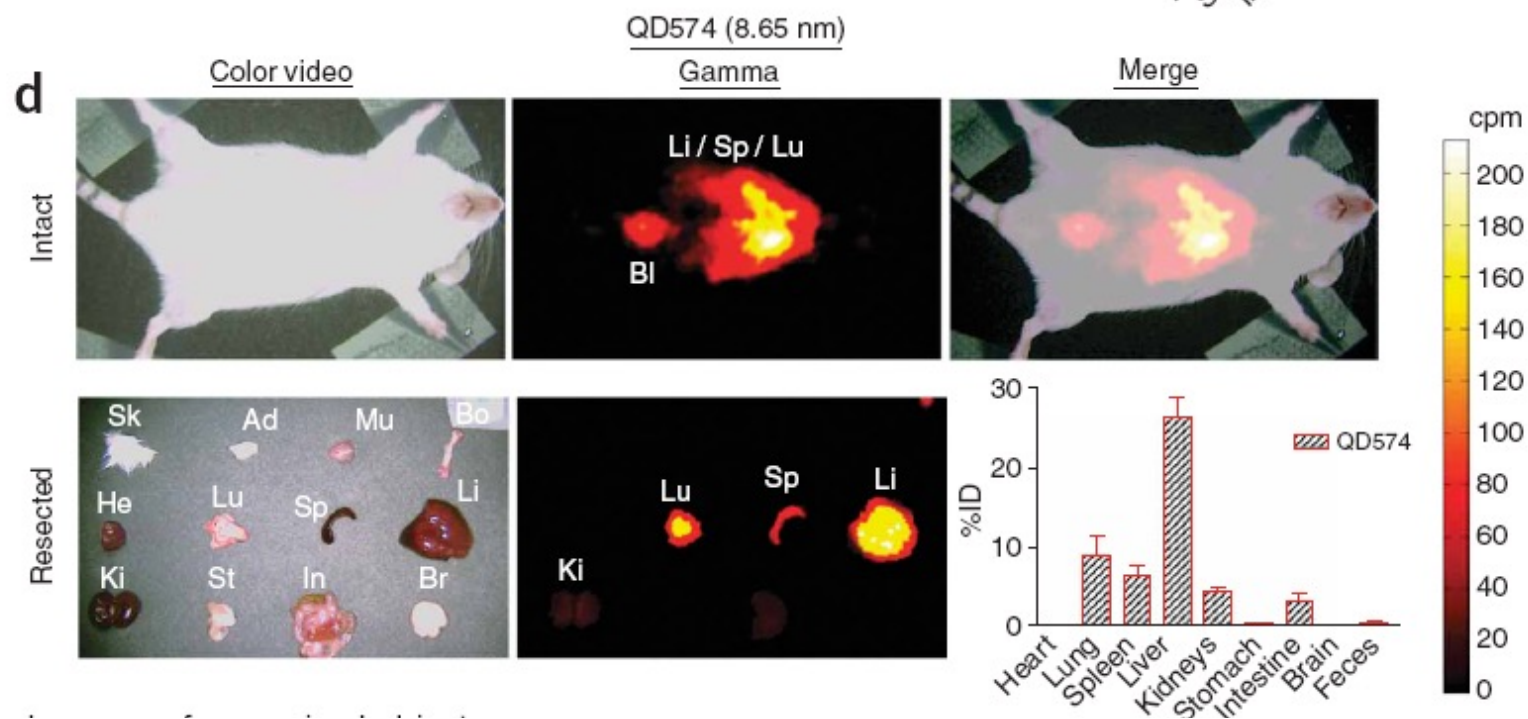
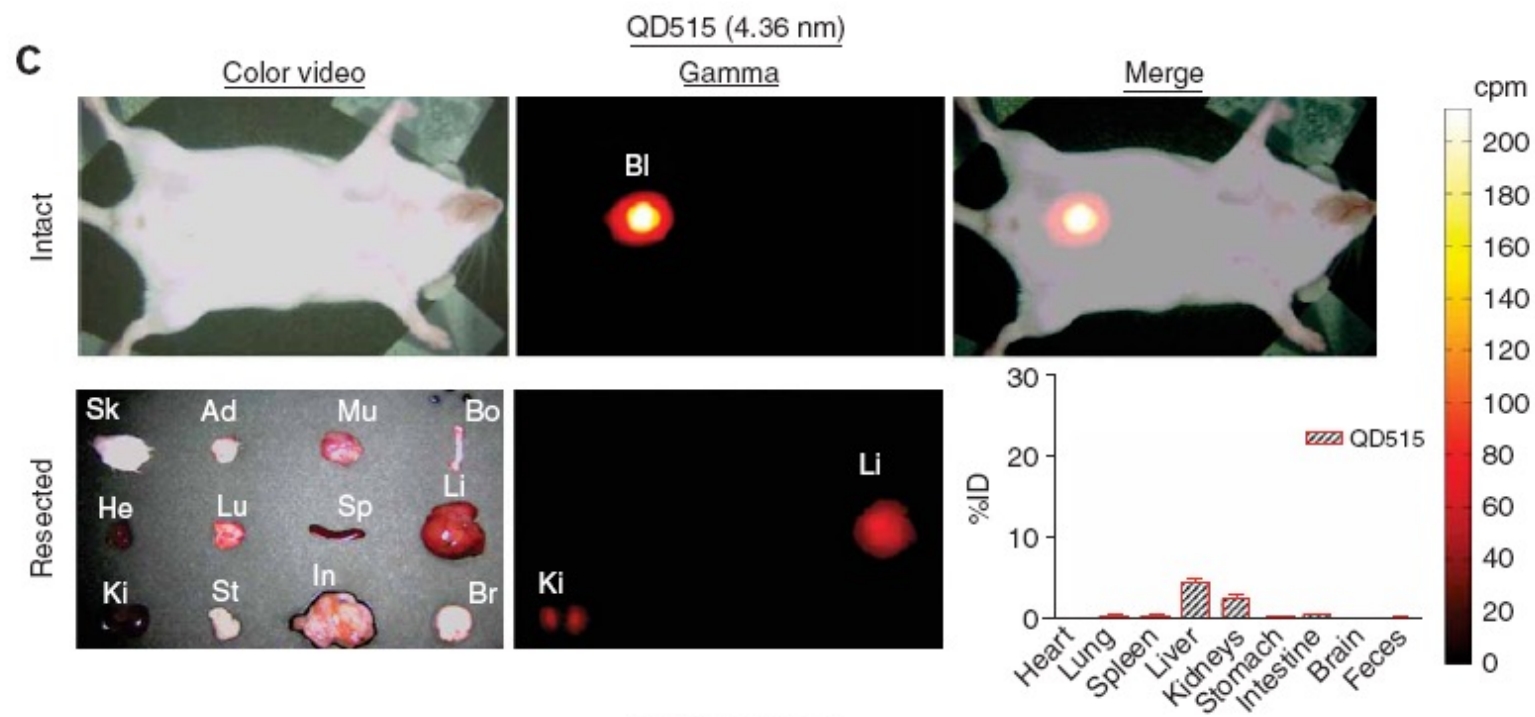
Quantum Dots



Renal clearance of quantum dots







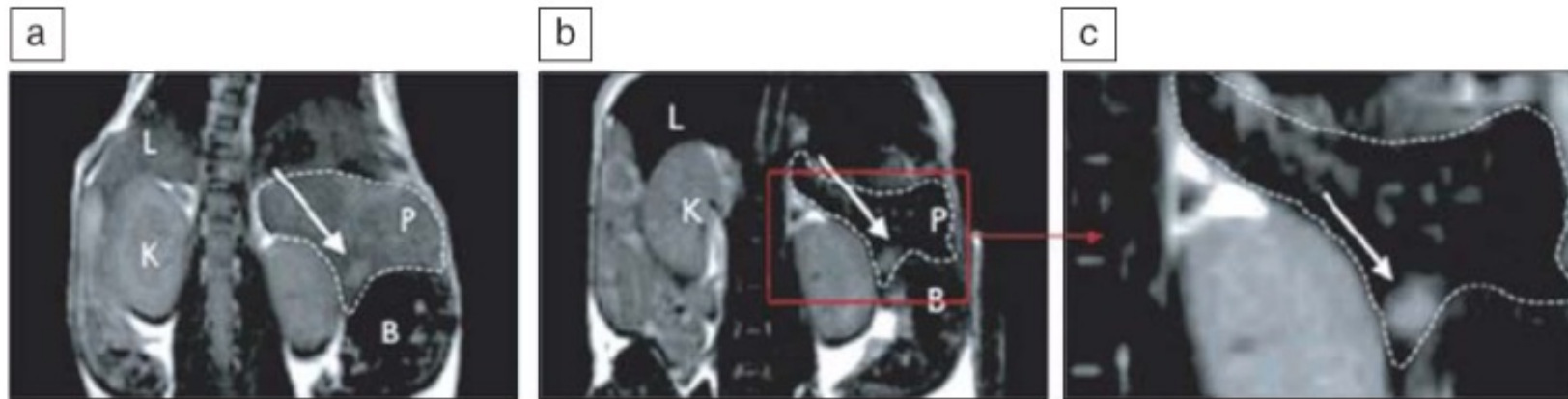


Figure 1. Cross-linked iron oxide (CLIO) nanoparticles for T_2 -weighted images of rodent pancreatic cancer: (a) preinjection of CLIO, (b) postinjection of CLIO, and (c) higher magnification of postinjection image with the arrow indicating tumor. L, liver; P, pancreas; K, kidney; B, bowel.¹⁶

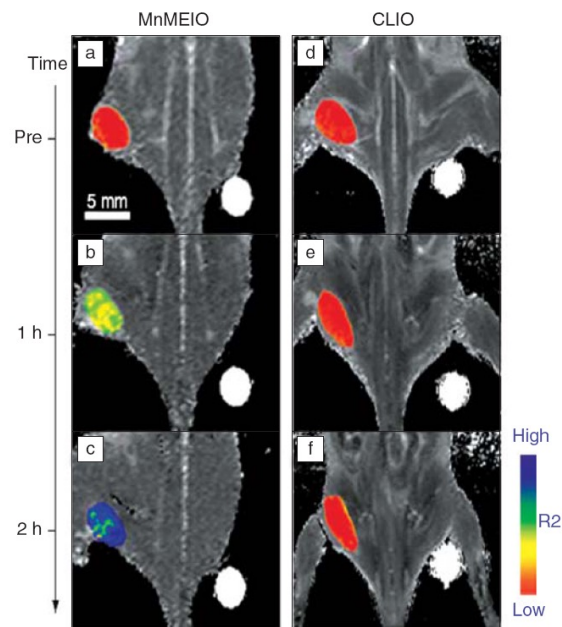
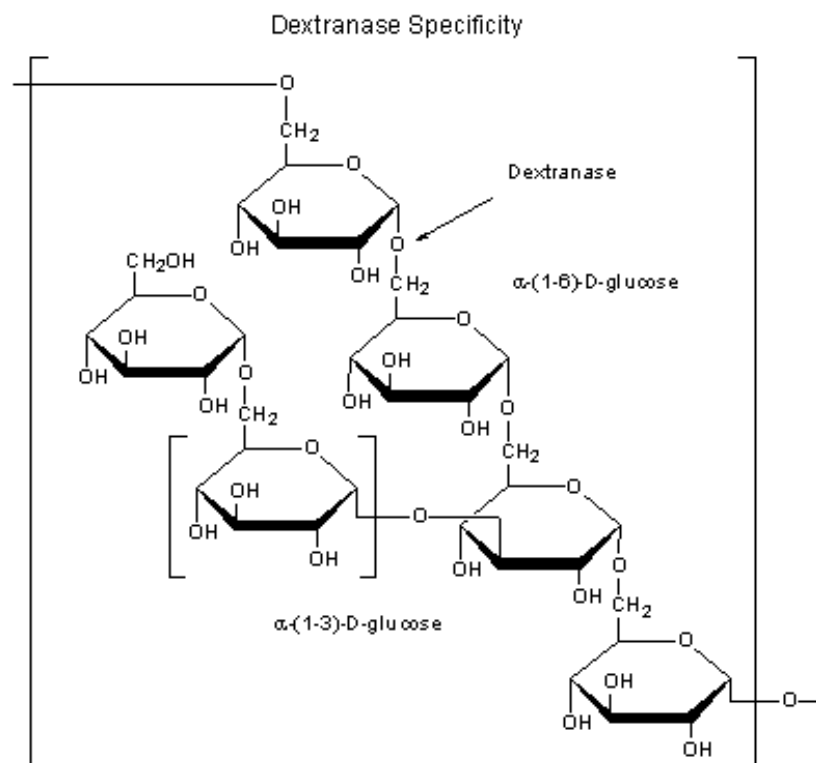
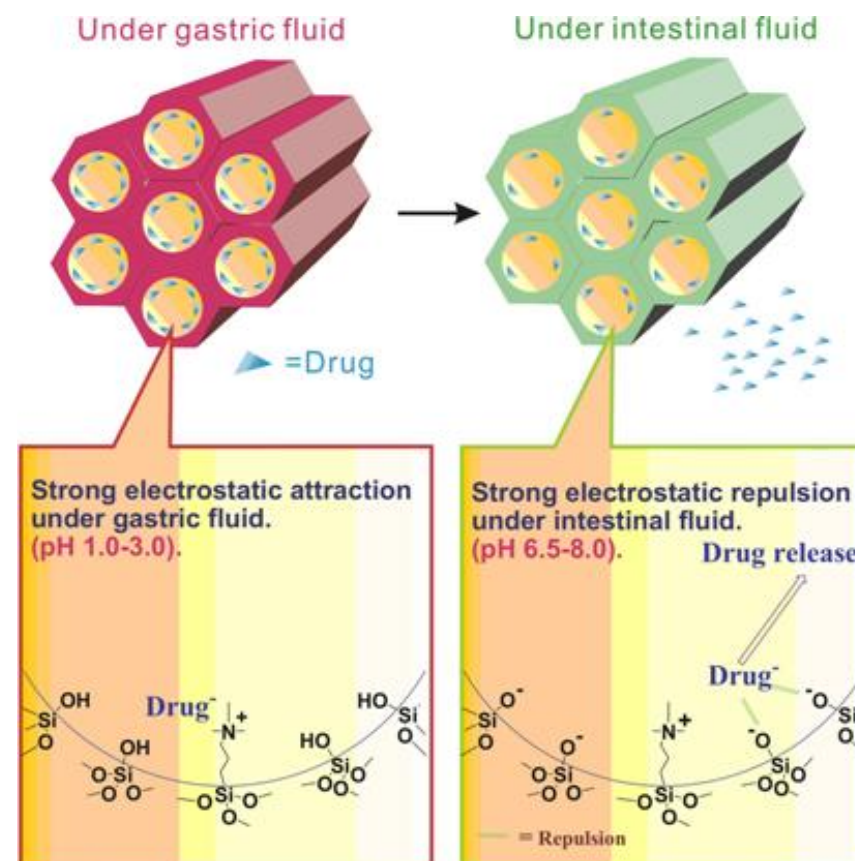
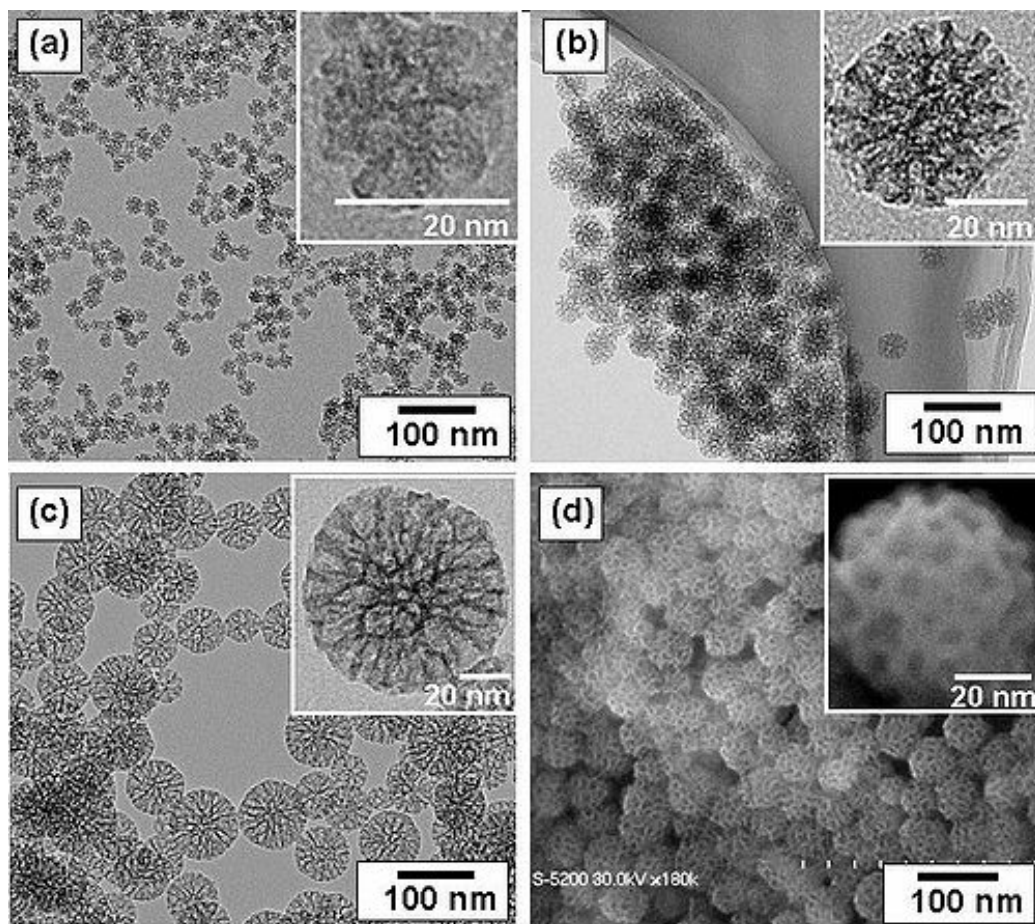
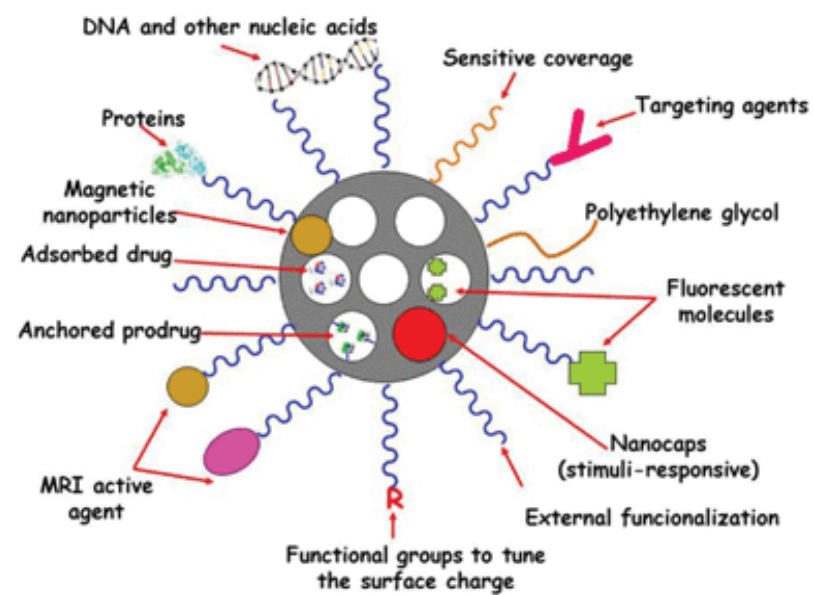
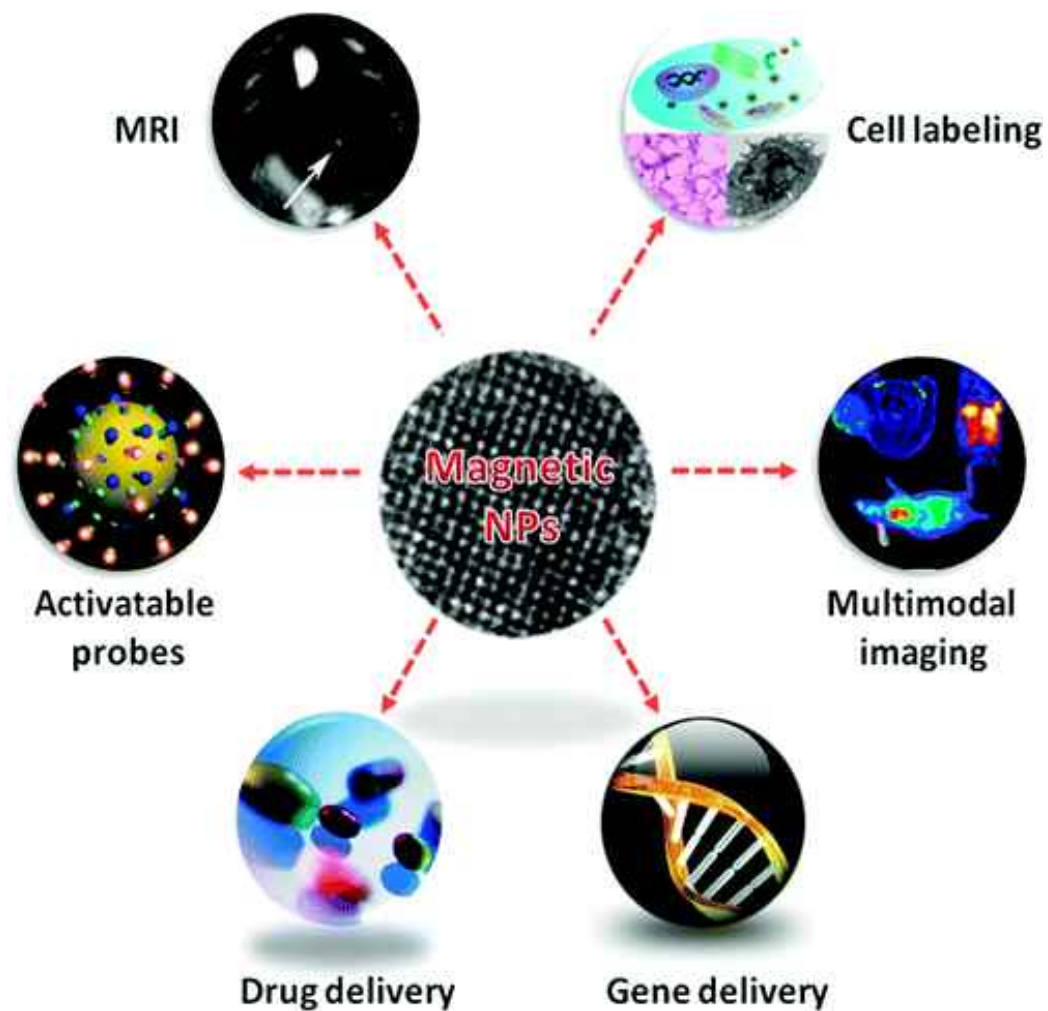


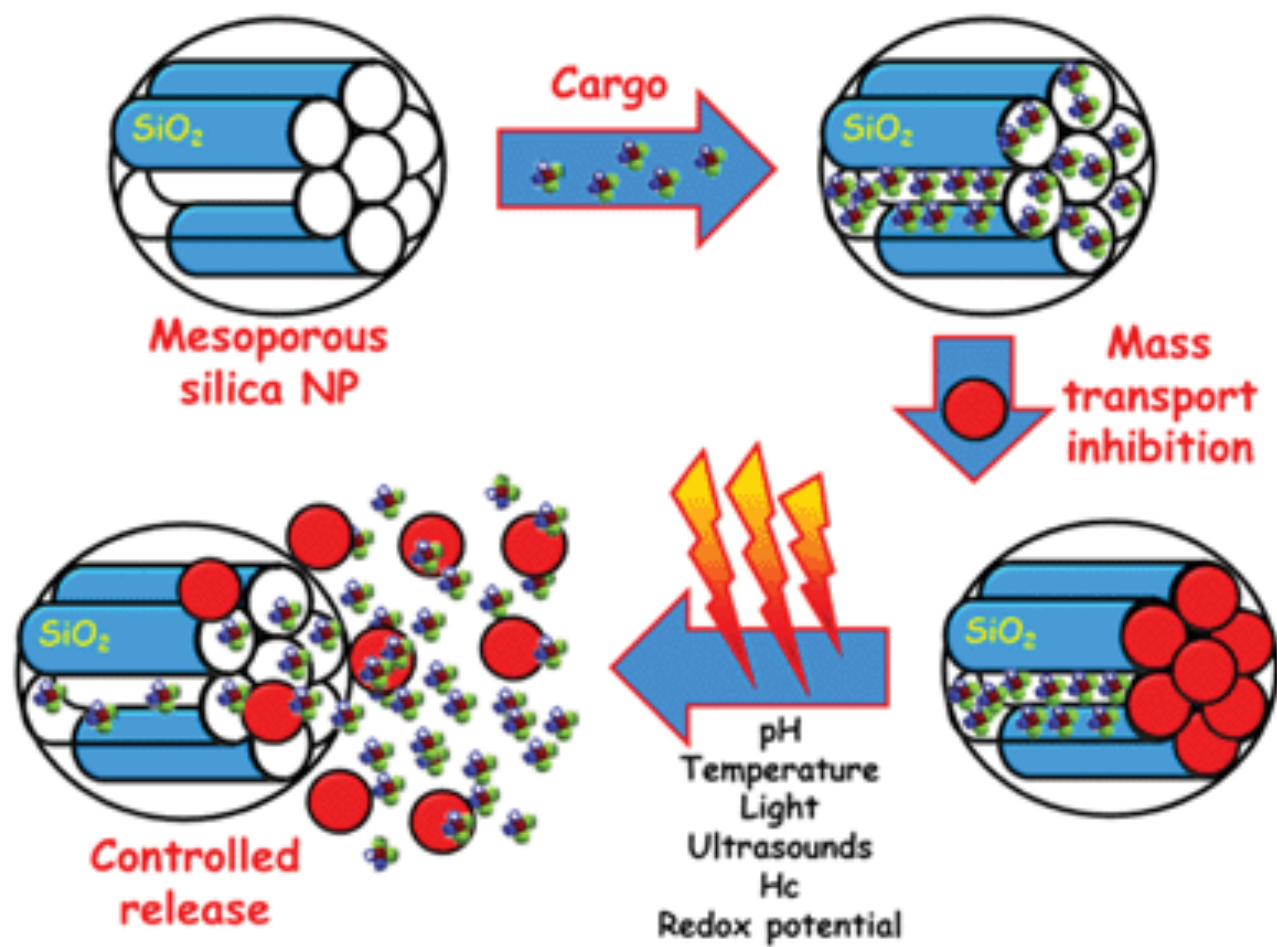
Figure 2. *In vivo* magnetic resonance detection of cancer after administration of magnetic nanoparticles Herceptin conjugates. MnFe_2O_4 nanoparticles (MnMEIO) (a–c) show higher signal enhancement than cross-linked iron oxide (CLIO) (d–f).²⁴ R2, inverse of transverse relaxation time.



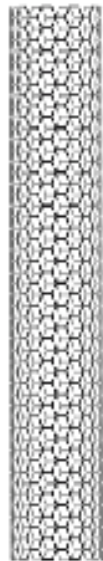
Mesoporous Silica







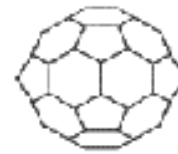
Carbon



SWNT



Poly-C₆₀

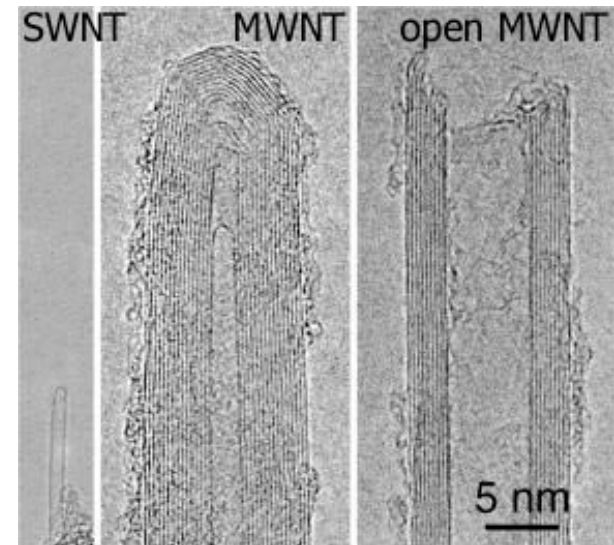
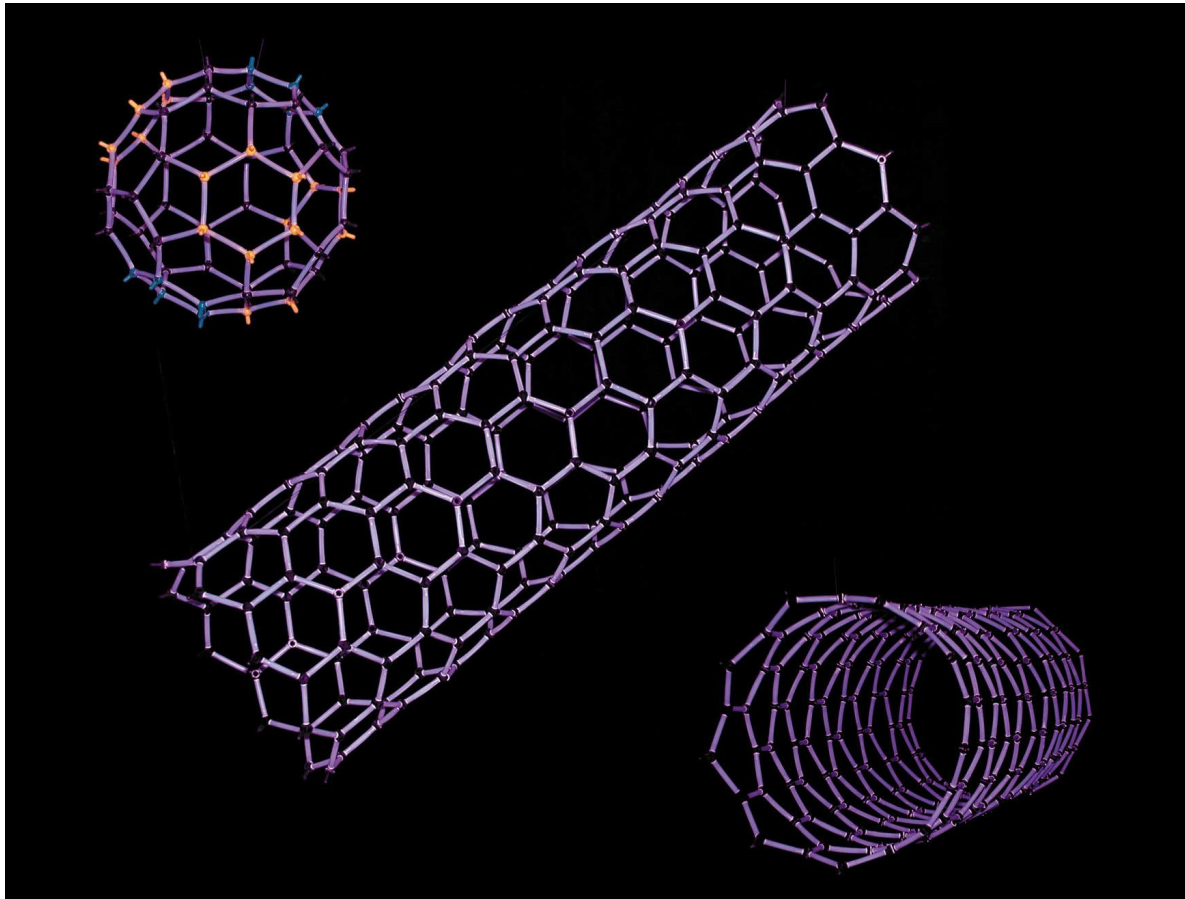


C₆₀



Nanodiamond
~ 2-10 nm

Carbon Nanotubes



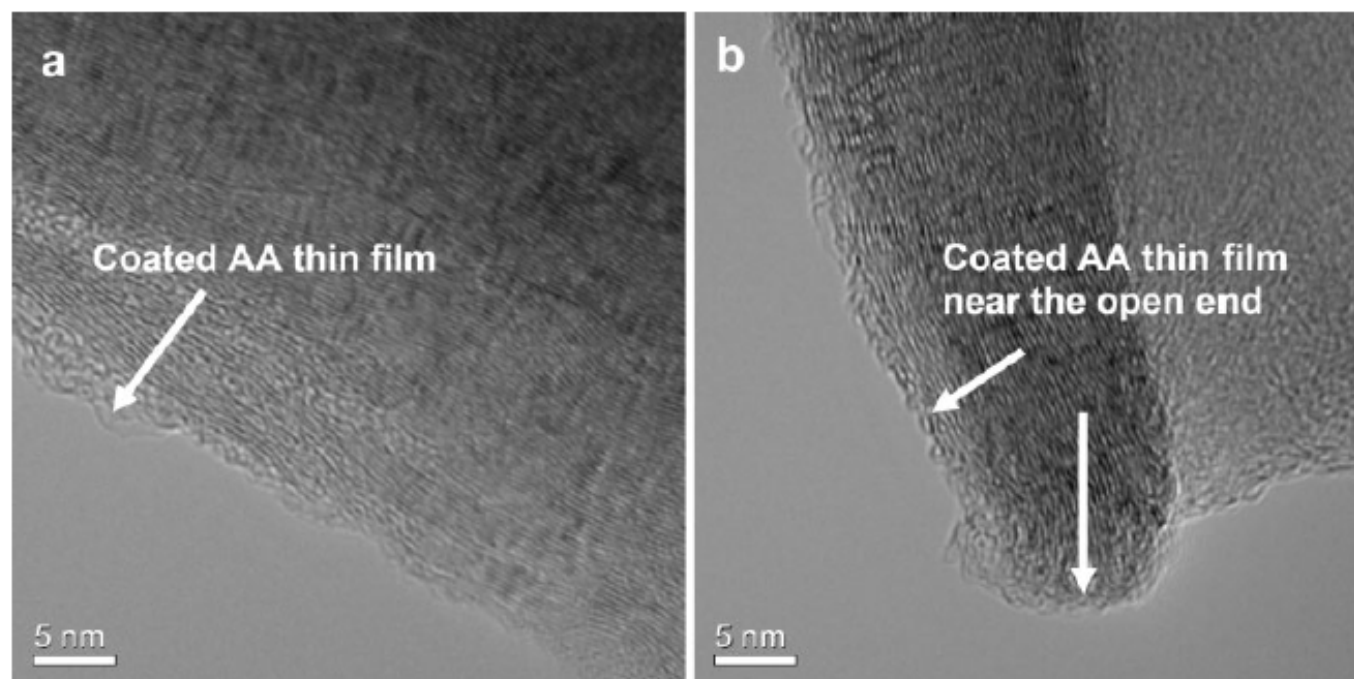
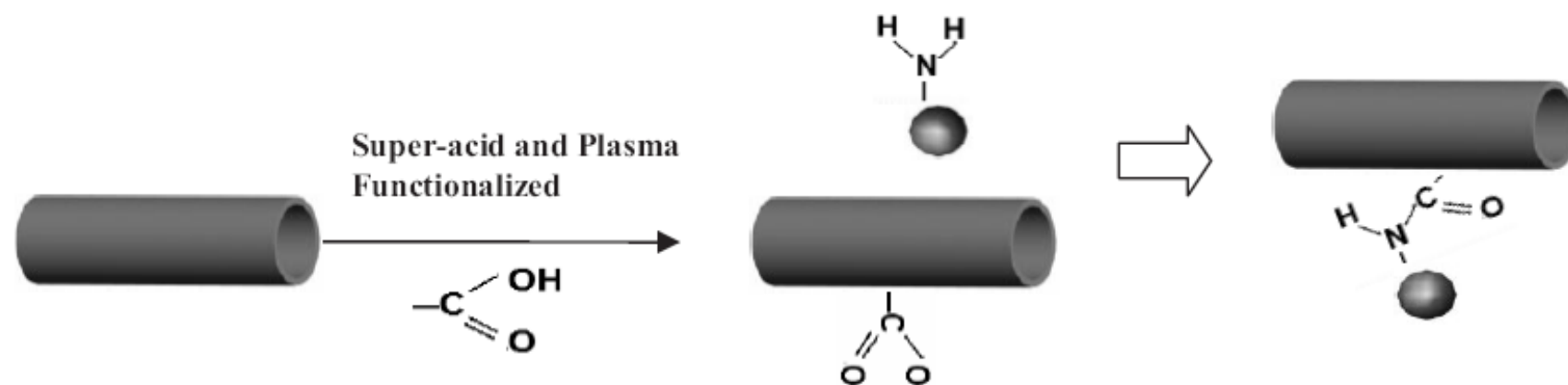


Figure 2. TEM images showing a) the plasma deposited acrylic acid (AA) polymer thin film on the carbon nanotube, the lattice image of carbon nanotube can be clearly seen with an extremely thin layer of polymer film (~ 2 nm); b) the thin film of AA was plasma deposited near the open end of the carbon nanotube.

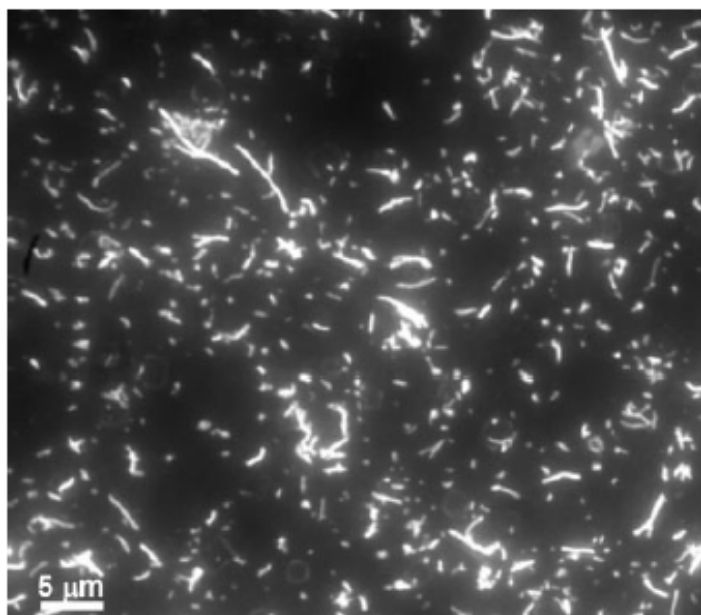
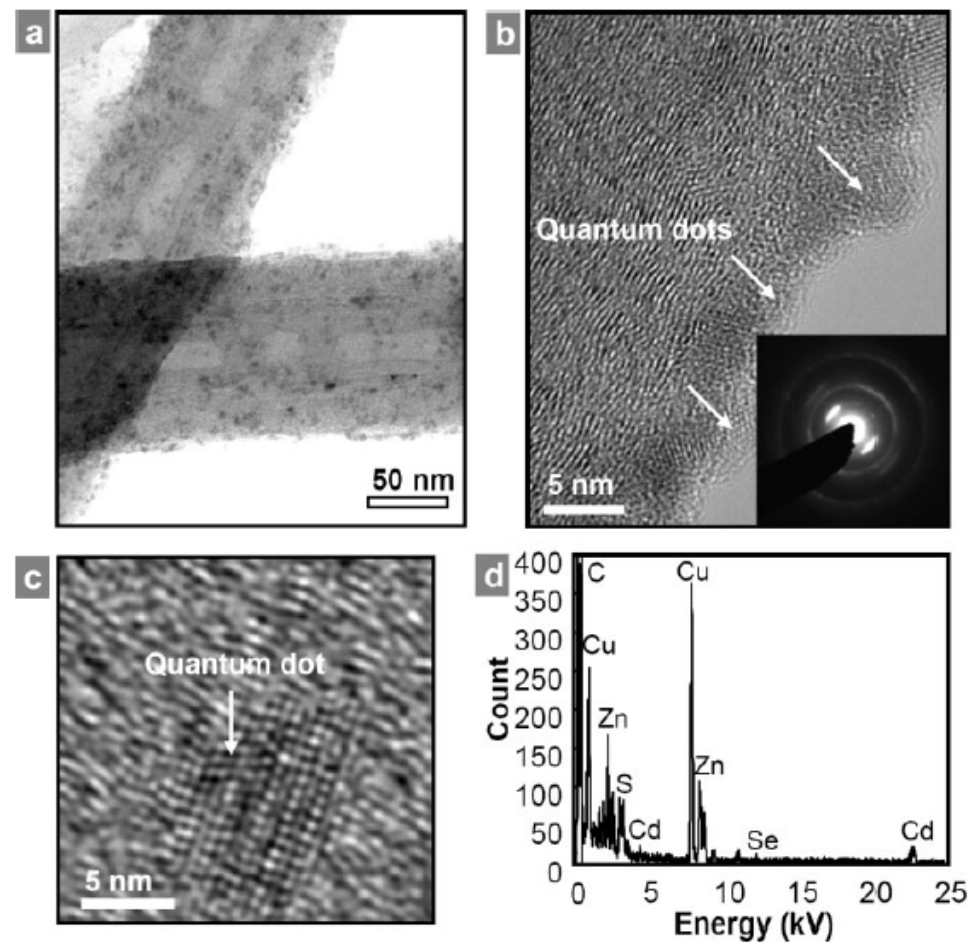
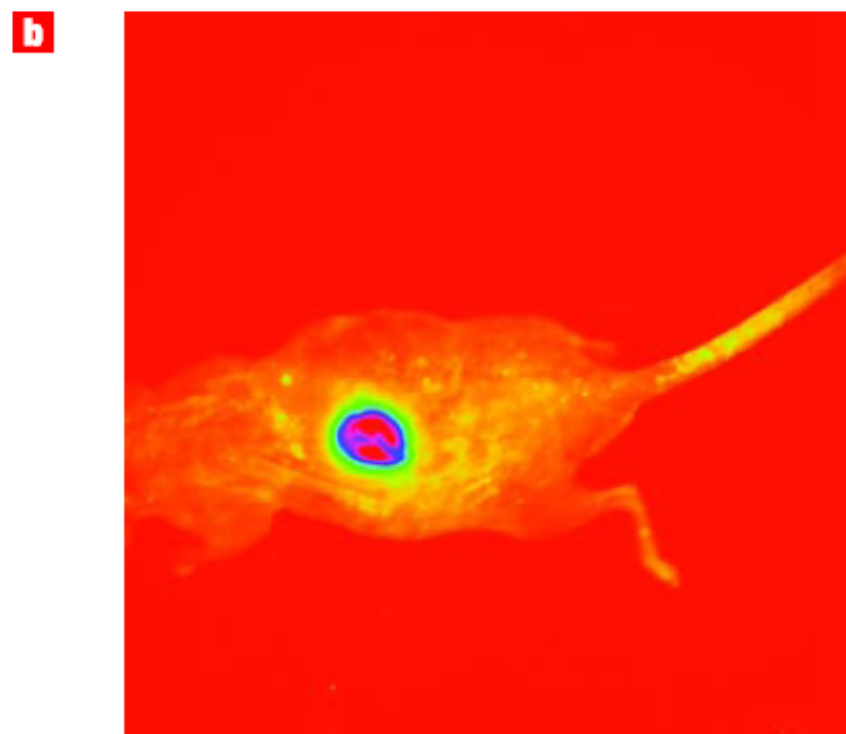
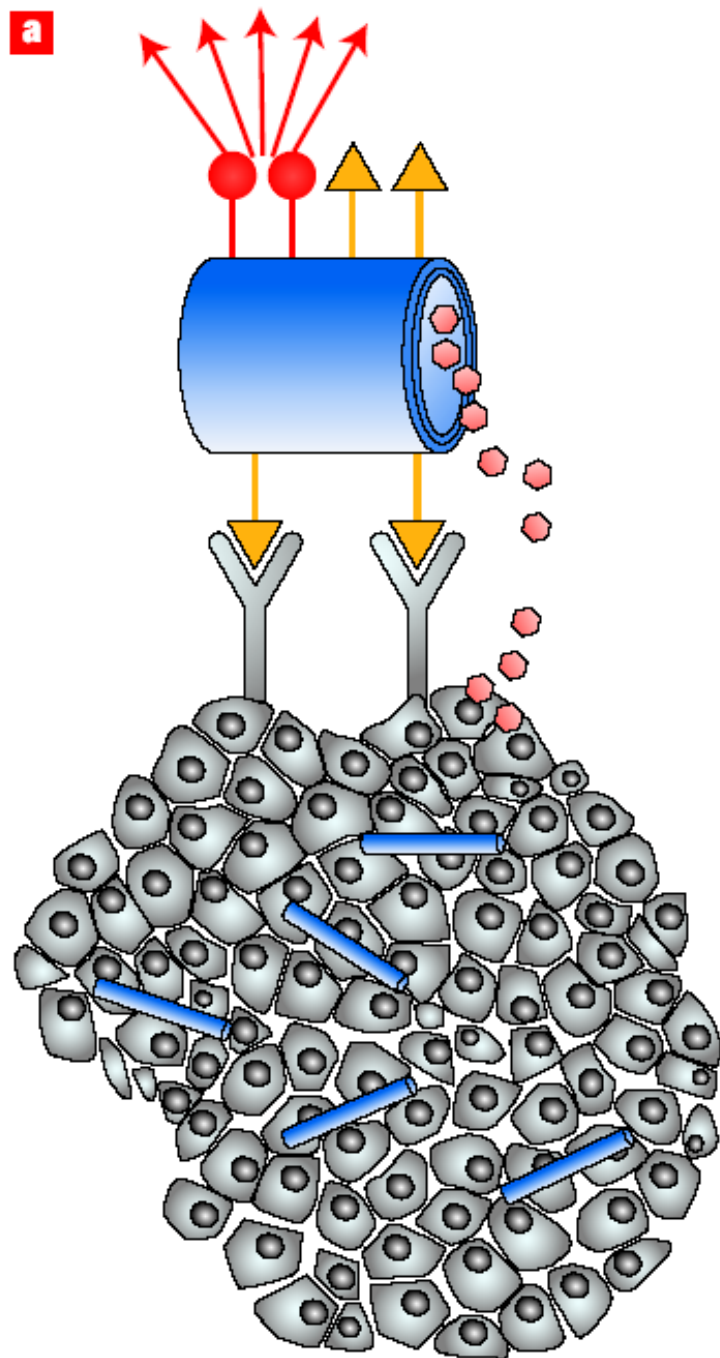


Figure 3. Fluorescent microscopy image (Olympus 350 nm excitation) showing that the MWCNTs are in with fluorescent QDs and exhibiting strong emissions background.





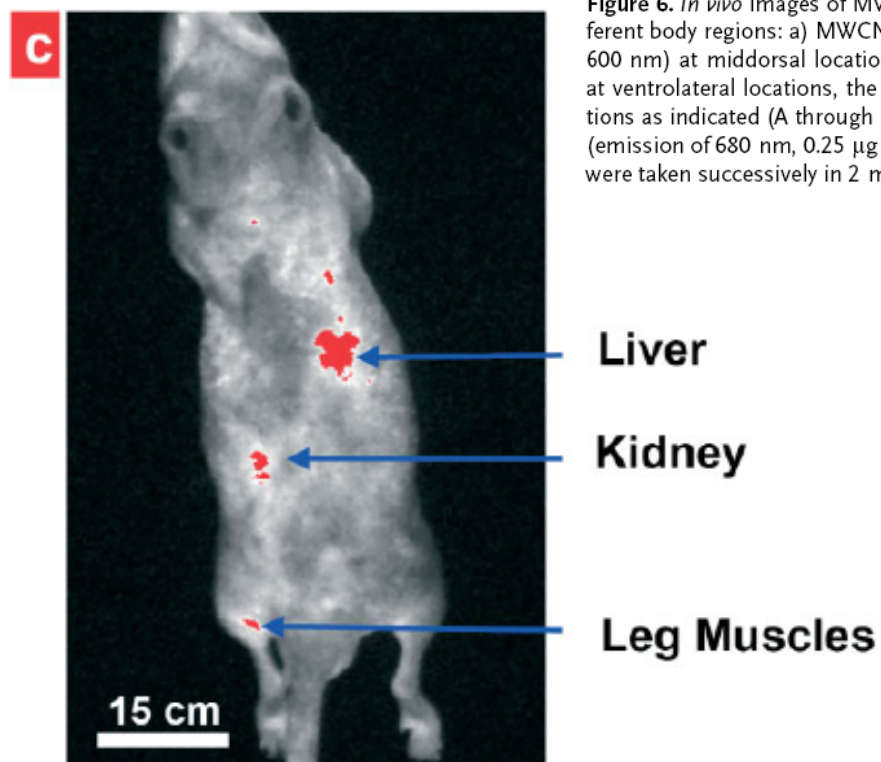
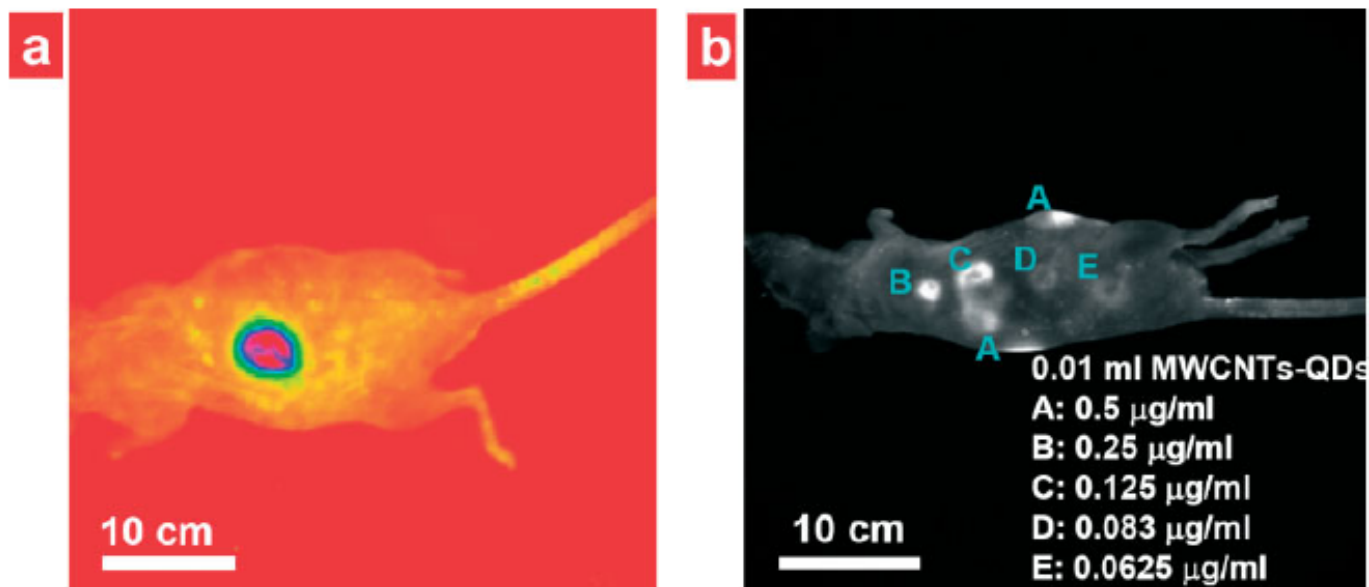
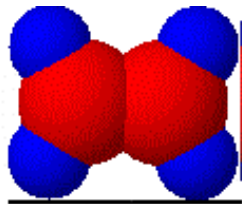
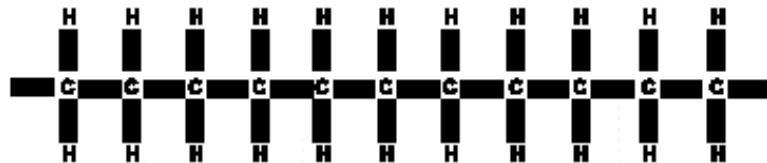
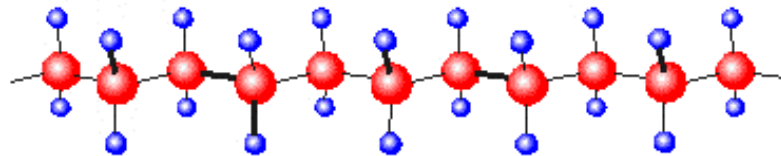
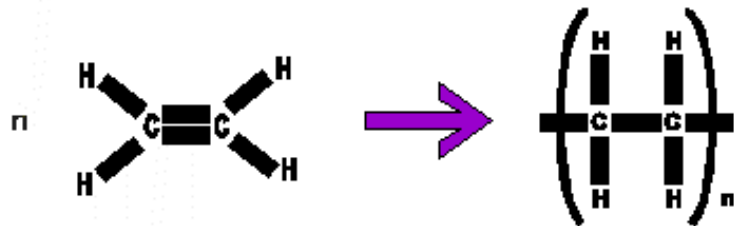
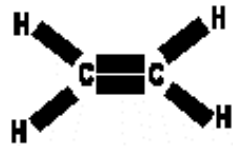


Figure 6. *In vivo* images of MWCNTs-QDs ($0.5 \mu\text{g ml}^{-1}$ in PBS) in mice injected at different body regions: a) MWCNTs attached with CdSe/ZnS quantum dots (emission of 600 nm) at middorsal location; b) MWCNTs attached with CdSe/ZnS quantum dots at ventrolateral locations, the suspensions were diluted by PBS at various concentrations as indicated (A through E); c) MWCNTs attached with InGaP/ZnS quantum dots (emission of 680 nm, $0.25 \mu\text{g ml}^{-1}$ in PBS) in liver, kidney, and leg muscles. All images were taken successively in 2 min under epi-UV illuminator with excitation of 435 nm.

Polymer

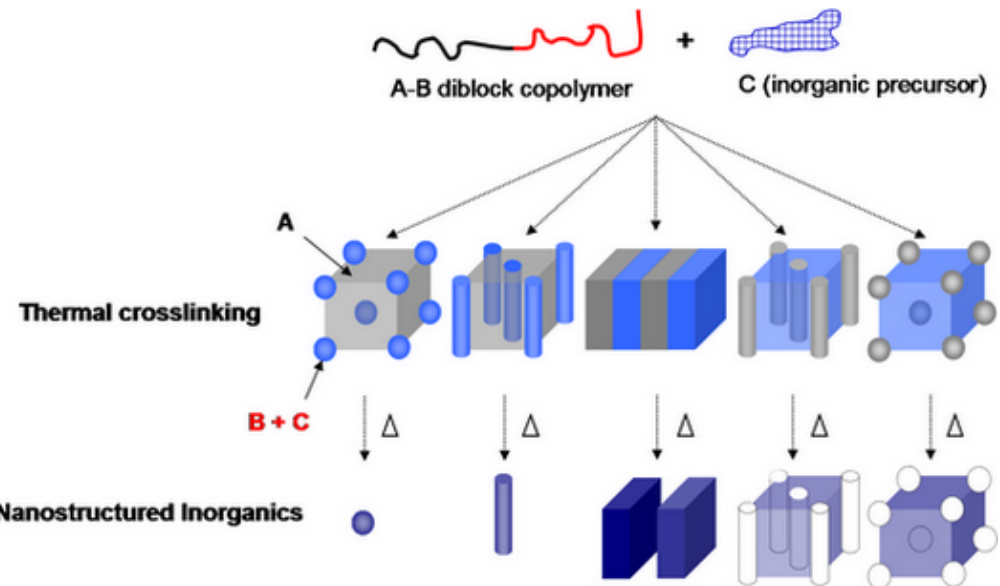


a monomer ethene



a polymer

poly(ethene)



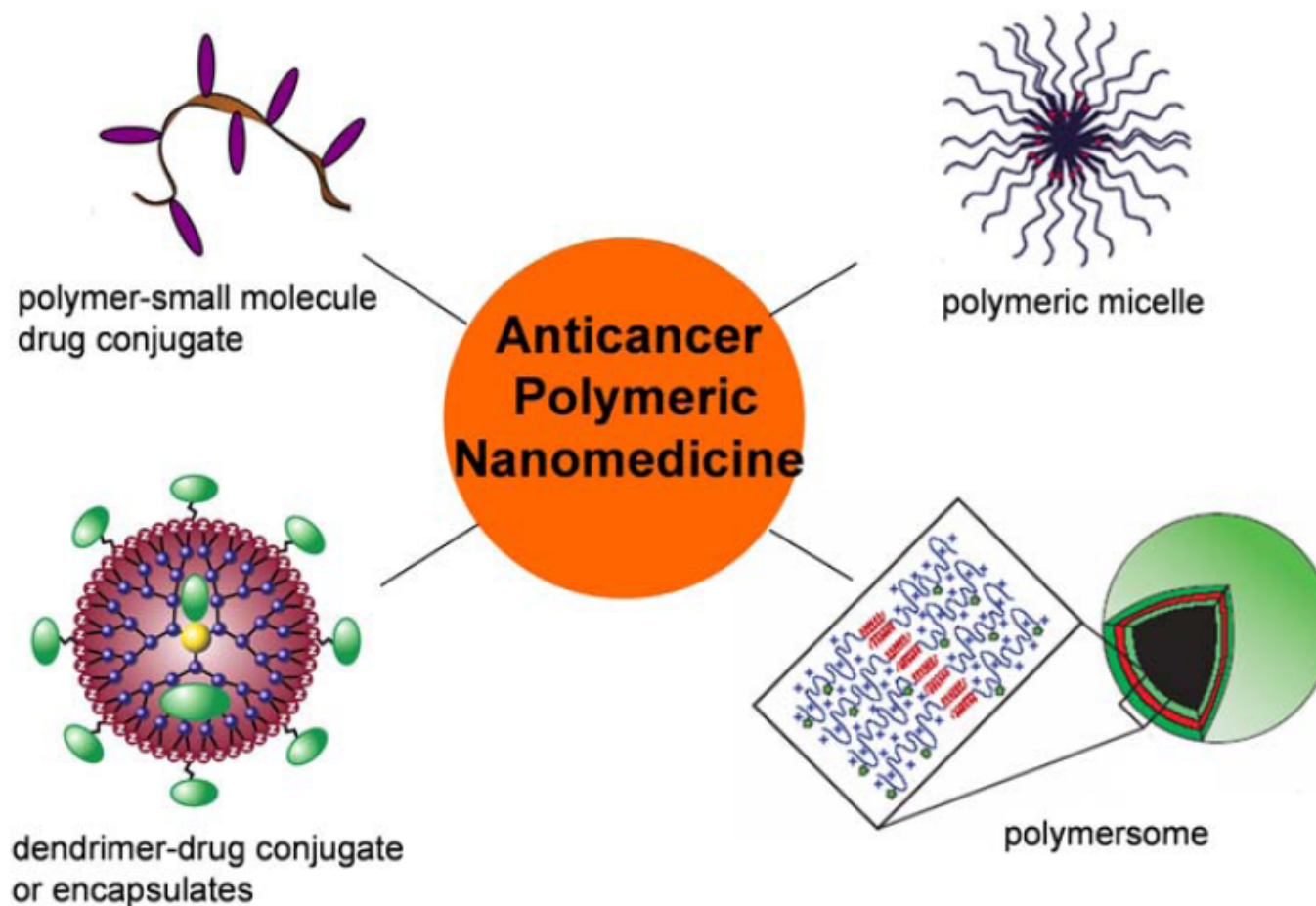


Figure 1. Illustration of various anticancer polymeric nanomedicines that have been developed and are used in cancer drug delivery. Polymer-small molecule drug conjugates are usually hydrophilic (water-soluble) polymers with covalently bound, releasable hydrophobic drug molecules. Polymeric micelles are core-shell micellar nanostructures with a hydrophobic core that can be used for the encapsulation of hydrophobic drug molecules and for the controlled release of hydrophobic therapeutics, and a hydrophilic shell can be used for micelle surface modification (e.g., incorporation of targeting ligands). Polymersomes are a class of hollow spherical nanostructures that enclose a solution and can be used to deliver hydrophilic therapeutics such as DNA and proteins. Dendrimer drug conjugate or encapsulates are a class of drug delivery systems with drugs conjugated to the periphery or encapsulated inside of monodisperse macromolecules with highly branched, symmetric, three-dimensional architectures.

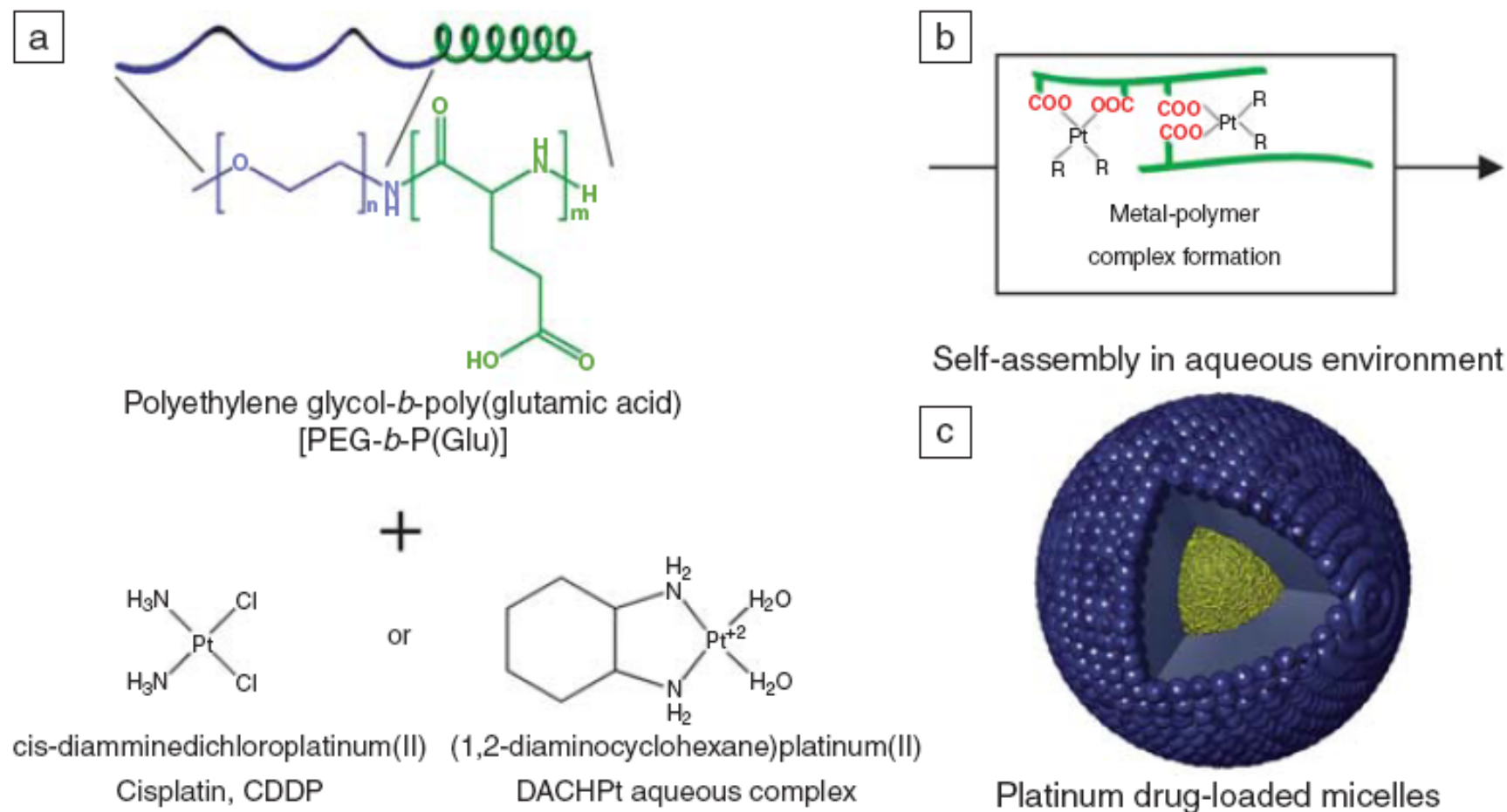


Figure 2. (a) Schematic diagram of proposed self-assembly of platinum drug-loaded polymeric micelles.^{101,102} (b) The self-assembly is mediated by the coordination of the platinum (II) and the carboxylate groups (COO) of the poly(glutamic acid) segments. (c) Narrowly distributed polymeric micelles with dense drug-loaded cores are formed.

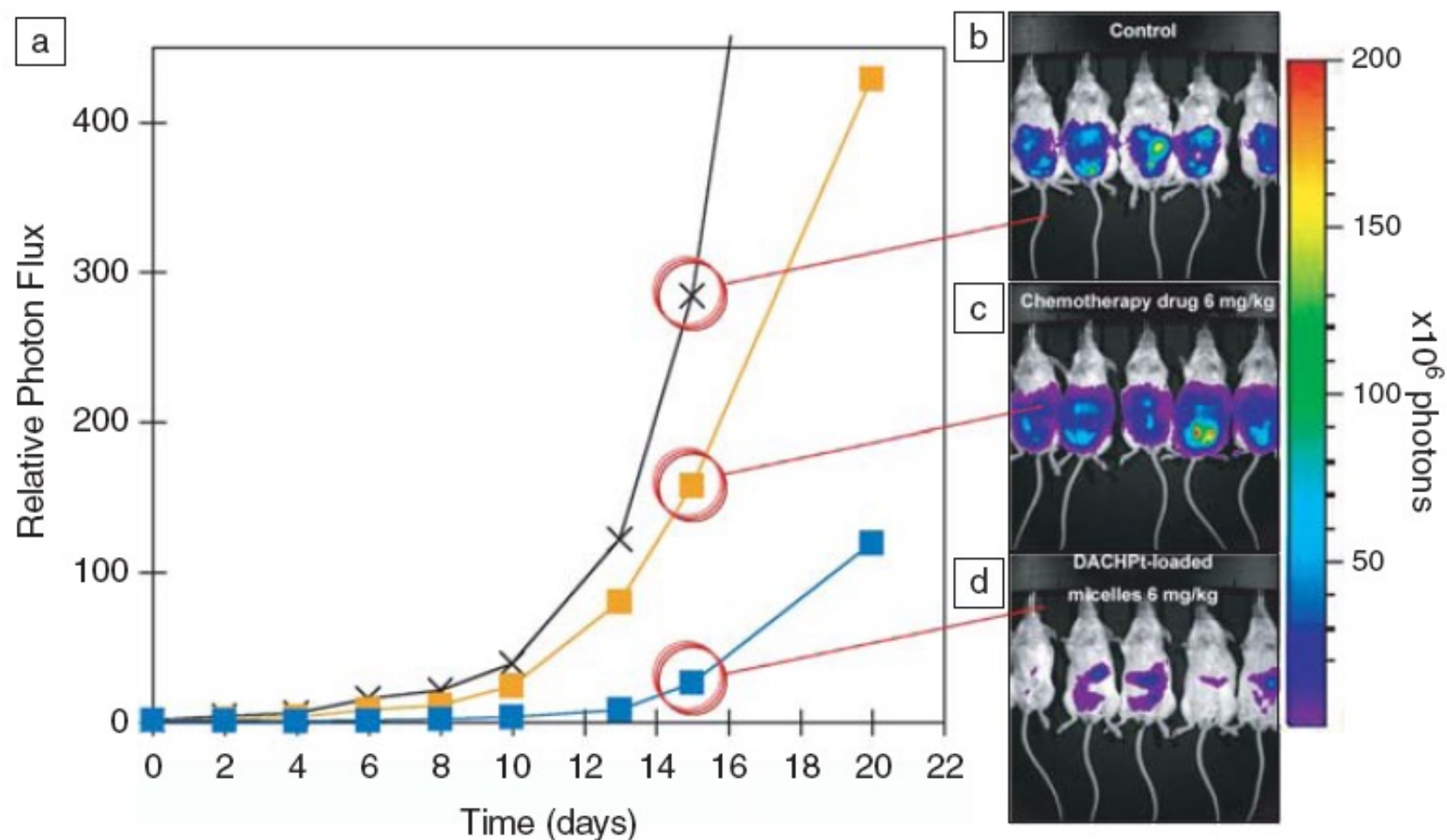


Figure 3. Platinum drug-loaded polymeric micelles.¹⁰³ (a) Antitumor activity measured as the relative photon flux, which is the ratio between the photon flux (photons/second) and the initial photon flux, from bioluminescent intraperitoneal (within the abdominal cavity) metastasis and the *in vivo* bioluminescent images corresponding to day 10. (b) Control (crosses), (c) the clinically used DACHPt derivative, oxaliplatin, 6 mg/kg (orange squares), (d) (1,2-diaminocycloheance) platinum (II) (DACHPt)-loaded micelle (blue squares).

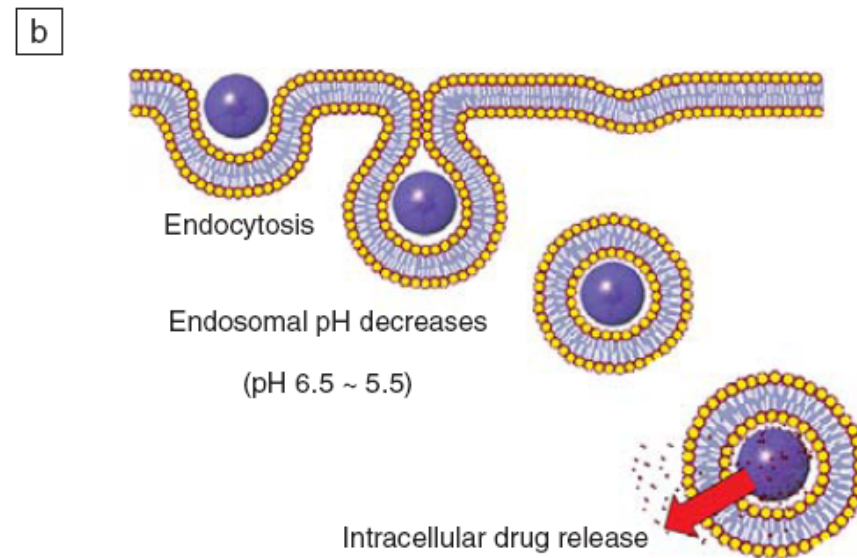
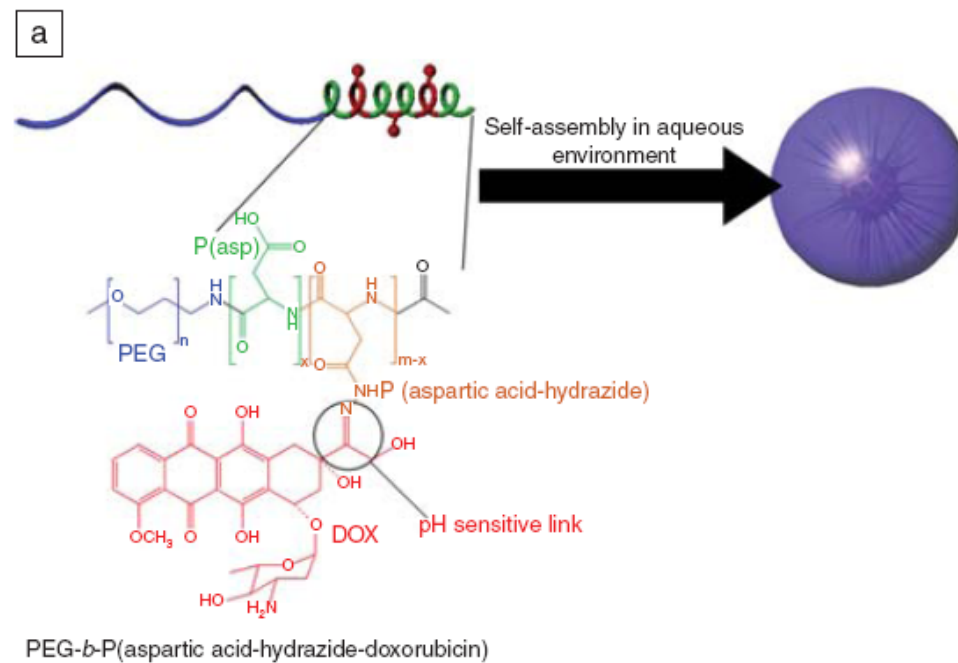


Figure 4. pH-sensitive doxorubicin-loaded polymeric micelles. (a) Molecular structure of PEG-poly(aspartic acid) conjugating with doxorubicin (DOX) by an acid-labile hydrazone bond. (b) Schematic diagram of selective drug release at endosomal pH.

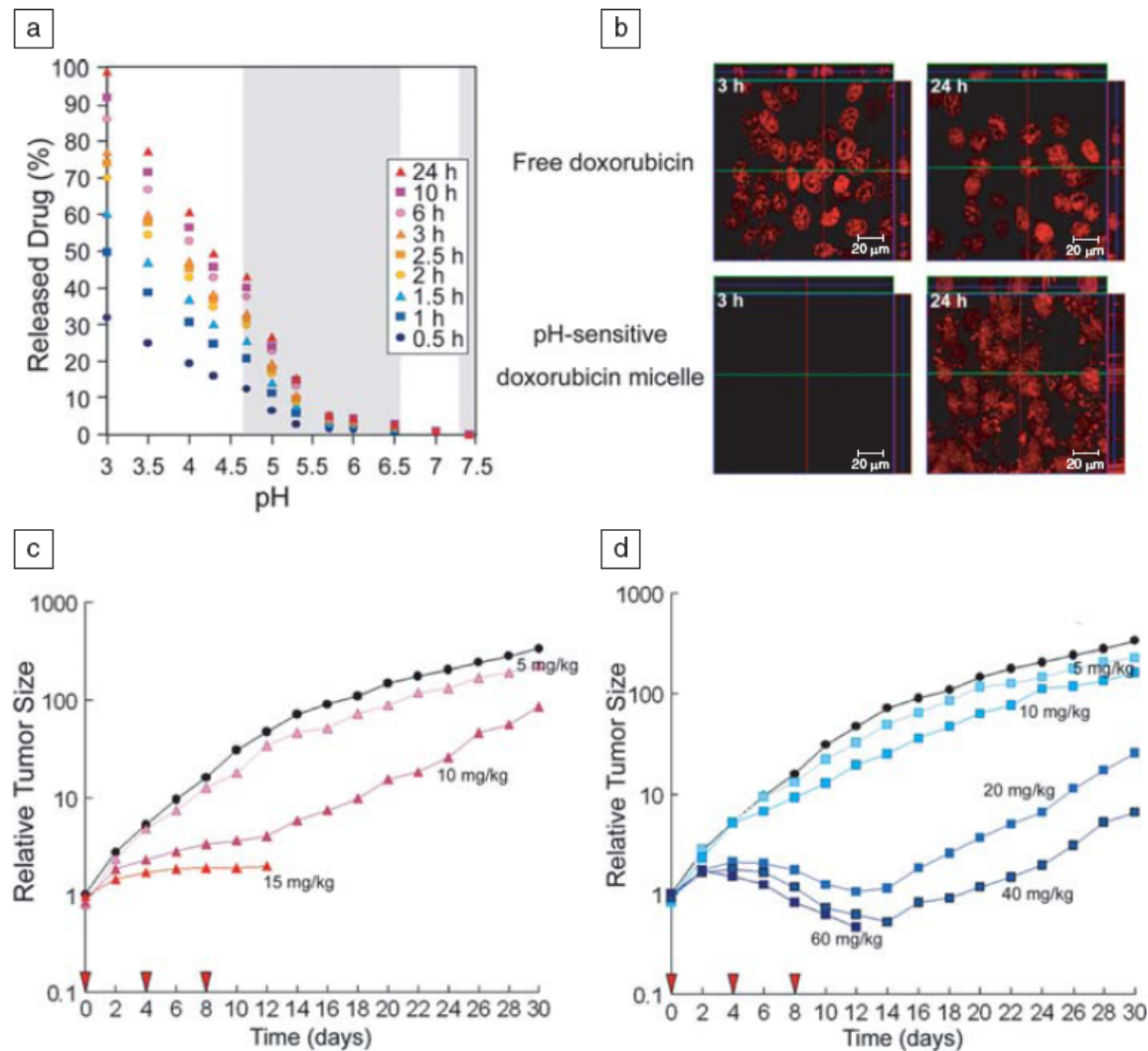


Figure 5. (a) Drug release profiles of pH-sensitive doxorubicin-loaded polymeric micelles at different pH values from 0.5 h to 24 h after release. Drug release amount increased with decreasing pH.¹⁰⁷ (b) Confocal microscopy of SBC-3 cancer cells incubated with free doxorubicin and pH-sensitive, doxorubicin-loaded polymeric micelles after 3 h and 24 h. Free doxorubicin rapidly penetrated the cancer cells by diffusion, while pH-sensitive, doxorubicin-loaded polymeric micelles were internalized by endocytosis and released the drug inside the cells. (c) Antitumor activity of free doxorubicin. The maximum tolerated dose was 15 mg/kg. (d) Antitumor activity of pH-sensitive doxorubicin-loaded polymeric micelles. The maximum tolerated dose was 60 mg/kg. Control (black circles); red arrows indicate intravenous injections.^{107,108}

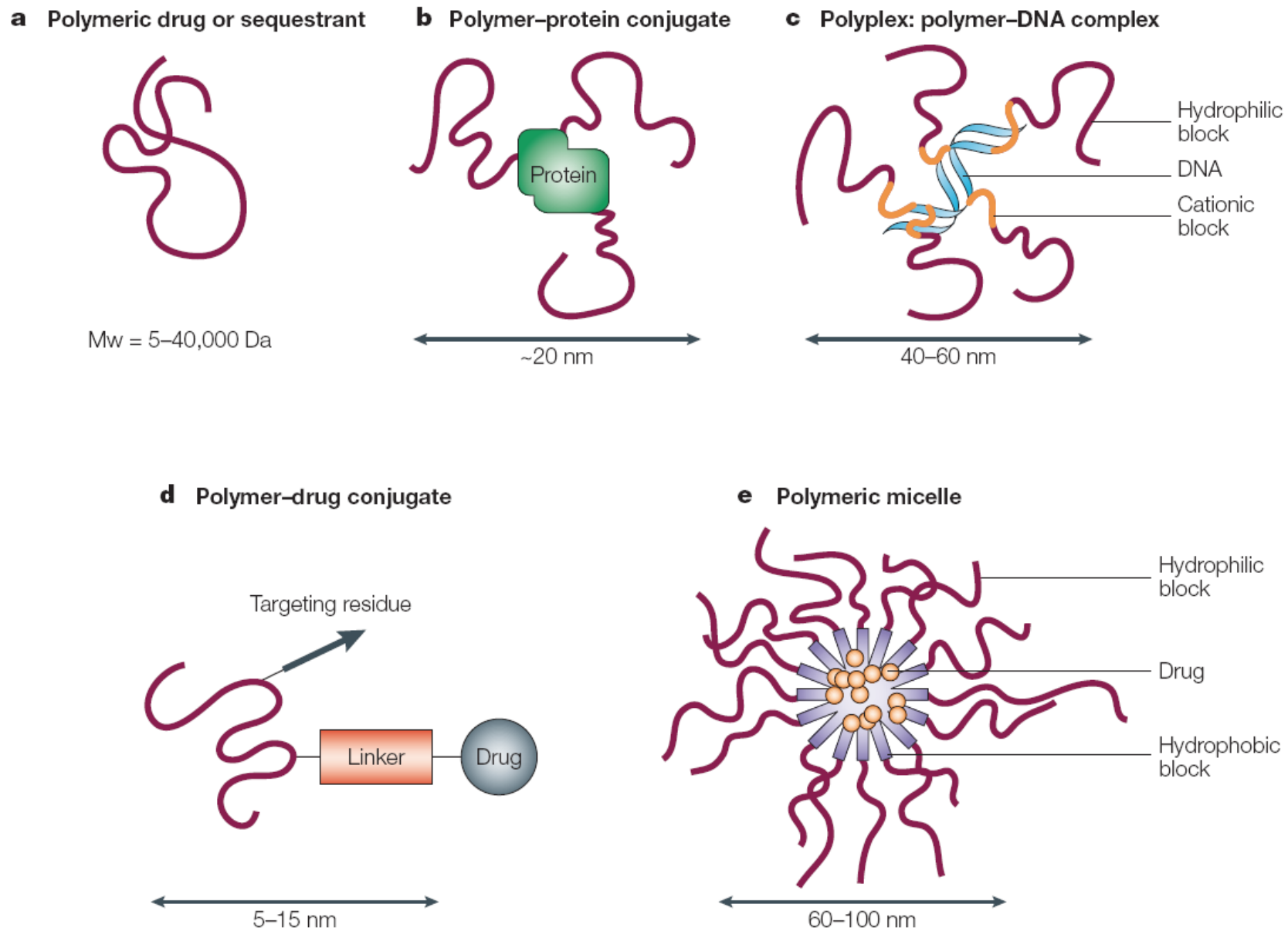
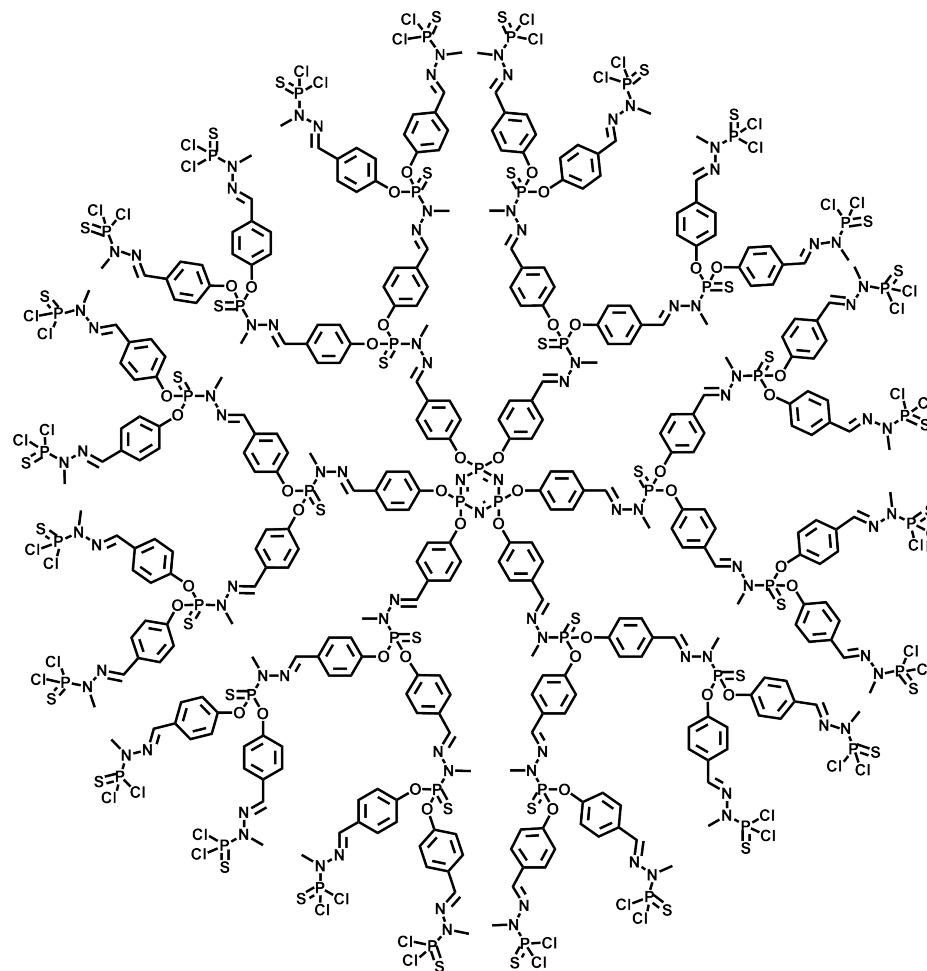
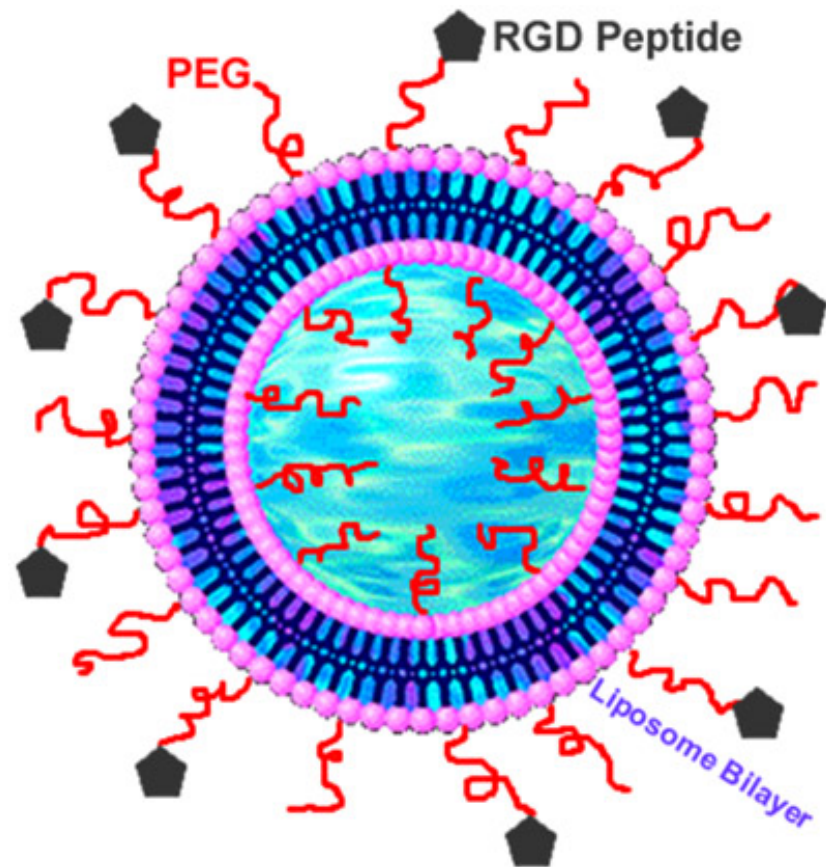
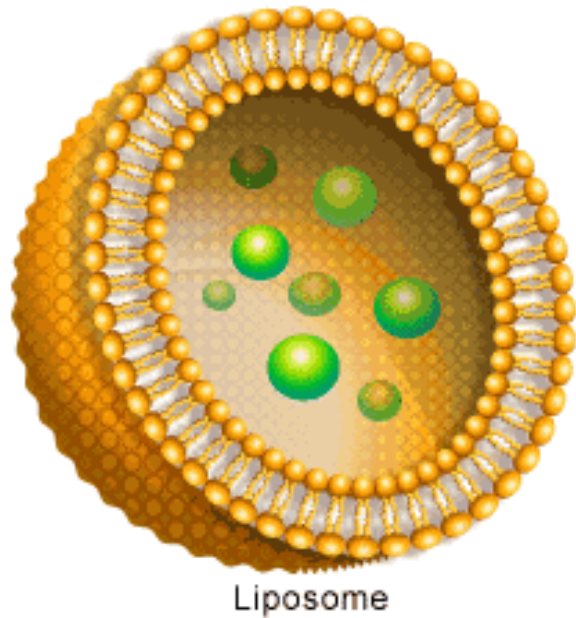


Figure 1 | **Schematic representation of polymer therapeutics now in, or progressing towards, clinical development.** The nano-sized and frequently multicomponent nature of these structures is visible. Mw, molecular weight.

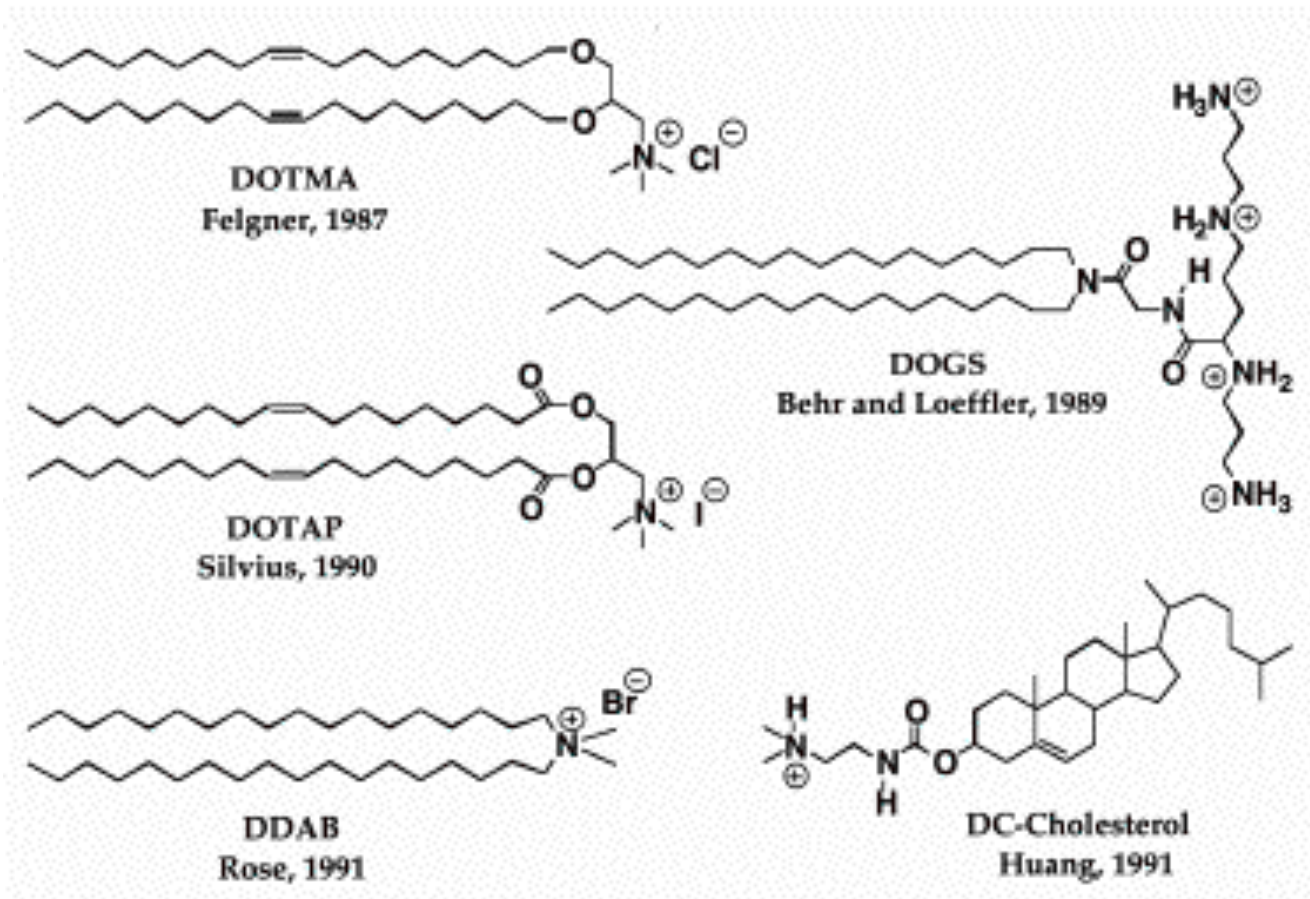
Dendrimer



Liposome



Cationic Lipids



DNA Origami

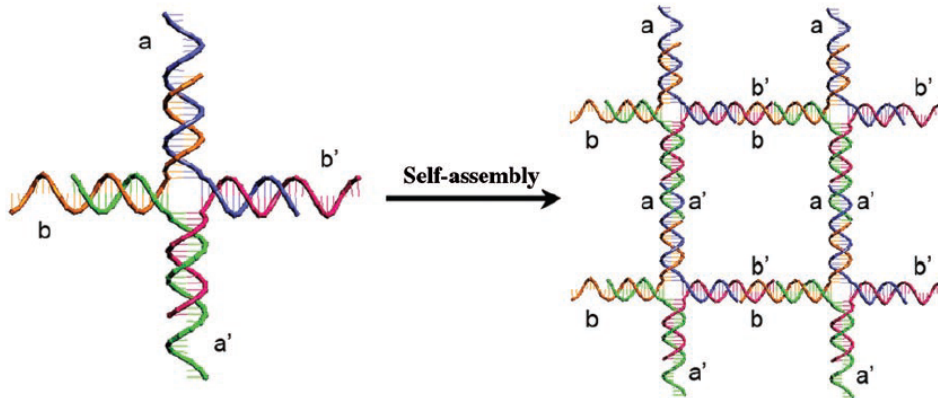
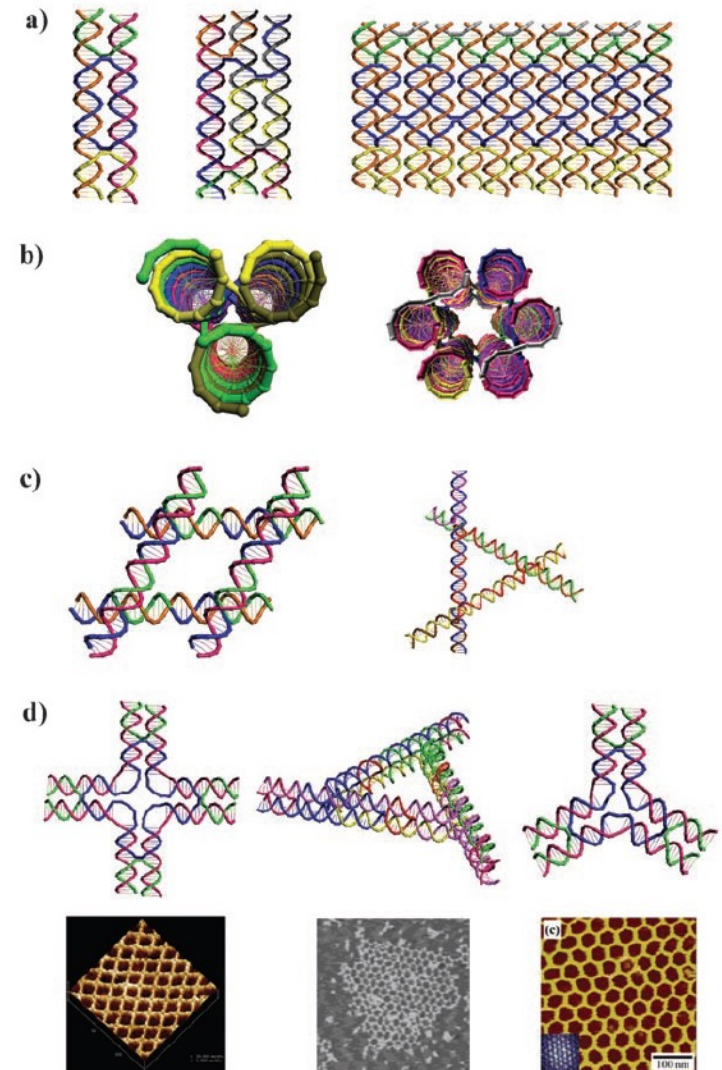


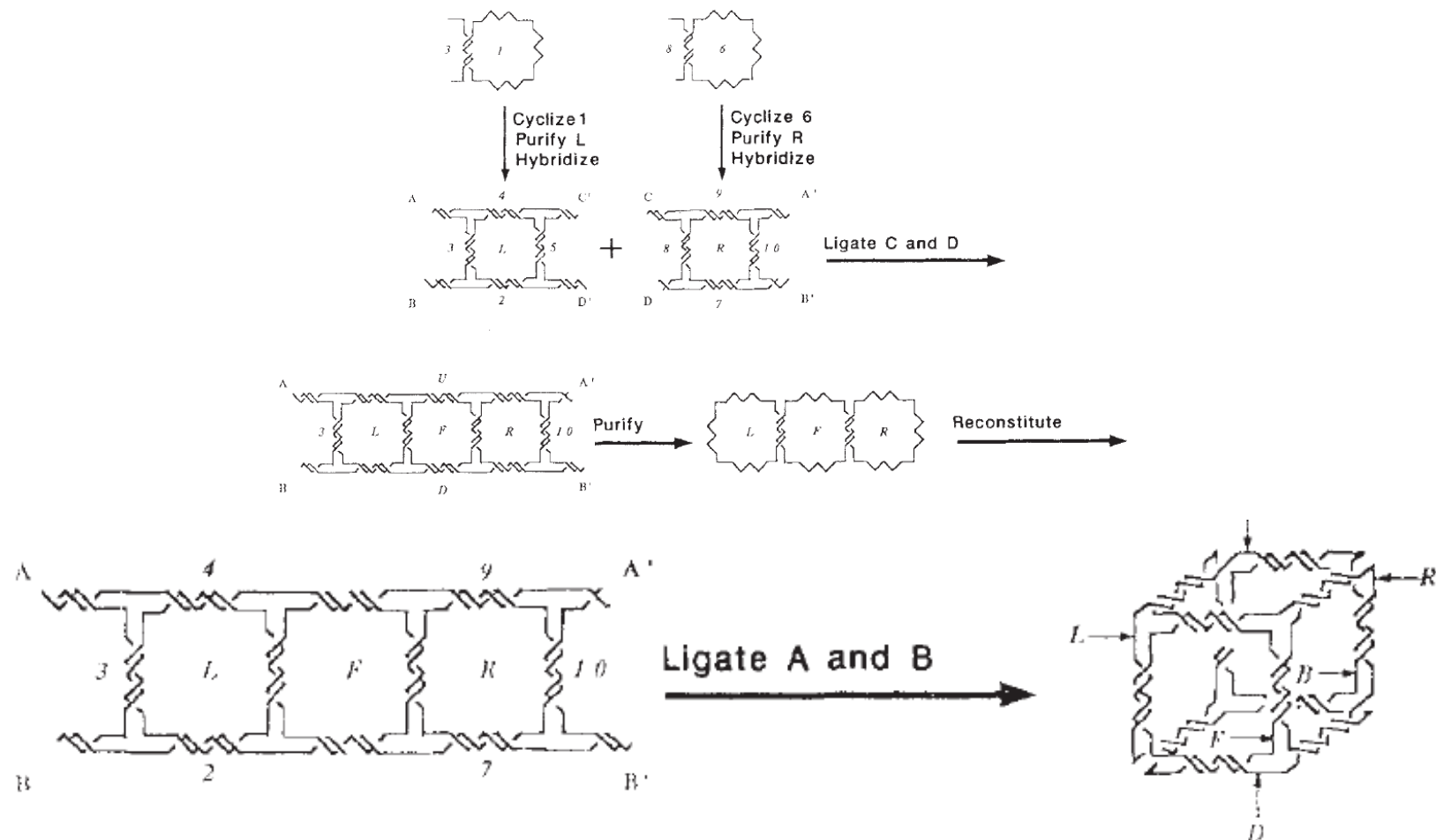
Figure 1. Key concept of DNA tile based self-assembly: combining branched DNA junction with sticky-end associations (e.g. *a*–*a'* and *b*–*b'* pairings) to self-assemble 2D lattices (adapted from ref. [1]). The DNA model was rendered using the Strata program (www.strata.com).



Synthesis from DNA of a molecule with the connectivity of a cube

Junghuei Chen & Nadrian C. Seeman

NATURE · VOL 350 · 18 APRIL 1991



Folding DNA to create nanoscale shapes and patterns

NATURE|Vol 440|16 March 2006

Paul W. K. Rothemund¹

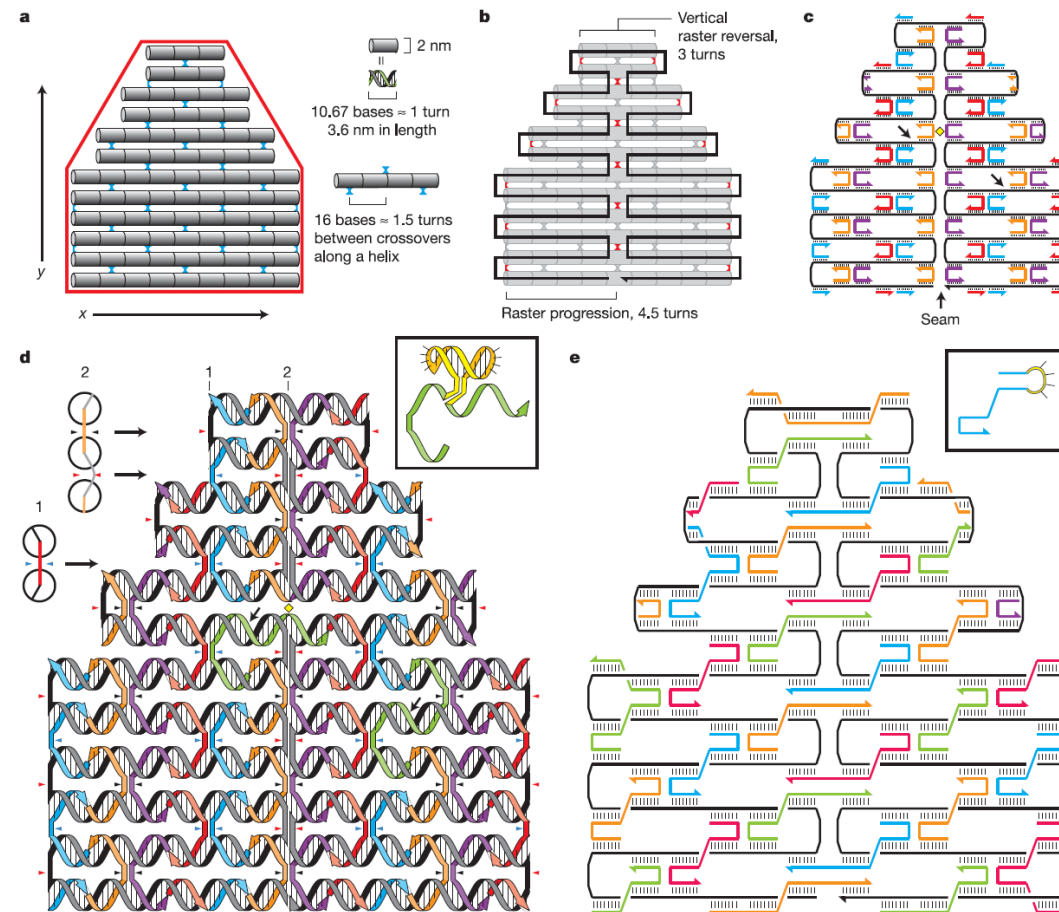
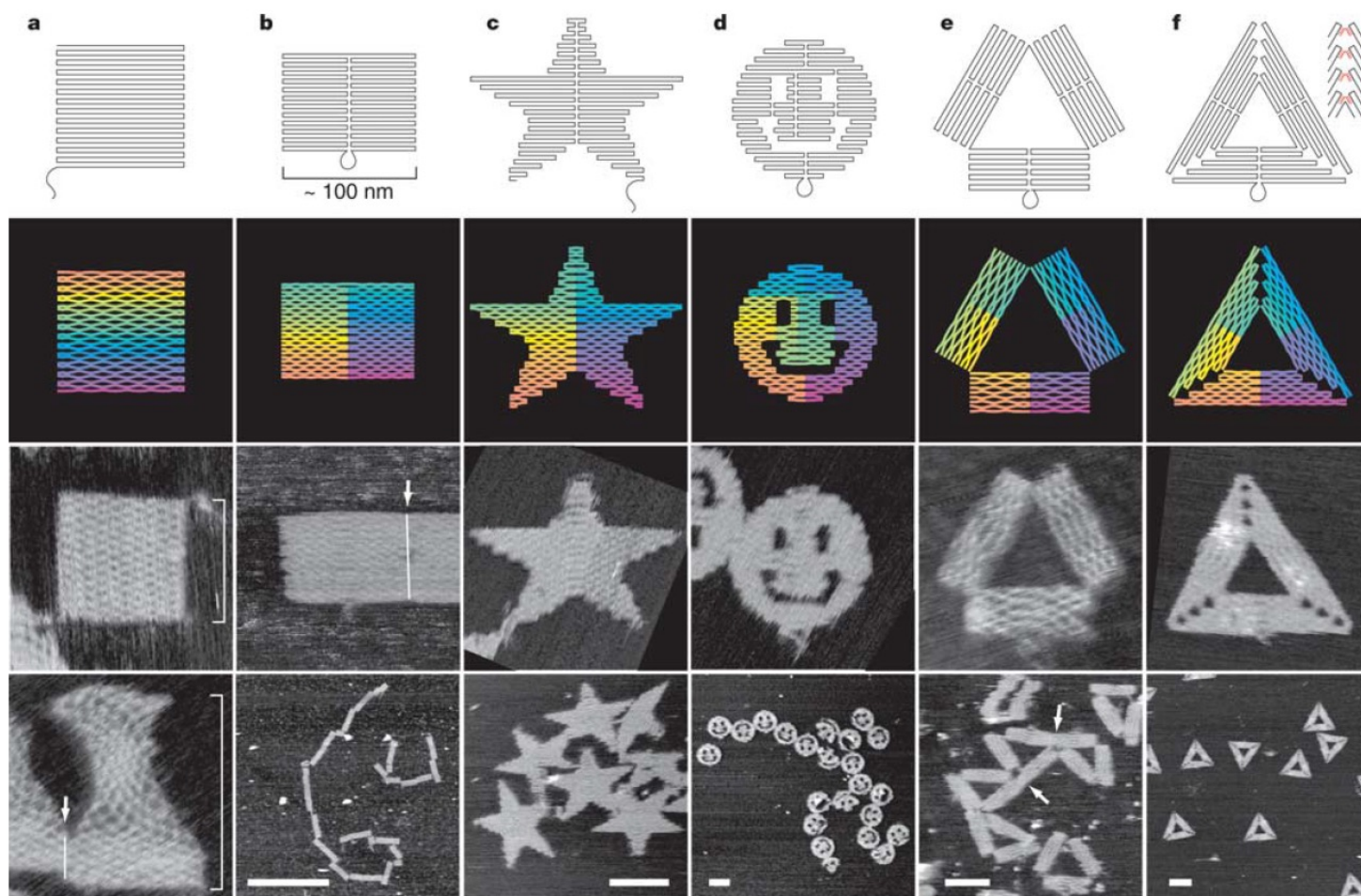
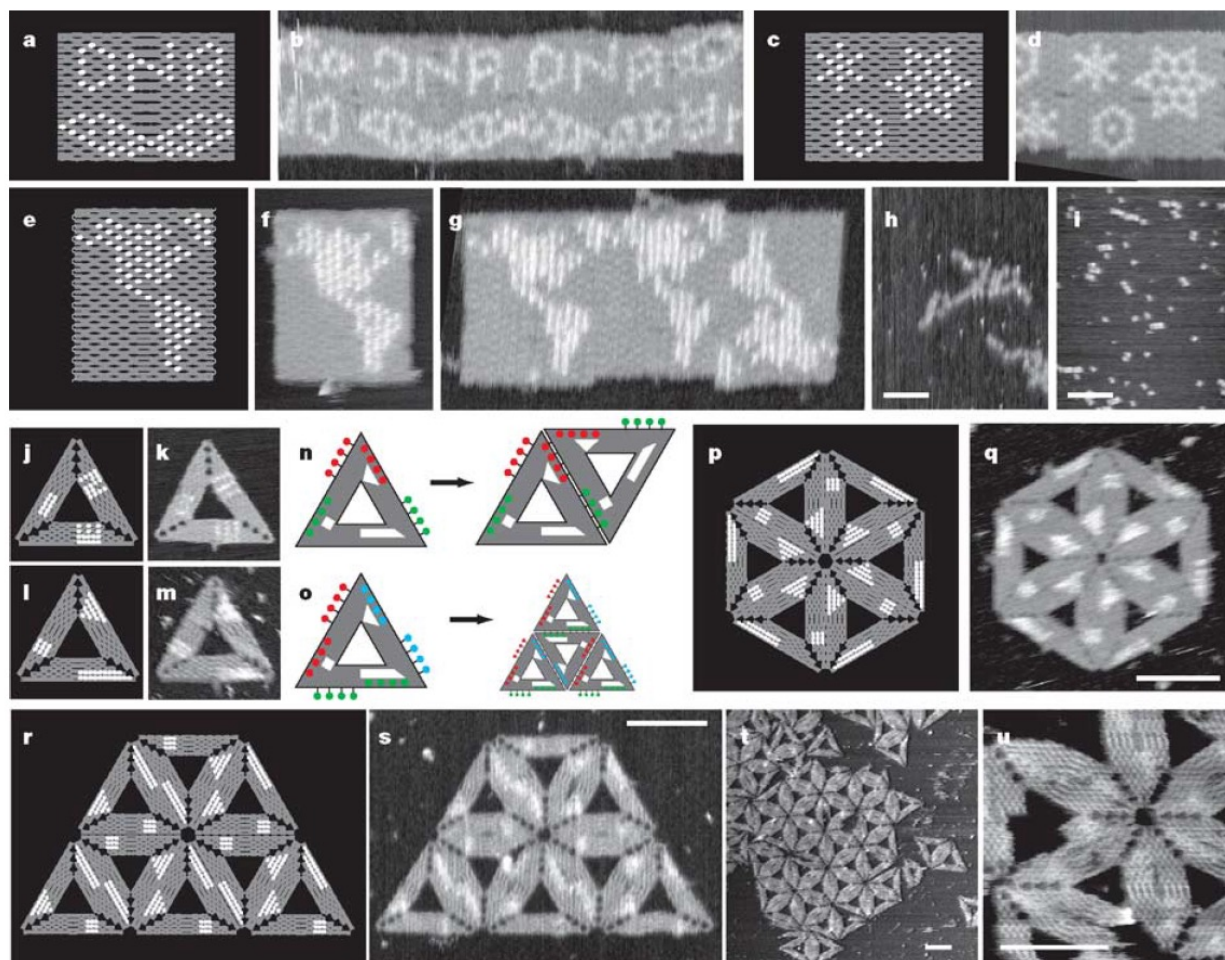


Figure 1 | Design of DNA origami. **a**, A shape (red) approximated by parallel double helices joined by periodic crossovers (blue). **b**, A scaffold (black) runs through every helix and forms more crossovers (red). **c**, As first designed, most staples bind two helices and are 16-mers. **d**, Similar to **c** with strands drawn as helices. Red triangles point to scaffold crossovers, black triangles to periodic crossovers with minor grooves on the top face of the shape, blue triangles to periodic crossovers with minor grooves on bottom. Cross-sections of crossovers (1, 2, viewed from left) indicate backbone positions

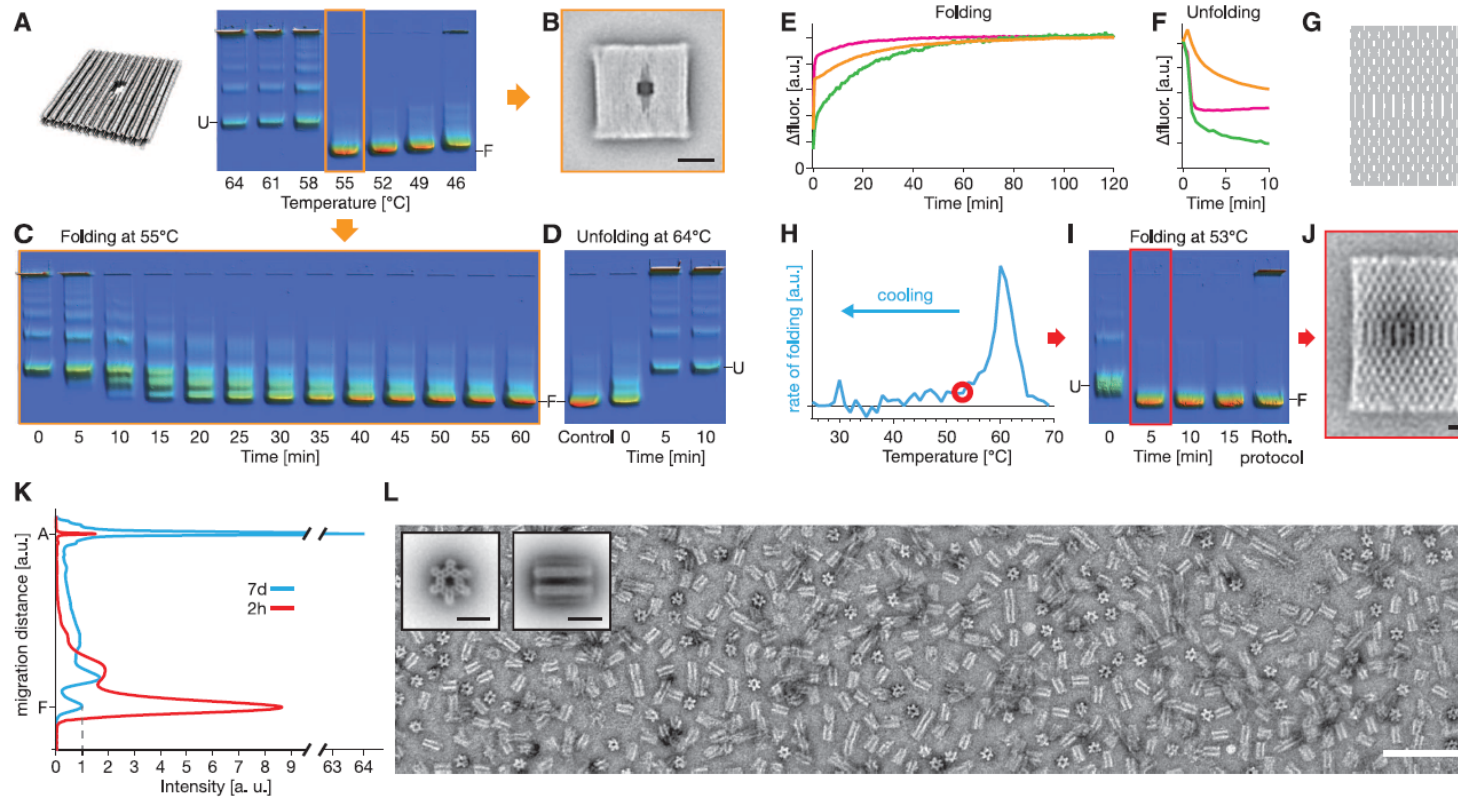
with coloured lines, and major/minor grooves by large/small angles between them. Arrows in **c** point to nicks sealed to create green strands in **d**. Yellow diamonds in **c** and **d** indicate a position at which staples may be cut and resealed to bridge the seam. **e**, A finished design after merges and rearrangements along the seam. Most staples are 32-mers spanning three helices. Insets show a dumbbell hairpin (**d**) and a 4-T loop (**e**), modifications used in Fig. 3.





Rapid Folding of DNA into Nanoscale Shapes at Constant Temperature

Jean-Philippe J. Sobczak *et al.*
Science **338**, 1458 (2012);
DOI: 10.1126/science.1229919



DNA Origami as a Carrier for Circumvention of Drug Resistance

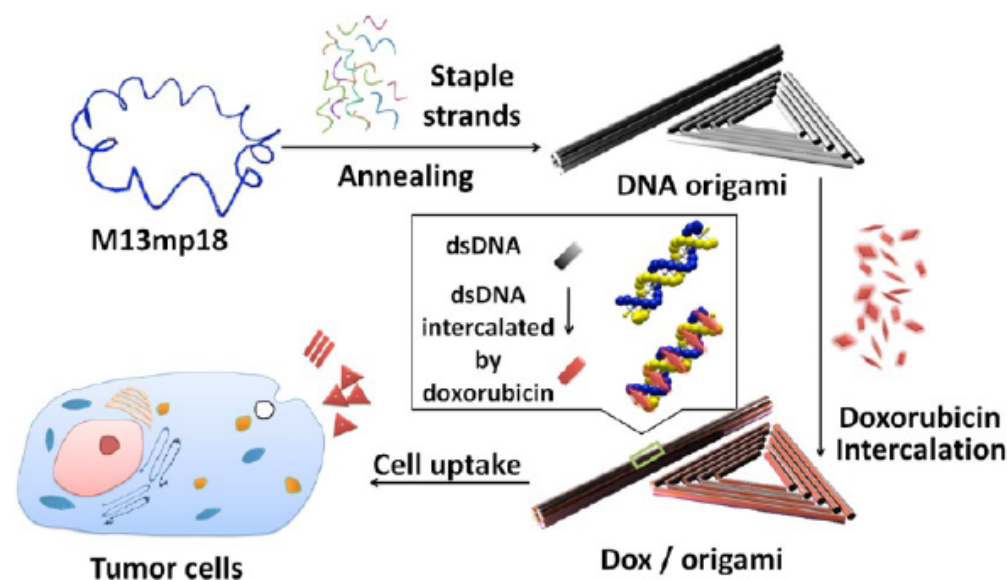
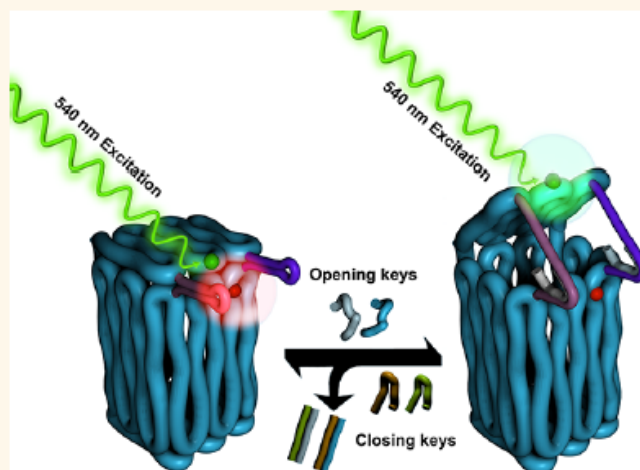


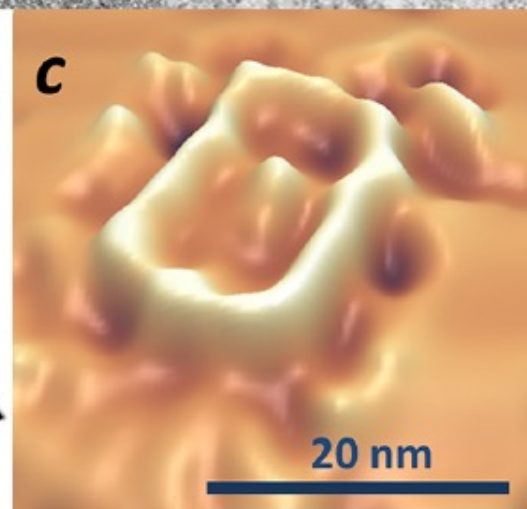
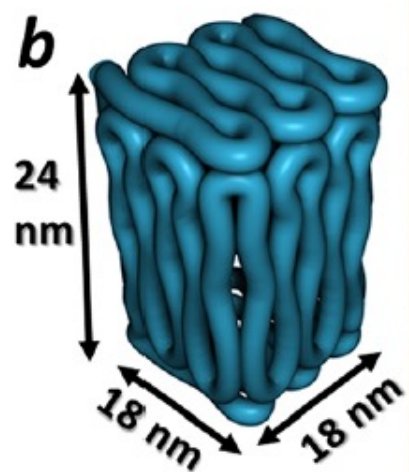
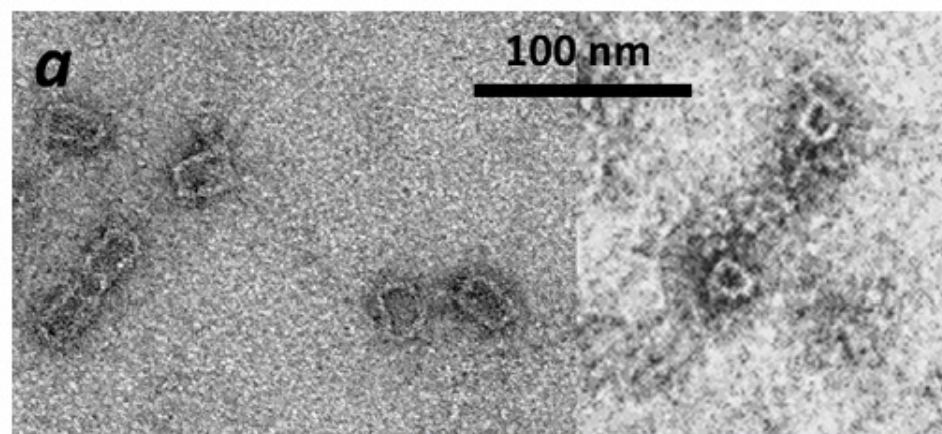
Figure 1. DNA origami and doxorubicin origami delivery system assembly. The long single-strand M13mp18 genomic DNA scaffold strand (blue) is folded into the triangle and tube structures through the hybridization of rationally designed staple strands. Watson–Crick base pairs in the double helices serve as docking sites for doxorubicin intercalation. After incubation with doxorubicin, the drug-loaded DNA nanostructure delivery vessels were administered to MCF 7 cells, and the effects were investigated.

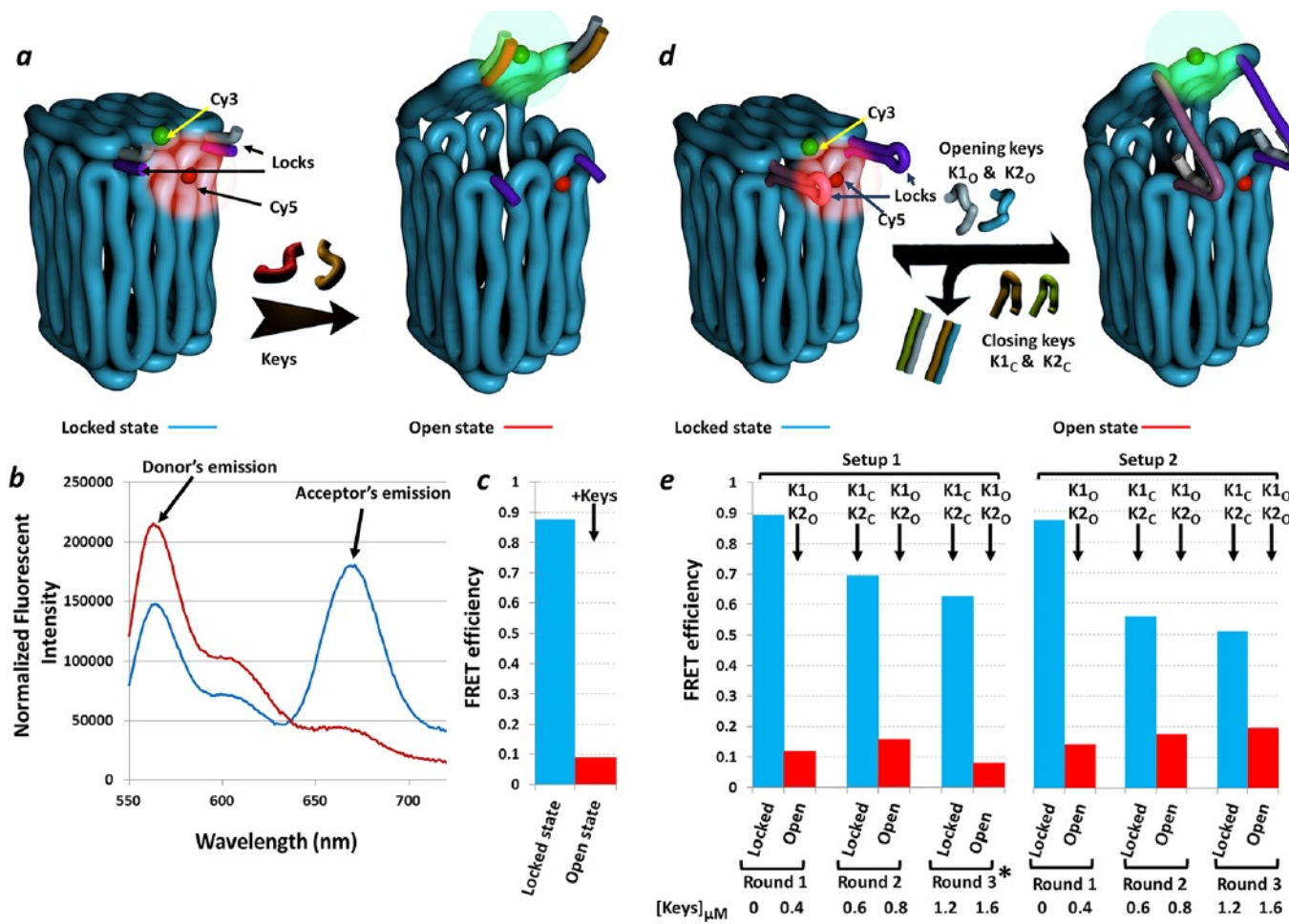
Construction of a 4 Zeptoliters Switchable 3D DNA Box Origami

ABSTRACT The DNA origami technique is a recently developed self-assembly method that allows construction of 3D objects at the nanoscale for various applications. In the current study we report the production of a $18 \times 18 \times 24 \text{ nm}^3$ hollow DNA box origami structure with a switchable lid. The structure

was efficiently produced and characterized by atomic force microscopy, transmission electron microscopy, and Förster resonance energy transfer spectroscopy. The DNA box has a unique reclosing mechanism, which enables it to repeatedly open and close in response to a unique set of DNA keys. This DNA device can potentially be used for a broad range of applications such as controlling the function of single molecules, controlled drug delivery, and molecular computing.

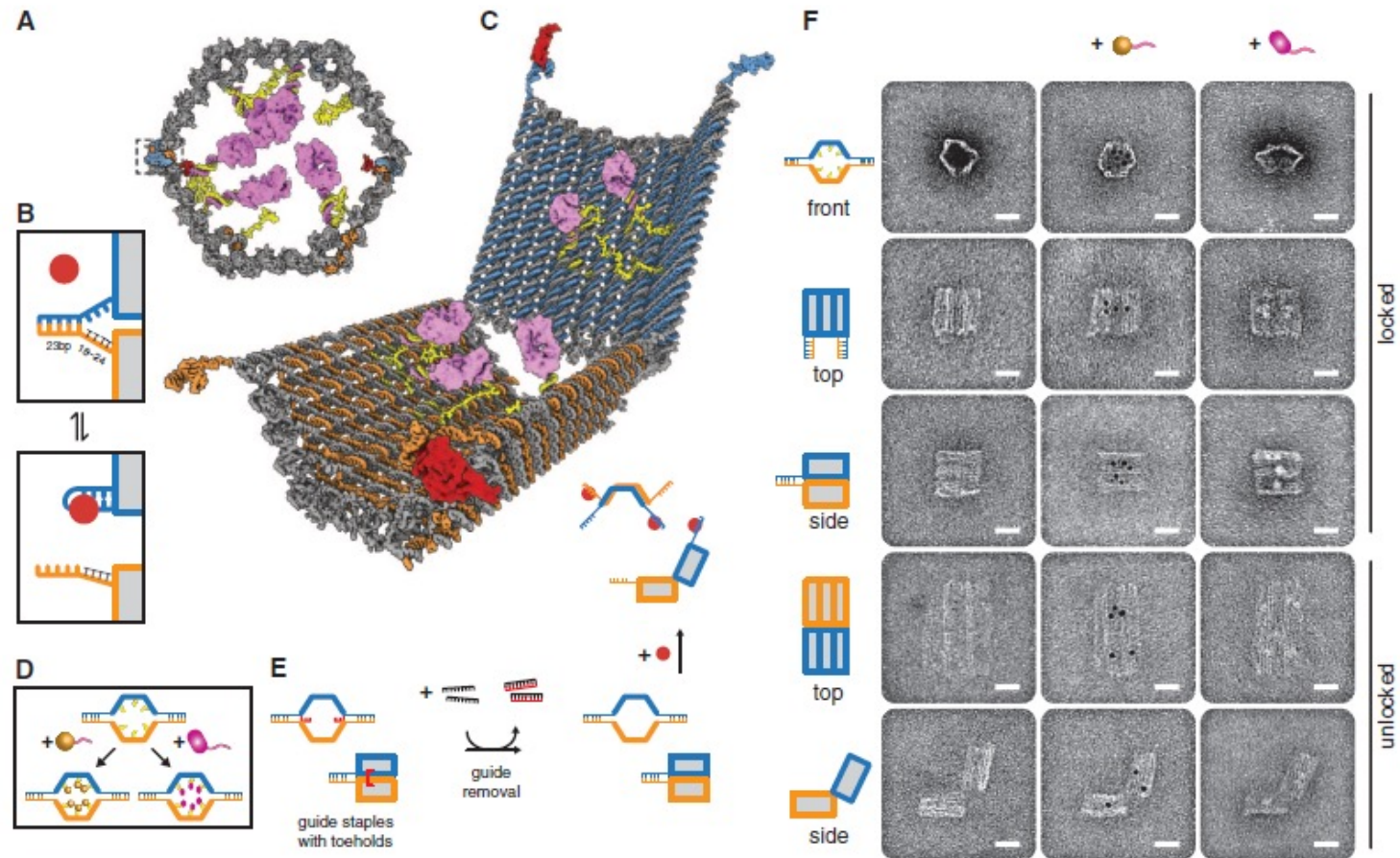






A Logic-Gated Nanorobot for Targeted Transport of Molecular Payloads

Shawn M. Douglas,* Ido Bachelet,* George M. Church†



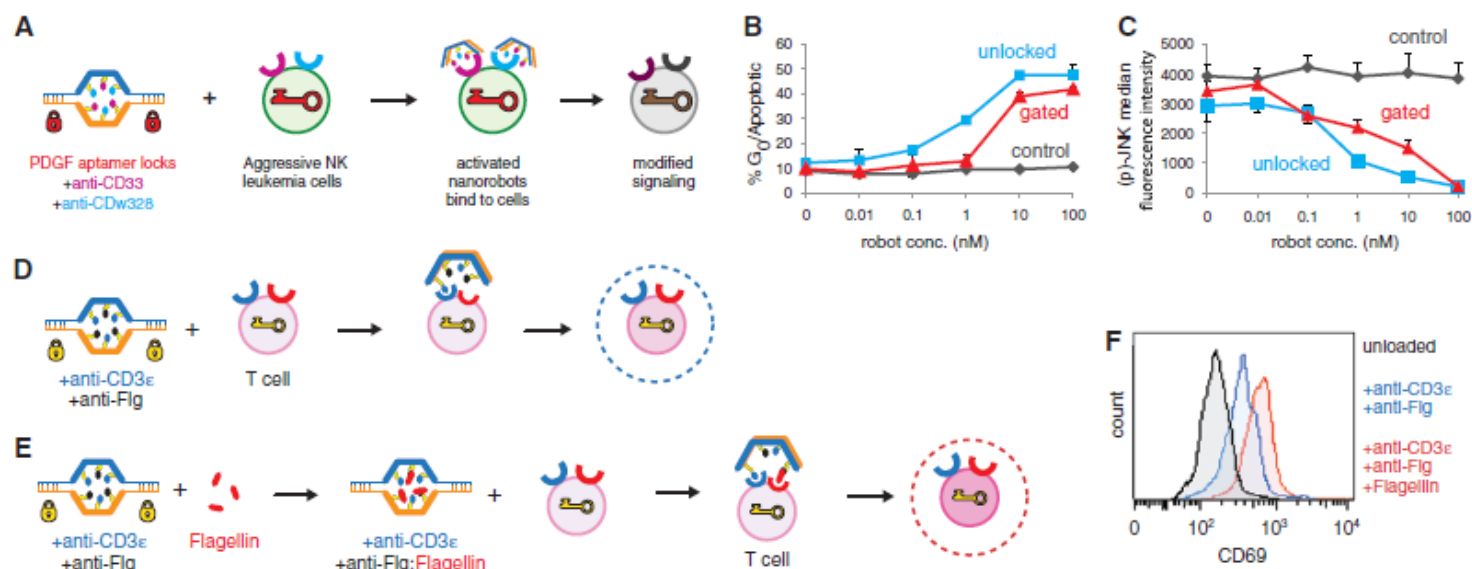


Fig. 3. Nanorobots manipulate target cell signaling. **(A)** Experimental scheme. A single dose of nanorobots loaded with an equal mixture of antibody to human CD33 and antibody to human CDw328/Siglec-7 Fab' fragments (cyan and magenta, respectively, each at a molar excess of 10 over nanorobots) and gated by 41t locks recognizing platelet-derived growth factor (PDGF) were used to treat NKL cells at various concentrations (0 to 100 nM). Phosphorylation of JNK was measured after 72 hours by intracellular flow cytometry. **(B)** NKL cells (10,000 per sample) treated with nanorobots were analyzed after 72 hours for cell cycle distribution by propidium

iodide (5 µg/ml). **(C)** Phosphorylation level of JNK as a function of robot concentration (lowest, 0; highest, 100 nM) after 72 hours. Error bars for **(B)** and **(C)** represent SEM of two biological replicates. **(D)** and **(E)** Incremental activation of T cells by nanorobots loaded with antibody to human CD3ε (blue) and antibody to flagellin Fab' (black). Nanorobots (50 nM) with **(E)** and without **(D)** pre-incubation with flagellin (red; 100 pg/ml) were reacted with Jurkat T cells (pink) for 1 hour at 37°C. **(F)** Histograms showing T cell activation after nanorobot treatment, as measured by labeling with FITC-labeled antibody to CD69.

Gene Therapy

- Gene therapy is a technique for correcting defective genes responsible for disease development. Researchers may use one of several approaches for correcting faulty genes:
 - **A normal gene may be inserted into a nonspecific location within the genome to replace a nonfunctional gene. This approach is most common.**
 - **An abnormal gene could be swapped for a normal gene through homologous recombination.**
 - **The abnormal gene could be repaired through selective reverse mutation, which returns the gene to its normal function.**
 - **The regulation (the degree to which a gene is turned on or off) of a particular gene could be altered.**

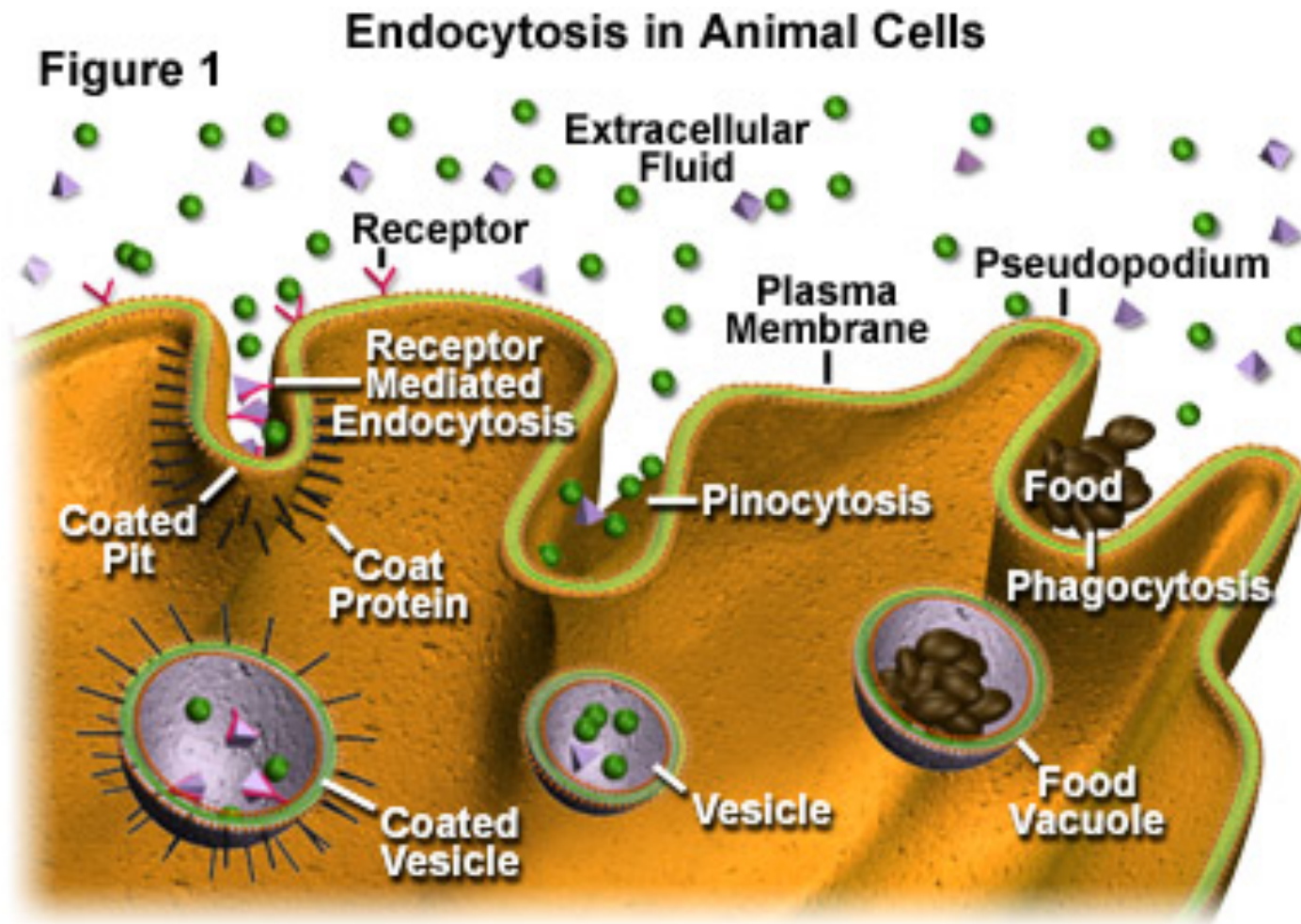
How Gene Therapy Works?

- In most gene therapy studies, a "normal" gene is inserted into the genome to replace an "abnormal," disease-causing gene. A carrier molecule called a vector must be used to deliver the therapeutic gene to the patient's target cells. Currently, the most common vector is a virus that has been genetically altered to carry normal human DNA. Viruses have evolved a way of encapsulating and delivering their genes to human cells in a pathogenic manner. Scientists have tried to take advantage of this capability and manipulate the virus genome to remove disease-causing genes and insert therapeutic genes.
- Target cells such as the patient's liver or lung cells are infected with the viral vector. The vector then unloads its genetic material containing the therapeutic human gene into the target cell. The generation of a functional protein product from the therapeutic gene restores the target cell to a normal state.

Gene Delivery

- Transfection- the delivery of foreign molecules such as DNA and RNA into eukaryotic cells
- Naked DNA is not suitable for in-vivo transport of genetic materials-> degradation by serum nucleases
- Ideal gene delivery system
 - Biocompatible
 - Non-immunogenic
 - Stable in blood stream
 - Protect DNA during transport
 - Small enough to extravagate
 - Cell and tissue specific

Endocytosis



Endocytic pathway in mammalian cells

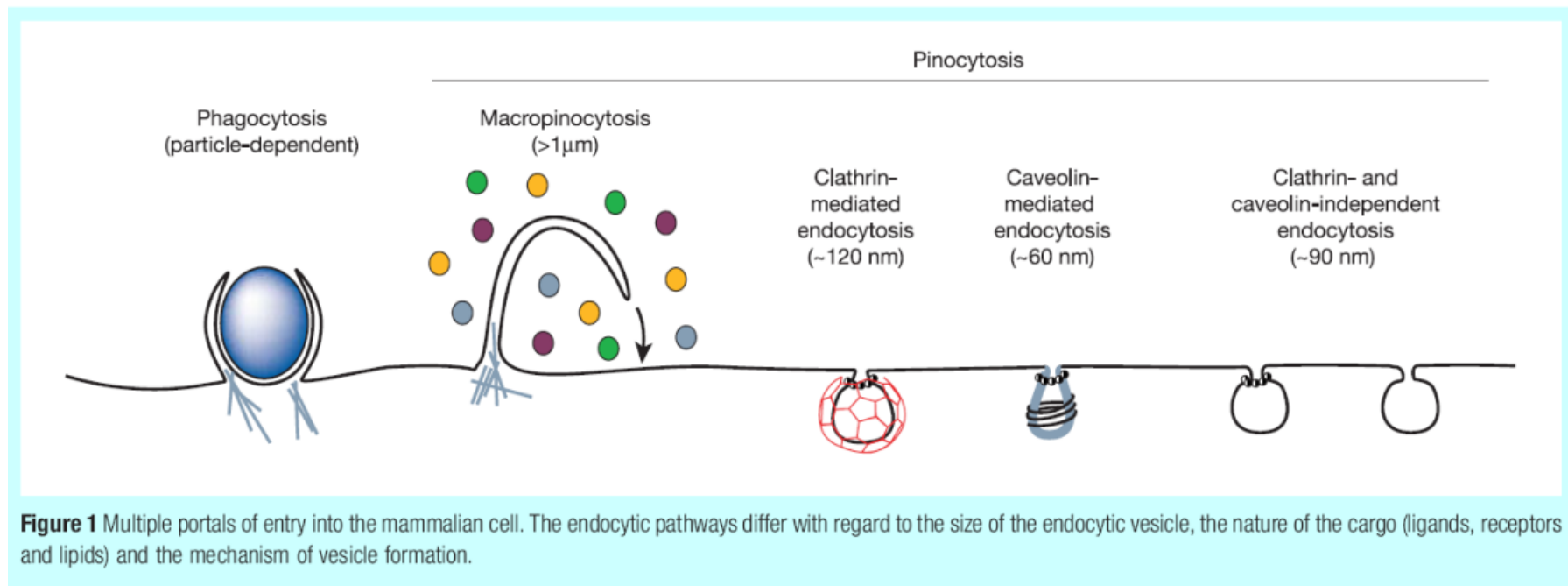


Figure 1 Multiple portals of entry into the mammalian cell. The endocytic pathways differ with regard to the size of the endocytic vesicle, the nature of the cargo (ligands, receptors and lipids) and the mechanism of vesicle formation.

Barrier to non-viral gene delivery

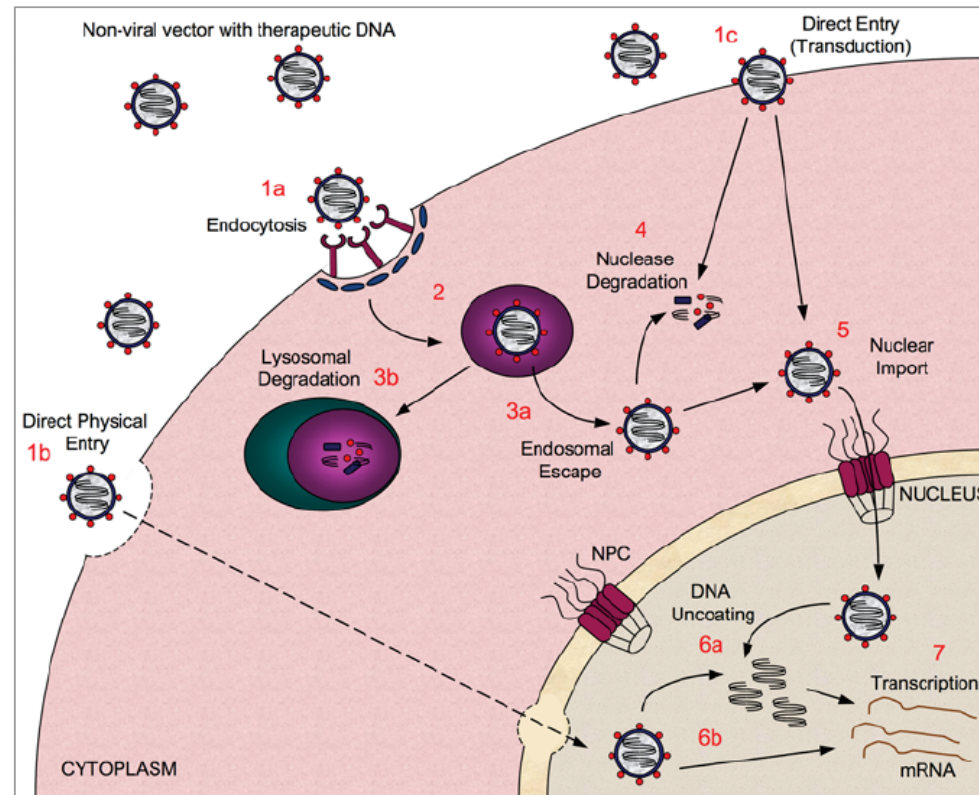


Figure 1 Barriers to non-viral gene delivery

Representation of the route travelled by a non-viral gene-delivery vector carrying therapeutic DNA to the nucleus. A non-viral vector, formed by interaction of the DNA with a carrier compound, must cross the plasma membrane to enter the cell. This can be via several routes, including endocytosis-based entry (1a), direct physical entry routes, such as electroporation or ballistic delivery (1b), or direct entry via protein transduction (1c). Depending on the mode of cellular entry, the vector may become encapsulated in an endosome (2), from which it must escape (3a) or it will become degraded when the endosome fuses with a lysosome (3b). The DNA will at some point be subjected to degradation by cytosolic nucleases (4), as it traverses through the cytoplasm to reach the nucleus. Finally, the vector must undergo nuclear transport (5) through NPCs embedded in the NE in order to gain access to the nucleoplasm. Once in the nucleus, the DNA may (6a) or may not (6b) need to be uncoated, depending upon the vector used, before it can ultimately be transcribed (7).

NLS-mediated nuclear import

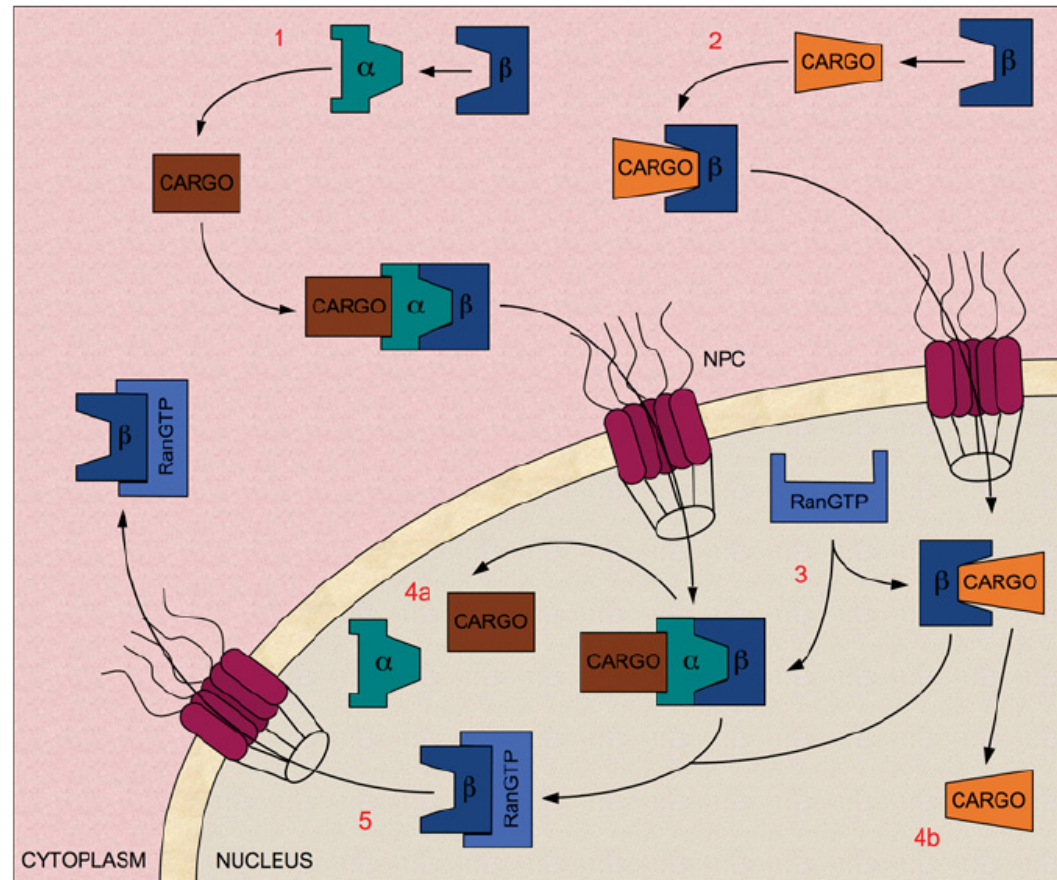


Figure 2 NLS-mediated nuclear import pathways

In classical nuclear import, the NLS found in cargo bound for the nucleus is recognized by the Imp α subunit of the Imp α/β heterodimer (1). However, there are also many examples where Imp β or one of its many homologues can mediate nuclear import of cargo proteins independently of Imp α (2). In both cases, transient interactions between the Imp β and the nucleoporin proteins that line the NE-embedded NPCs mediate translocation into the nucleus. Once inside, RanGTP binds to Imp β (3), releasing Imp α and the cargo into the nucleoplasm (4a and 4b). RanGTP itself is then recycled back to the cytoplasm (5), where it is converted into its RanGDP state (not shown). An animated version of this Figure can be found at <http://www.BiochemJ.org/bj/406/0185/bj4060185add.htm>

Barriers to DNA Delivery

BOX 1

A number of challenges and barriers face the successful delivery of therapeutic DNA to target cells in the body. Physicochemical, economic and sterilization challenges complicate formulation; the complex environment of the human body hinders its successful transport to the target cell population; and endocytic pathway barriers hinder its successful transport to the nucleus of the cell (the site of action). Each known and major barrier is listed in Fig. B1, using nanoscale DNA-delivery systems as representative examples. Each barrier exists independent of length scale. L = lysosome. A number of clever systems have been devised to overcome these barriers, the general design criteria of which are given in Tables B1 and B2.

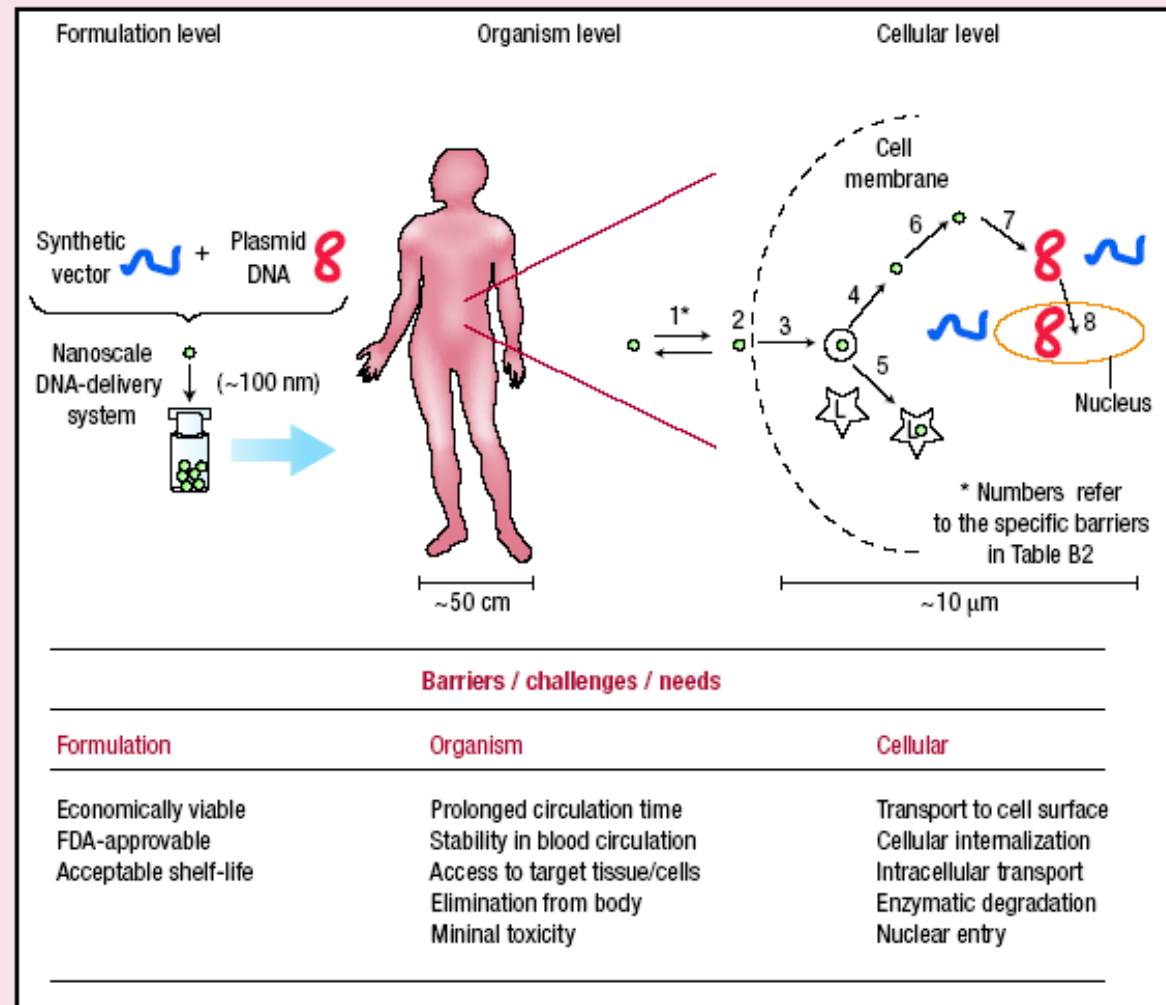


Figure B1 Barriers to DNA delivery.

Organism Level

Barrier/challenge/need	Rationale	Example approaches	Materials design criteria
Prolonged circulation time	Maximize total flux past target cell type	PEG conjugates to minimize interaction with serum proteins	Hydrophilic Uncharged
Stability within blood circulation	Maintenance of designed functionality	Crosslinking to maximize overall stability	Stable crosslinks within bloodstream, but reversible upon entry into target cell
Access to target tissue/cells	Transport from capillary lumen to extracellular space to reach target cell surface	Vaso-active protein conjugates (for example, vascular endothelial growth factor) Targeting restricted to 'leaky' vessel tissues (for example, tumour, liver, spleen).	Retention of protein activity post conjugation Small diameter delivery system (for example, <100 nm)
Elimination from body	Minimal build-up of delivery vector over time	Control over molecular weight Engineered biodegradation sites	Filterable through kidneys Biodegradable
Minimal toxicity and immunogenicity	Safety over treatment duration and beyond that required for FDA-approval	Minimize cation density Avoid protein-based materials/conjugates	Non-cytotoxic Non-immunogenic

Cellular Level

Barrier number (from Fig. B1)	Barrier/challenge/need	Example approaches	Materials design criteria
1, 2 and 3	Transport to cell surface, association with cell membrane, internalization	<p>Receptor/ligand interaction (for example, antibody/polymer conjugates, recombinant protein–polymer fusions, carbohydrate conjugates)</p> <p>Non-specific interaction with cell surface (for example, positive zeta potential, lipid conjugates)</p>	<p>Cell-type specificity, low cross reactivity, if desired</p> <p>Promiscuous attachment, high cross reactivity, if desired (for example, positive zeta potential, lipid conjugation)</p> <p>Endocytic pathway trigger (for example, clathrin-dependent, clathrin-independent, caveolin-dependent)</p>
4 and 5	Escape endosomal vesicle and avoid transport to lysosome	<p>Buffering capacity between pH ~7.2 and ~5.0</p> <p>Fusogenic peptide conjugate</p>	Ability to disrupt endosomal membrane and/or fusion of endosome with lysosome
6	Transport through cytosol to perinuclear space with minimal degradation	'Higher' molecular weight to maintain complex stability within cytosol	<p>Thermodynamic and kinetic stability of complex within cytosol</p> <p>Minimize DNA degradation within cytosol</p>
7	Separation of complex to allow nuclear translocation	Hydrolytically or reductively degradable polymers to reduce molecular weight	'Triggered' degradation of polymer to reduce thermodynamic and kinetic stability of complex. Release of intact DNA at or near nuclear envelope
8	Nuclear entry	<p>Nuclear localization sequence conjugates</p> <p>Mitosis</p>	<p>Facilitate nuclear uptake of DNA using virus-derived signals</p> <p>Facilitate nuclear uptake during mitosis when the nuclear envelope is dissolved.</p>

CANCER NANOTECHNOLOGY: OPPORTUNITIES AND CHALLENGES

NATURE REVIEWS |

CANCER
Summary

VOLUME 5 | MARCH 2005 | 161

- Nanotechnology concerns the study of devices that are themselves or have essential components in the 1–1,000 nm dimensional range (that is, from a few atoms to subcellular size).
- Two main subfields of nanotechnology are nanovectors — for the administration of targeted therapeutic and imaging moieties — and the precise patterning of surfaces.
- Nanotechnology is no stranger to oncology: liposomes are early examples of cancer nanotherapeutics, and nanoscale-targeted magnetic resonance imaging contrast agents illustrate the application of nanotechnology to diagnostics.
- Photolithography is a light-directed surface-patterning method, which is the technological foundation of microarrays and the surface-enhanced laser desorption/ionization time-of-flight approach to proteomics. Nanoscale resolution is now possible with photolithography, and will give rise to instruments that can pack a much greater density of information than current biochips.
- The ability of nanotechnology to yield advances in early detection, diagnostics, prognostics and the selection of therapeutic strategies is predicated based on its ability to ‘multiplex’ — that is, to detect a broad multiplicity of molecular signals and biomarkers in real time. Prime examples of multiplexing detection nanotechnologies are arrays of nanocantilevers, nanowires and nanotubes.
- Multifunctionality is the fundamental advantage of nanovectors for the cancer-specific delivery of therapeutic and imaging agents. Primary functionalities include the avoidance of biobarriers and biomarker-based targeting, and the reporting of therapeutic efficacy.
- Thousands of nanovectors are currently under study. By systematically combining them with preferred therapeutic and biological targeting moieties it might be possible to obtain a very large number of novel, personalized therapeutic agents.
- Novel mathematical models are needed, in order to secure the full import of nanotechnology into oncology.

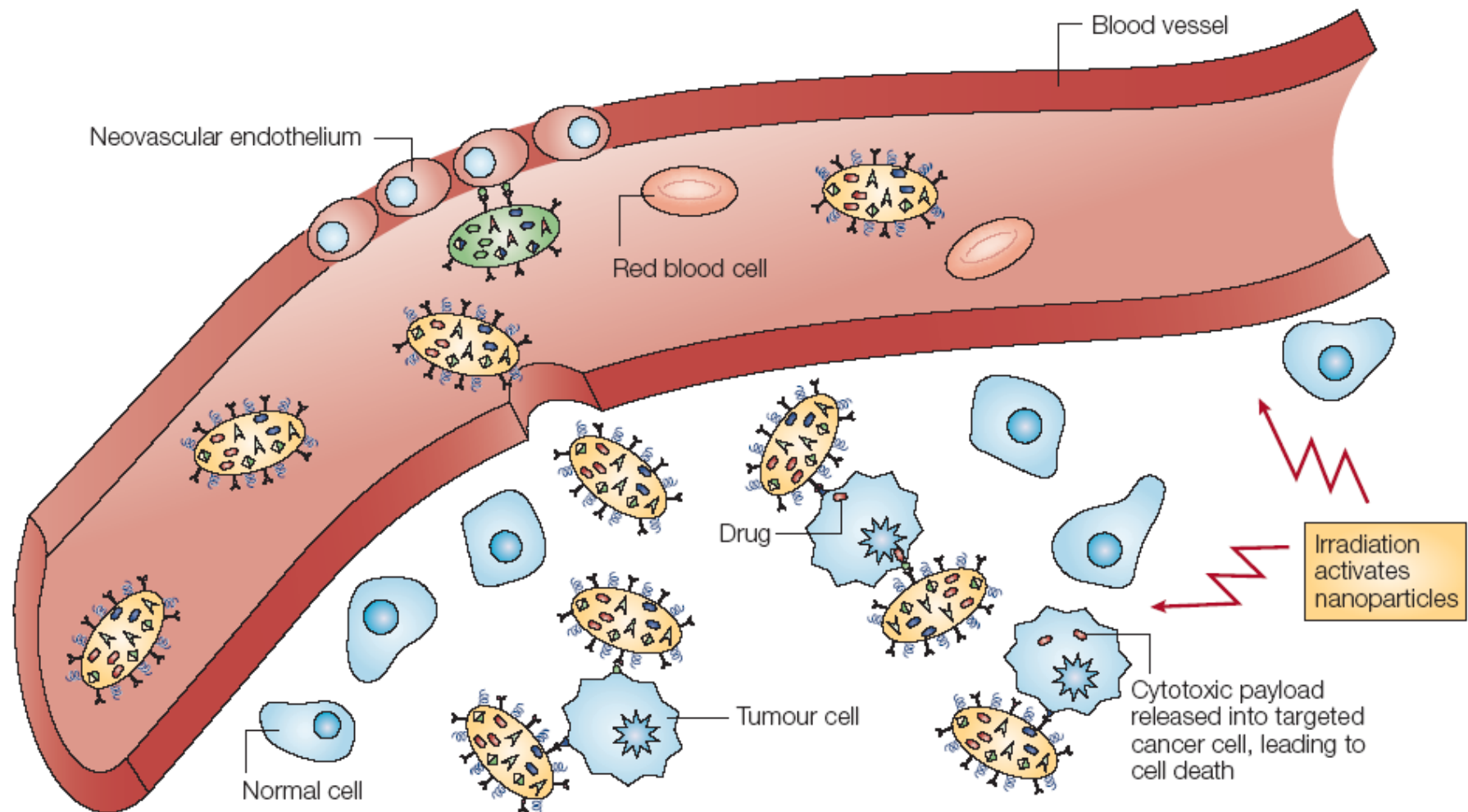


Figure 4 | **Multicomponent targeting strategies.** Nanoparticles extravasate into the tumour stroma through the fenestrations of the angiogenic vasculature, demonstrating targeting by enhanced permeation and retention. The particles carry multiple antibodies, which further target them to epitopes on cancer cells, and direct antitumour action. Nanoparticles are activated and release their cytotoxic action when irradiated by external energy. Not shown: nanoparticles might preferentially adhere to cancer neovasculature and cause it to collapse, providing anti-angiogenic therapy. The red blood cells are not shown to scale; the volume occupied by a red blood cell would suffice to host 1–10 million nanoparticles of 10 nm diameter.

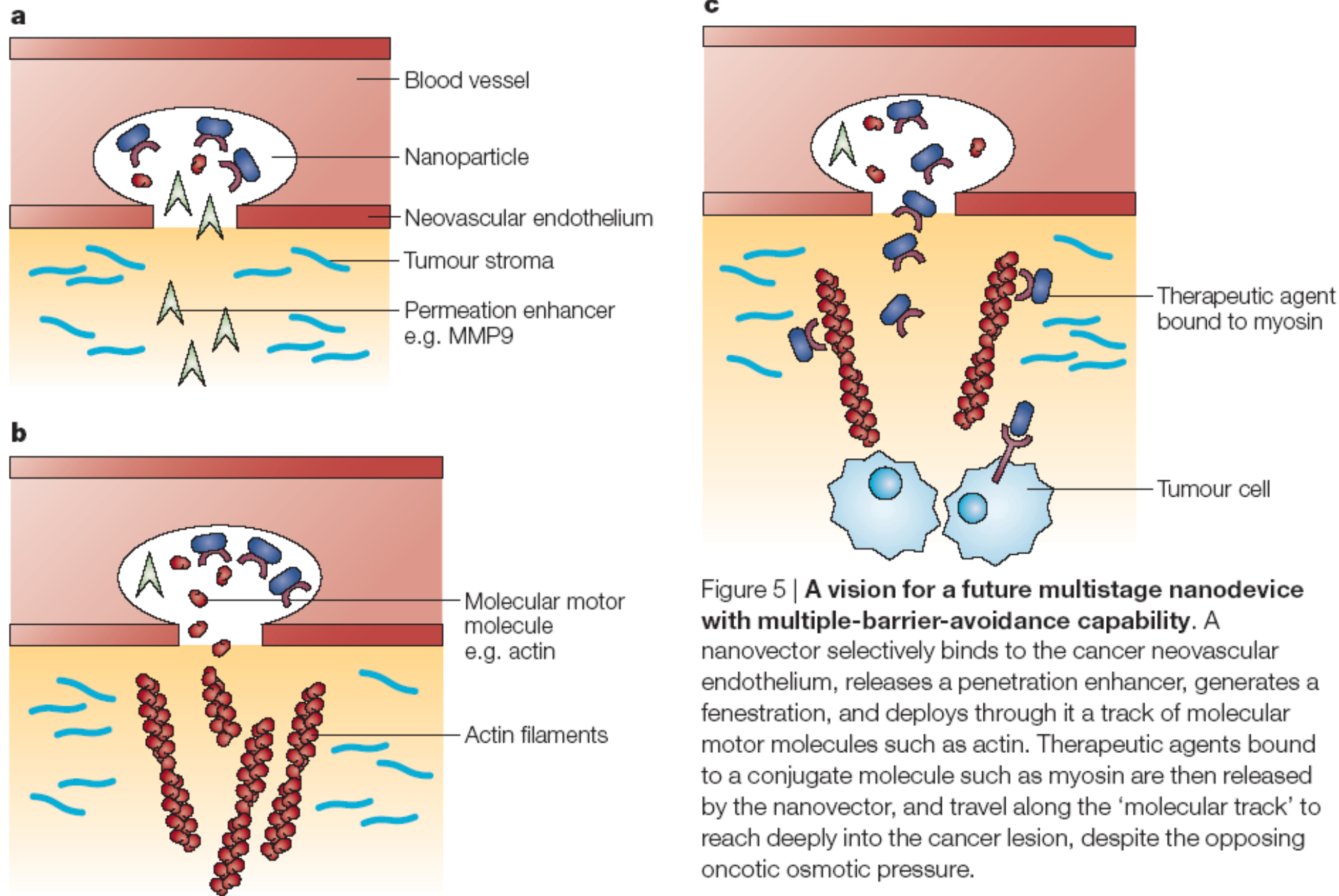


Figure 5 | A vision for a future multistage nanodevice with multiple-barrier-avoidance capability. A nanovector selectively binds to the cancer neovascular endothelium, releases a penetration enhancer, generates a fenestration, and deploys through it a track of molecular motor molecules such as actin. Therapeutic agents bound to a conjugate molecule such as myosin are then released by the nanovector, and travel along the 'molecular track' to reach deeply into the cancer lesion, despite the opposing oncotic osmotic pressure.

Polymer conjugates as anticancer nanomedicines

NATURE REVIEWS | CANCER | VOLUME 6 | SEPTEMBER 2006 | 689

At a glance

- Water-soluble polymers conjugated to proteins and anticancer drugs are in routine clinical use and clinical development as both single agents and components of combination therapy. This is establishing polymer therapeutics as one of the first classes of anticancer nanomedicine. There is growing optimism about the use of ever more sophisticated polymer-based vectors for cancer therapy.
- The covalent conjugation of synthetic polymers, particularly poly(ethyleneglycol) (PEG), to protein drugs increases their plasma residence, reduces protein immunogenicity and can increase their therapeutic index. Several PEGylated enzymes (such as L-asparaginase) and cytokines (including interferon- α and granulocyte colony-stimulating factor) have now entered routine clinical use.
- Polymer conjugation alters the biodistribution of low-molecular-weight drugs, enabling tumour-specific targeting with reduced access to sites of toxicity. More than ten polymer–anti-tumour conjugates have been transferred into clinical development. They have been designed for lysosomotropic delivery following passive tumour targeting by the enhanced permeability and retention effect (EPR effect) or, in one case, for receptor-mediated targeting by the introduction of a cell-specific ligand. Polyglutamic acid–paclitaxel is showing particular promise in phase III trials in women with non-small-cell lung cancer.
- New strategies are making polymer conjugates active against new molecular targets (for example, anti-angiogenics), and the combination of polymer conjugates with low-molecular-weight drugs (which are routinely used in chemotherapy), radiotherapy or tailor-made prodrugs is showing promise. Moreover, the polymer platform provides an ideal opportunity to deliver a drug combination from a single carrier, and combined endocrine therapy and chemotherapy is showing preclinical potential as a breast cancer therapy.
- The polymers that have been used clinically so far have a linear polymer architecture. The principles for the design of polymer therapeutics are now being applied to new hyperbranched dendrimers and dendritic polymer architectures. Before clinical evaluation it is essential to establish the safety of new polymers, particularly in respect of general toxicity, immunogenicity and metabolic fate.

Box 1 | **Rationale for design of PEG–protein conjugates**

Recombinant DNA and monoclonal antibody technology has created a growing number of peptide, protein and antibody-based drugs. The conjugation of poly(ethyleneglycol) (PEG) to proteins (PEGylation) is proving a useful tool to:

- Increase protein solubility and stability, and also to reduce protein immunogenicity^{29,30}.
- Prevent the rapid renal clearance of small proteins and receptor-mediated protein uptake by cells of the reticuloendothelial (RES) system.
- Prolong plasma half-life — leading to the need for less frequent dosing, which is of great patient benefit.

Although several water-soluble polymers have been successfully used for protein conjugation, PEG is particularly attractive because:

- PEG is used as a pharmaceutical excipient and is known to be non-toxic and non-immunogenic.
- PEG has a flexible, highly water-soluble chain that extends to give a hydrodynamic radius some 5–10 times greater than that of a globular protein of equivalent molecular weight. Its high degree of hydration means the polymer chain effectively has a ‘water shell’, and this helps to mask the protein to which it is bound.
- PEG can be prepared with a single reactive group at one terminal end, and this aids site-specific conjugation to a protein and avoids protein crosslinking during conjugation.

Although first generation protein conjugates were synthesized using linear monomethoxyPEGs (molecular weight (Mw) of $\sim 5,000 \text{ g mol}^{-1}$), with many polymer chains randomly attached to each protein molecule, various sophisticated conjugation chemistries have now emerged that use linear or branched PEGs of Mw $\sim 5,000$ – $40,000 \text{ g mol}^{-1}$. Several techniques, most recently including phage display, enable site-specific peptide and protein modification. The specific linking chemistries and synthetic strategies being used are described in more detail elsewhere^{29,30,44,45}.

Box 2 | Rationale for the design of polymer–drug conjugates

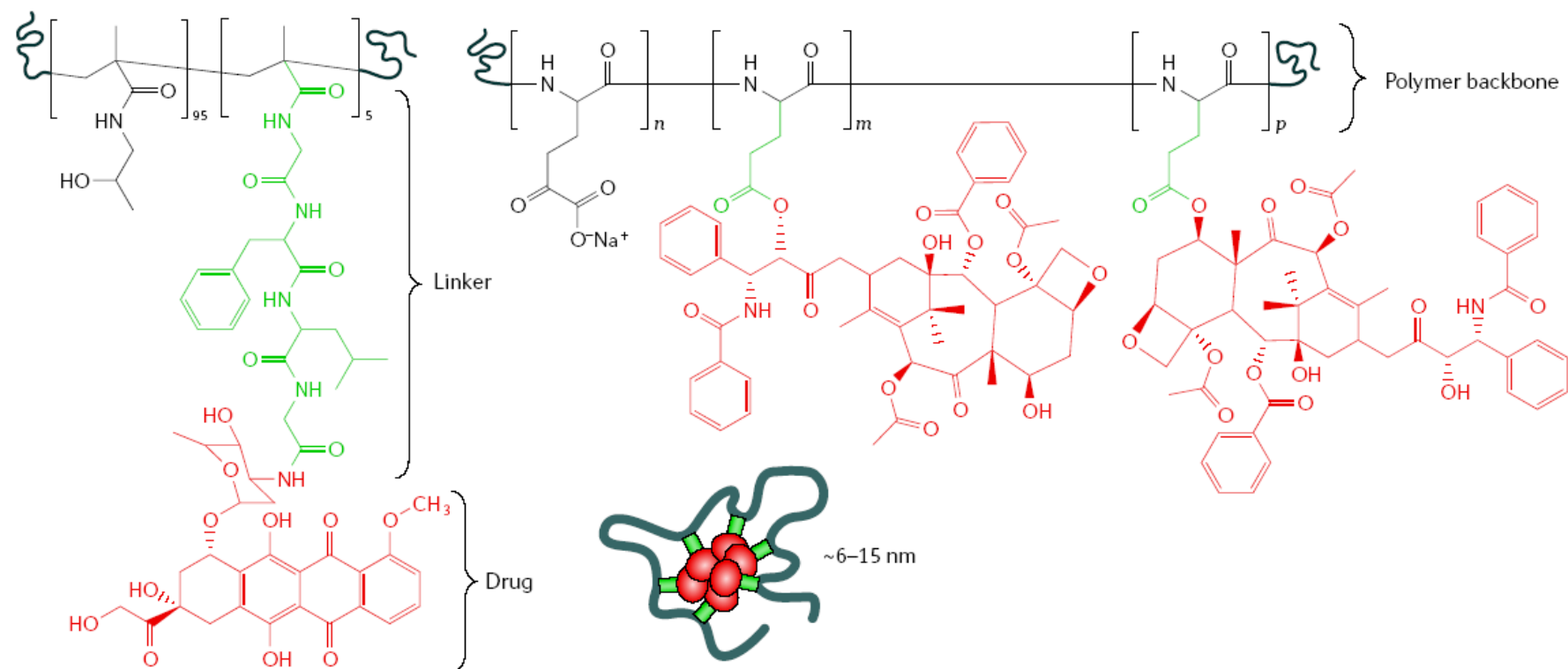
Ringsdorf's vision of the idealized polymer chemistry for drug conjugation⁶⁷ and Trouet and De Duve's realization that the endocytic pathway might be useful for lysosomotropic drug delivery¹⁵⁶ led to the concept of targetable anticancer polymer–drug conjugates. Low-molecular-weight anticancer agents typically distribute randomly throughout the body, and this often leads to side effects. The attachment of drugs to polymeric carriers can:

- Limit cellular uptake to the endocytic route.
- Produce long-circulating conjugates. Most of the dose of low-molecular-weight drug typically leaves the circulation within minutes, whereas a polymer conjugate will ideally circulate for several hours to facilitate passive tumour targeting caused by the leakiness of angiogenic tumour blood vessels by the enhanced permeability and retention effect (EPR effect)³⁹. Conjugates have also been synthesized to contain targeting ligands (such as antibodies, peptides and sugars) with the aim of further promoting increased (building on the EPR effect) tumour targeting by receptor-mediated delivery^{26,28}.

Several features are needed for the effective design of polymer–drug conjugates:

- The polymer must be non-toxic and non-immunogenic. It must also be suitable for industrial-scale manufacture. Polymer molecular weight should be high enough to ensure long circulation, but for non-biodegradable polymeric carriers this molecular weight (Mw) must be less than 40,000 g mol⁻¹ to enable the renal elimination of the carrier following drug delivery. Therefore, the optimum (usually Mw 30,000–100,000 g mol⁻¹) must be tailored to suit the particular polymer being used.
- The polymer must be able to carry an adequate drug payload in relation to its potency.
- The polymer–drug linker must be stable during transport to the tumour, but able to release the drug at an optimum rate on arrival within tumour cells.
- If the drug exerts its effects through an intracellular pharmacological receptor, access to the correct intracellular compartment is essential. Peptidyl and ester polymer–drug linkers have been widely used. In particular, peptide sequences designed for cleavage by the lysosomal thiol-dependent protease cathepsin B^{81,82}, but pH-sensitive *cis*-aconityl, hydrazone and acetal linkages have also been used¹⁵⁷. They are hydrolysed within endosomal and lysosomal vesicles because of the local acidic pH (6.5–4.0). The ideal rate of release will vary according to the mechanism of action of the drug being delivered. Typically, conjugates containing doxorubicin linked by Gly-Phe-Leu-Gly release the drug payload over 24–48 h.
- The intracellular delivery and transfer of a drug out of the endosomal or lysosomal compartment is in many cases not only essential for therapeutic activity¹⁵⁸, it also provides the opportunity to bypass mechanisms of drug resistance that are reliant on membrane efflux pumps such as p-glycoprotein¹⁵⁹. The limitation of polymer Mw to <100,000 g mol⁻¹ ensures that the conjugate will be small enough to extravasate easily into the tumour, and will enable endocytic internalization by all types of tumour cell.

a Polymer-drug conjugate



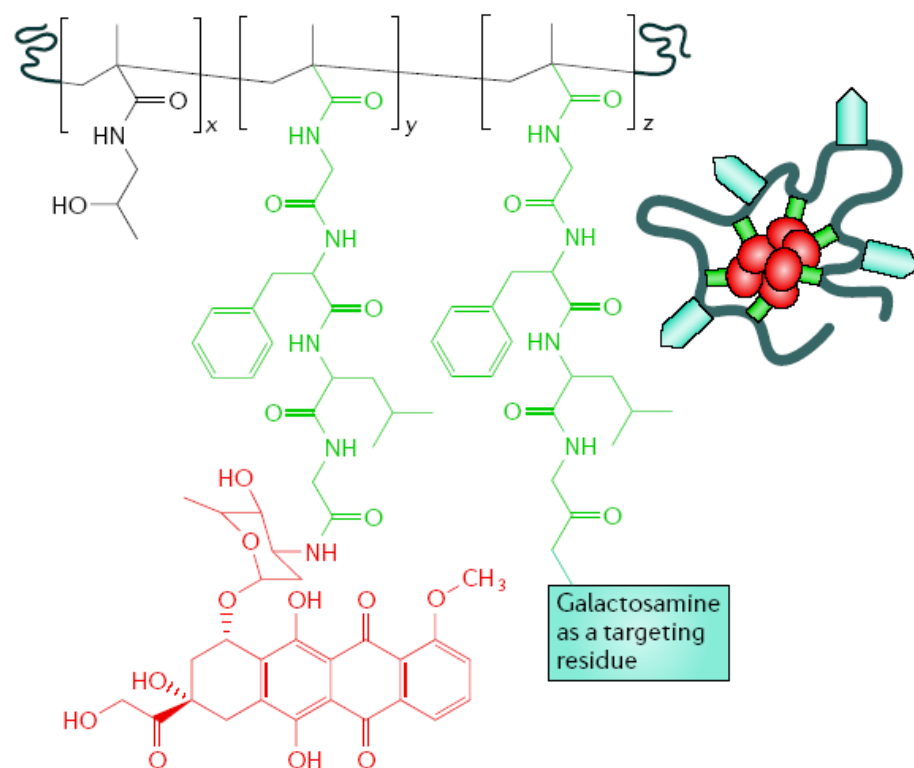
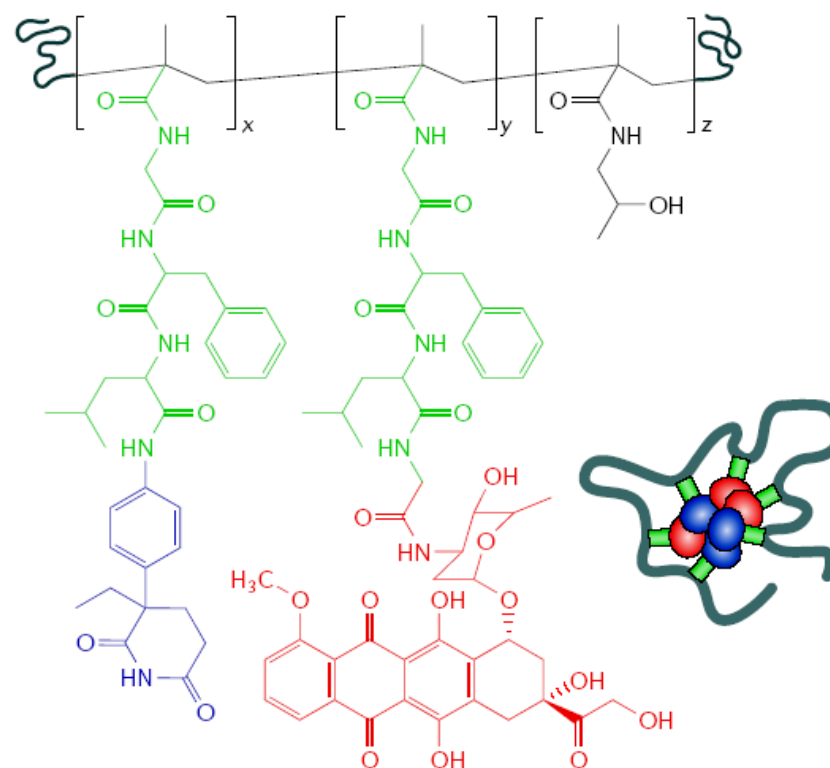
b Targeted conjugate**c Polymeric combination therapy**

Figure 1 | **Polymer–anticancer drug conjugates.** Each panel shows both the detailed chemical structure and a cartoon of the general structure. The polymer backbone is shown in black, linker region in green, drug in red and additional components (for example, a targeting residue) in blue. **a** | Two examples of more ‘simple’ polymer–drug conjugates containing doxorubicin (left) and paclitaxel (right) that have progressed to clinical trial. **b** | A multivalent receptor-targeted conjugate containing galactosamine (light blue) to promote liver targeting. **c** | Polymeric combination therapy containing the aromatase inhibitor aminoglutethimide (red) and doxorubicin (blue).

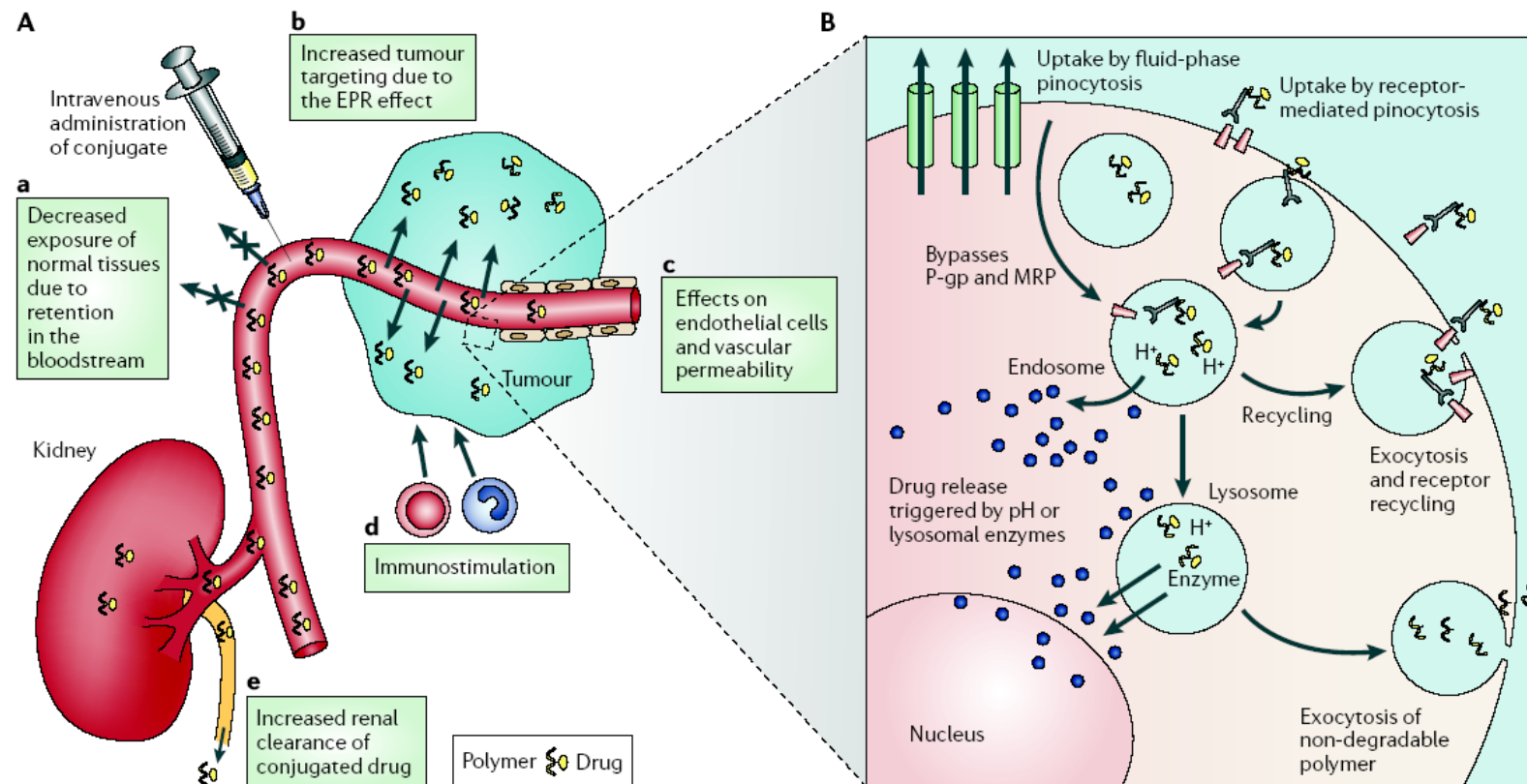


Figure 2 | Current understanding of the mechanism of action of polymer–drug conjugates. **A** | Hydrophilic polymer–drug conjugates administered intravenously can be designed to remain in the circulation — their clearance rate depends on conjugate molecular weight, which governs the rate of renal elimination. **a** | Drug that is covalently bound by a linker that is stable in the circulation is largely prevented from accessing normal tissues (including sites of potential toxicity), and biodistribution is initially limited to the blood pool. **b** | The blood concentration of drug conjugate drives tumour targeting due to the increased permeability of angiogenic tumour vasculature (compared with normal vessels), providing the opportunity for passive targeting due to the enhanced permeability and retention effect (EPR effect). **c** | Through the incorporation of cell-specific recognition ligands it is possible to bring about the added benefit of receptor-mediated targeting of tumour cells. **d** | It has also been suggested that circulating low levels of conjugate (slow drug release) might additionally lead to immunostimulation. **e** | If the polymer–drug linker is stable in the circulation, for example, *N*-(2-hydroxypropyl)methacrylamide (HPMA) copolymer–Gly–Phe–Leu–Gly–doxorubicin, the relatively high level of renal elimination (whole body $t_{1/2}$ clearance >50% in 24 h) compared with free drug ($t_{1/2}$ clearance ~50% in 4 days) can increase the elimination rate. **B** | On arrival in the tumour interstitium, polymer-conjugated drug is internalized by tumour cells through either fluid-phase pinocytosis (in solution), receptor-mediated pinocytosis following non-specific membrane binding (due to hydrophobic or charge interactions) or ligand–receptor docking. Depending on the linkers used, the drug will usually be released intracellularly on exposure to lysosomal enzymes (for example, Gly–Phe–Leu–Gly and polyglutamic acid (PGA) are cleaved by cathepsin B) or lower pH (for example, a hydrazone linker degrades in endosomes and lysosomes (pH 6.5–<4.0)). The active or passive transport of drugs such as doxorubicin and paclitaxel out of these vesicular compartments ensures exposure to their pharmacological targets. Intracellular delivery can bypass mechanisms of resistance associated with membrane efflux pumps such as p-glycoprotein. If >10-fold, EPR-mediated targeting will also enable the circumvention of other mechanisms of drug resistance. Non-biodegradable polymeric platforms must eventually be eliminated from the cell by exocytosis. Rapid exocytic elimination of the conjugated drug before release would be detrimental and prevent access to the therapeutic target. In general, polymeric carriers do not access the cytosol. MRP, multidrug resistance protein.

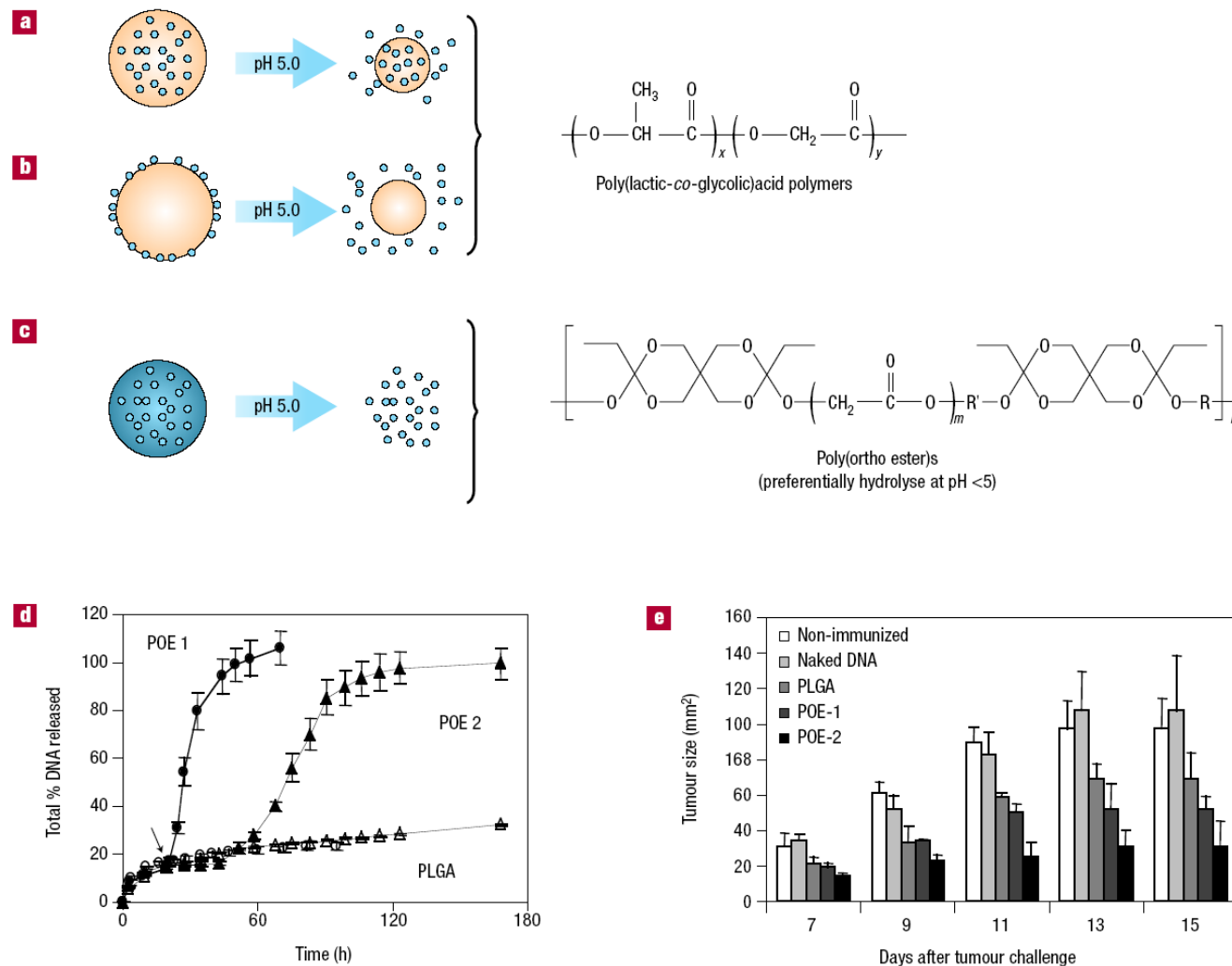


Figure 4 Degradation of polymeric microspheres as a function of pH. Microspheres <10 micrometres in diameter are preferentially internalized by APCs, providing a mechanism by which to target vaccines to the immune system. Following internalization by APCs, the spheres are sequestered within acidic vesicles, providing a mechanism through which to modulate the release of encapsulated DNA intracellularly. **a**, Poly(lactic-*co*-glycolic)acid (PLGA) microspheres degrade relatively independent of the extracellular and acidic vesicle pH and release DNA as a function of polymer degradation. **b**, DNA adsorbed to the surface of PLGA-based microspheres release DNA more quantitatively than encapsulated DNA, but relatively independent of pH. **c**, Poly(orthoesters) degrade more rapidly at pH ~5.0, allowing triggered release of the DNA in the acidic environment of the phagosome. **d**, The pH-sensitive release of plasmid DNA from microspheres comprised of poly(orthoesters) (POE-1 and POE-2) described in ref. 63 and the pH-independent release of plasmid DNA from PLGA-based microspheres. The arrow shows the time at which the pH was changed from 7.4 to 5.0. The error bars represent the standard deviations over three samples. **e**, The influence that different DNA release kinetics can have on the efficacy of an anticancer DNA-therapeutic (adapted from ref. 63). The error bars represent the standard error from the average over five samples.

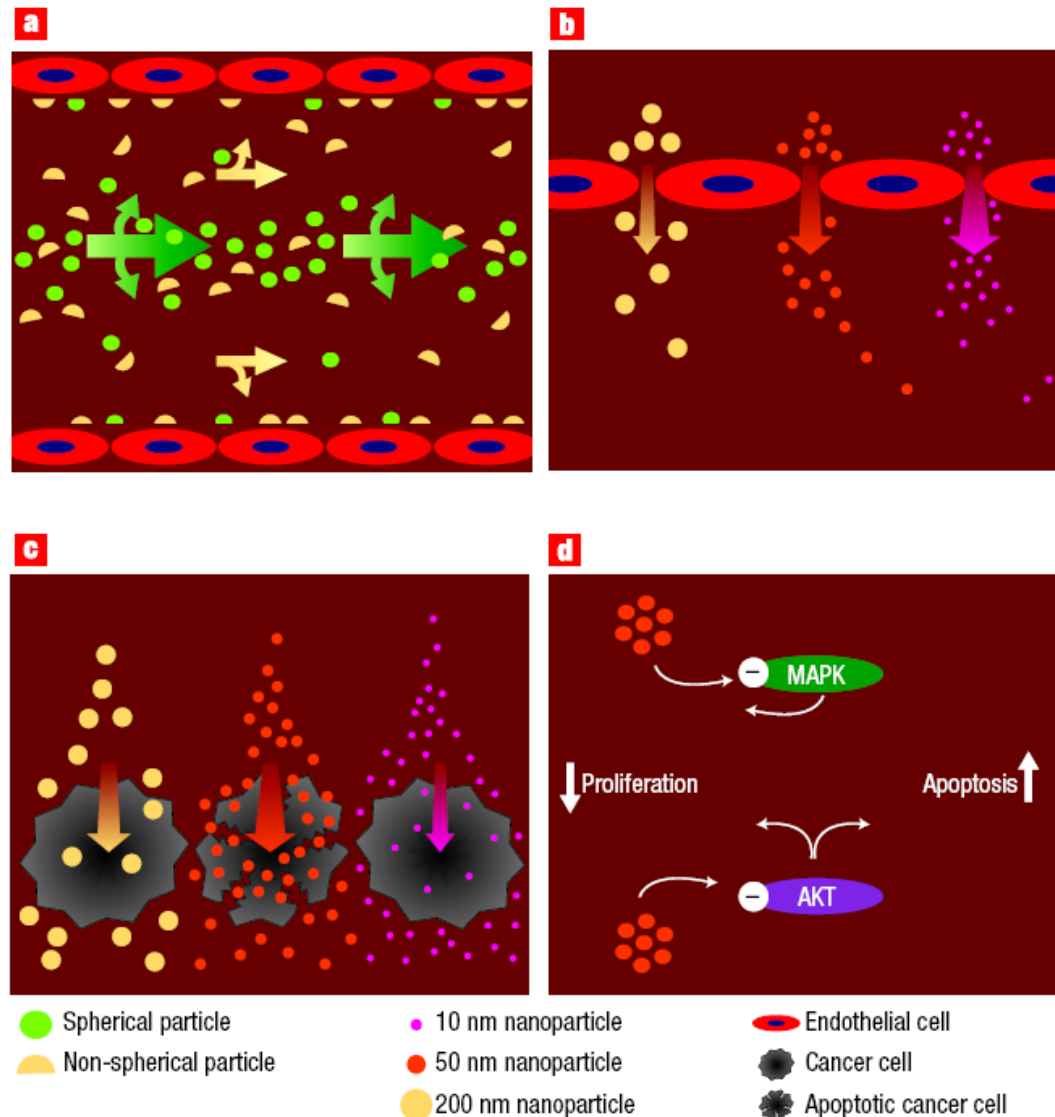
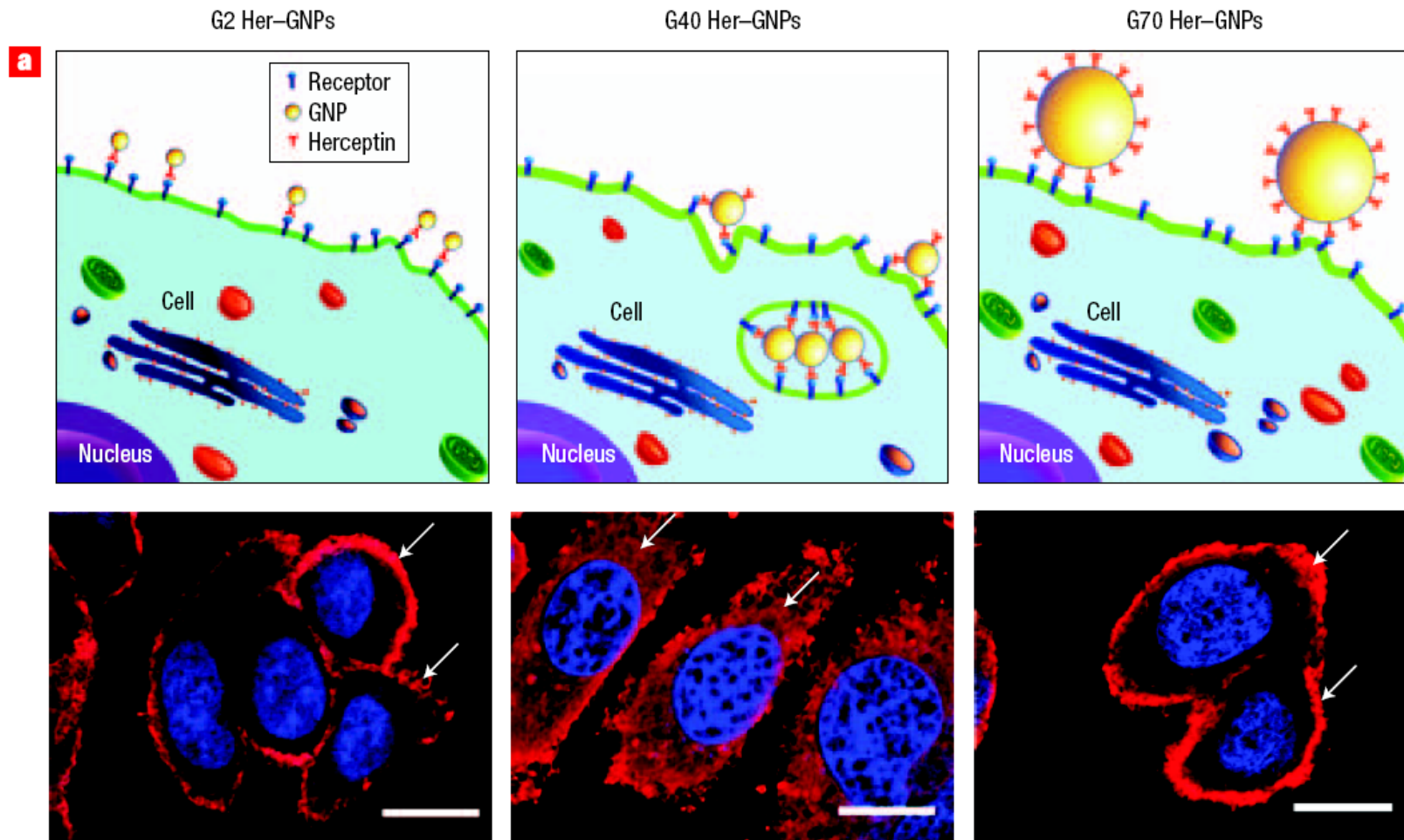
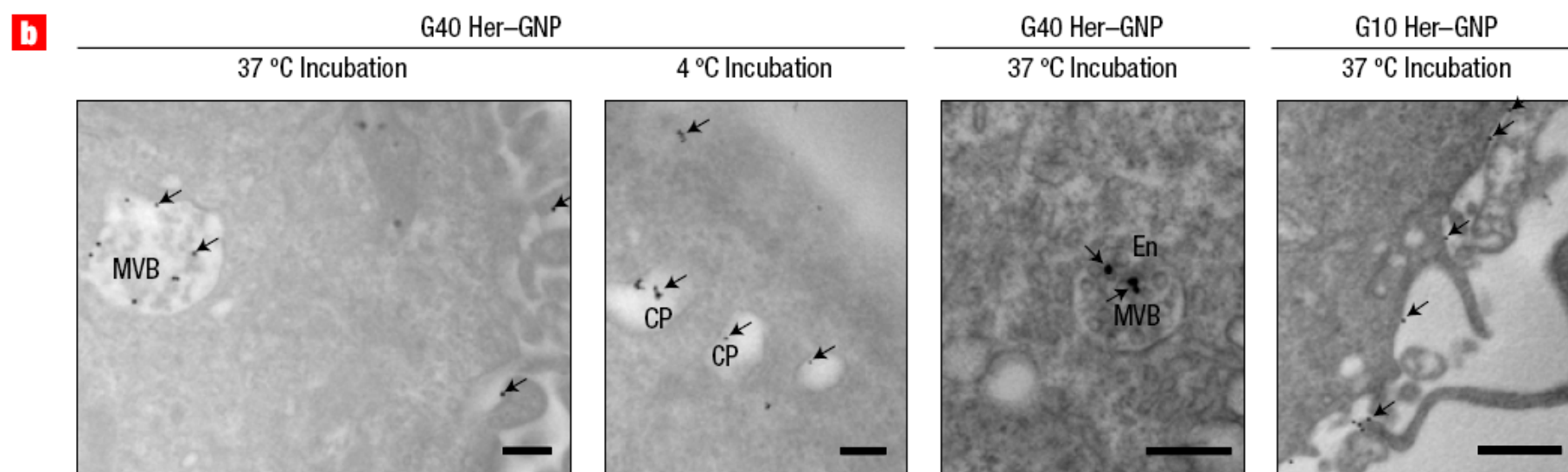
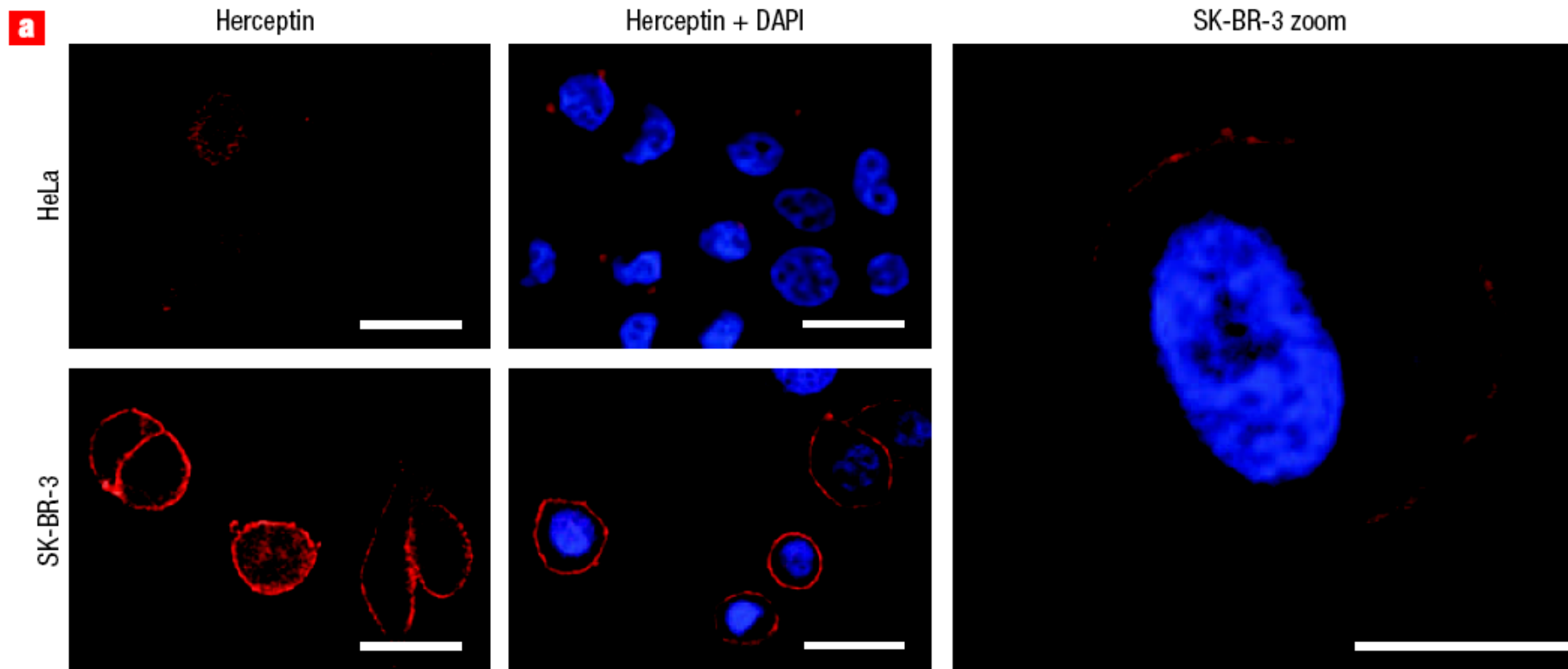


Figure 1 The geometry of a nanoparticle impacts its ability to perform its four basic functions. **a**, Navigation: non-spherical particles are more likely to be near the capillary walls and adhere to the cancer-specific molecules expressed on the vascular walls. **b**, Avoidance of biological barriers: particles of the right size fit through cancer-associated capillary wall fenestrations and localize preferentially in cancer lesions. **c**, Site- and cell-specific localization: nanoparticles of different sizes are taken up by cancer cells with different efficiency. **d**, Targeting of biological pathways. Chan and colleagues¹ showed that nanoparticles of different size can affect two signalling pathways, MAPK and AKT, to decrease proliferation and increase apoptotic cell death. These properties show that nanoparticles themselves can be candidate anticancer agents, even if they do not carry drugs.

Nanoparticle-mediated cellular response is size-dependent

nature nanotechnology | VOL 3 | MARCH 2008 |





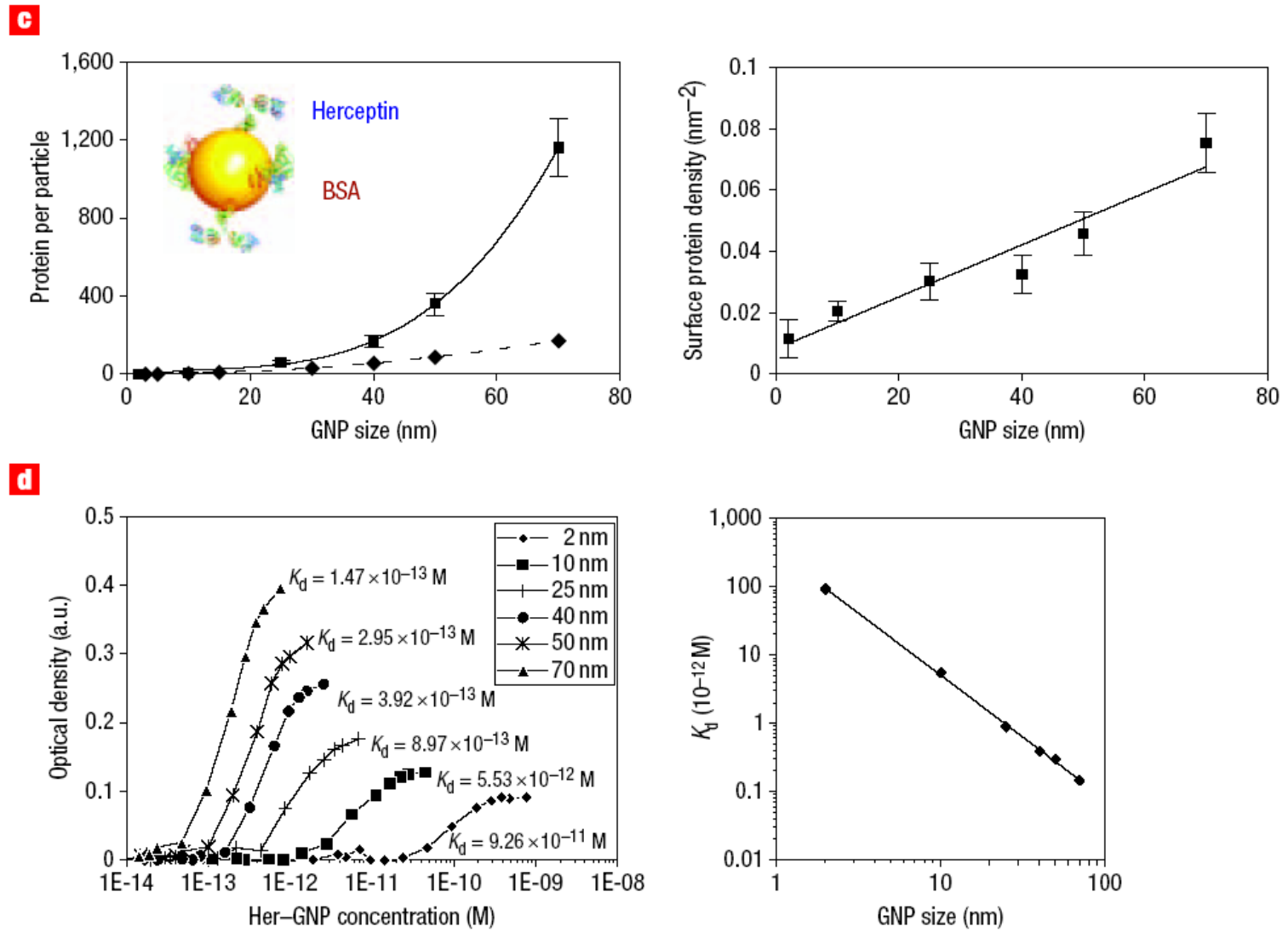


Figure 1 Specific interactions between Her–GNPs and ErbB2 receptors determine their internalization fate. **a**, Fluorescence images showing specific binding of Herceptin antibody (labelled with the Texas red dye molecule) to the ErbB2 receptors in SK-BR-3 cells. The cell nucleus is labelled with DAPI (blue). HeLa cells served as control. The enlarged view represents a single SK-BR-3 cell (scale bars = 5 μ m). **b**, TEM images of cells incubated with G40 Her–GNPs at 37 °C and 4 °C and G40 and G10 Her–GNPs at 37 °C. Arrows indicate Her–GNPs (scale bars = 0.5 μ m). MVB, multivesicular bodies; En, endosomes; CP, clathrin-coated pits. **c**, Antibody loading analysis. Left panel: Herceptin adsorption as a function of nanoparticle size (filled squares, experimental measurement; filled diamonds, calculation assuming constant Herceptin coverage area). Right panel: Surface-bound Herceptin density correlates with GNP size. Error bars, \pm s.d.; $n = 6$. **d**, Binding avidity analysis. Left panel: Effect of dissociation constant K_d for different-sized Her–GNPs. Right panel: K_d is inversely proportional to GNP size.

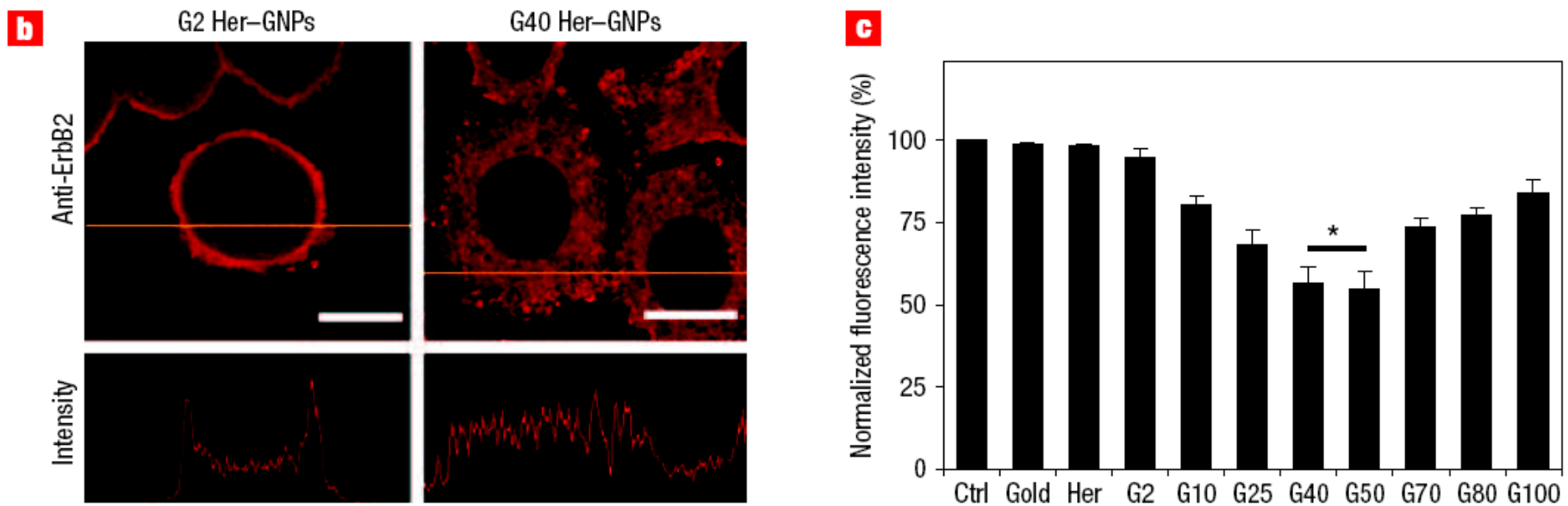
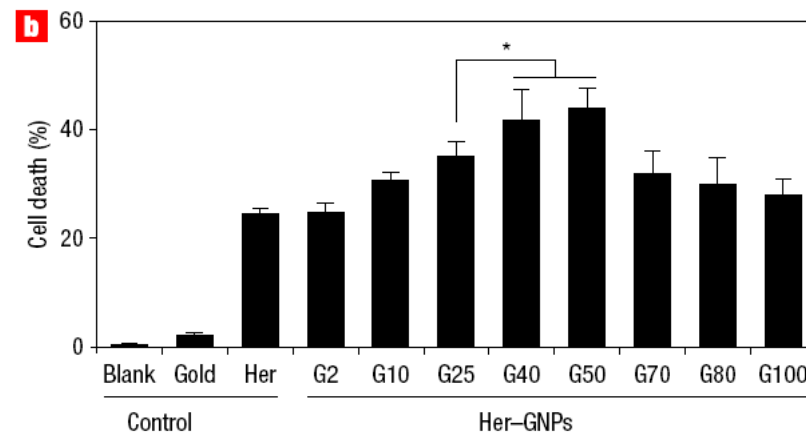


Figure 3 Dependence of downregulation of membrane ErbB2 expression on nanoparticle size. **a**, Illustrations with corresponding fluorescence images of ErbB2 receptor localization after treatment with different-sized Her-GNPs. Arrows indicate ErbB2 receptors, and the nucleus is counterstained with DAPI (blue) (scale bars=10 μ m). **b**, Cross-sectional fluorescence intensity measurements of ErbB2 receptor localization patterns with G2 and G40 Her-GNPs (scale bars = 10 μ m). **c**, Surface ErbB2 expression analysis using untreated cells normalized as 100% expression level (Ctrl). Cells were treated with unmodified 40-nm GNPs (Gold), Herceptin (Her) and Herceptin-modified GNPs of various sizes (* denotes statistical significance for G40/G50 compared to Her-GNPs of other sizes, $p < 0.05$, ANOVA). Error bars, \pm s.d.; $n = 4$.



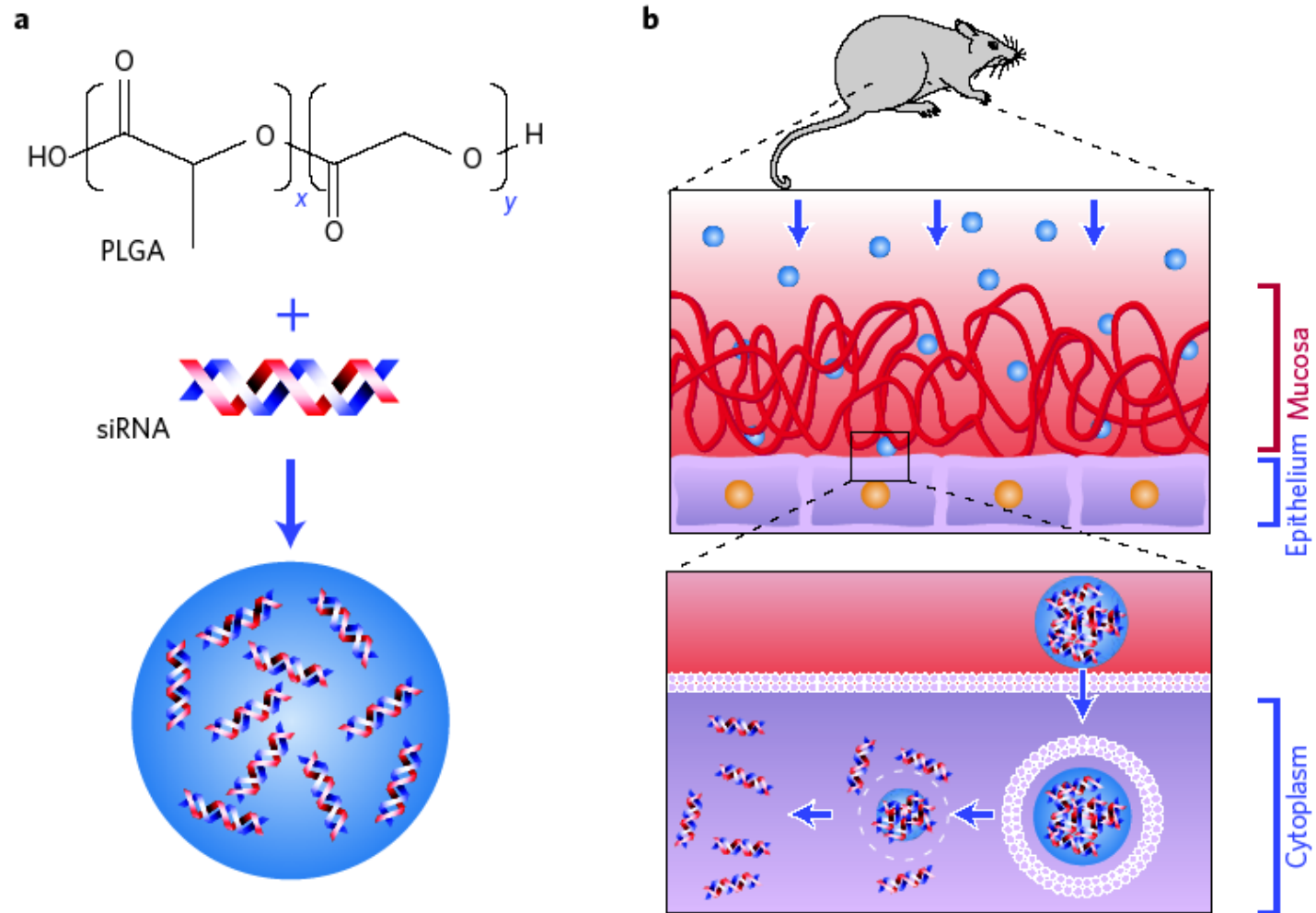


Figure 1 | Schematic illustration of the preparation and delivery of siRNA-loaded PLGA nanoparticles. **a**, Nanoparticles are formed using a double-emulsion solvent evaporation technique in which siRNA and a complexing agent (such as spermidine) are added to PLGA in an organic solvent. Particles are formed by sonication followed by solvent evaporation, and are then subsequently collected and freeze-dried. **b**, A single dose of siRNA-loaded nanoparticles is administered vaginally to mice. The particles must first diffuse through a mucosal layer; they are eventually taken up by epithelial cells and degrade, releasing their siRNA payloads.

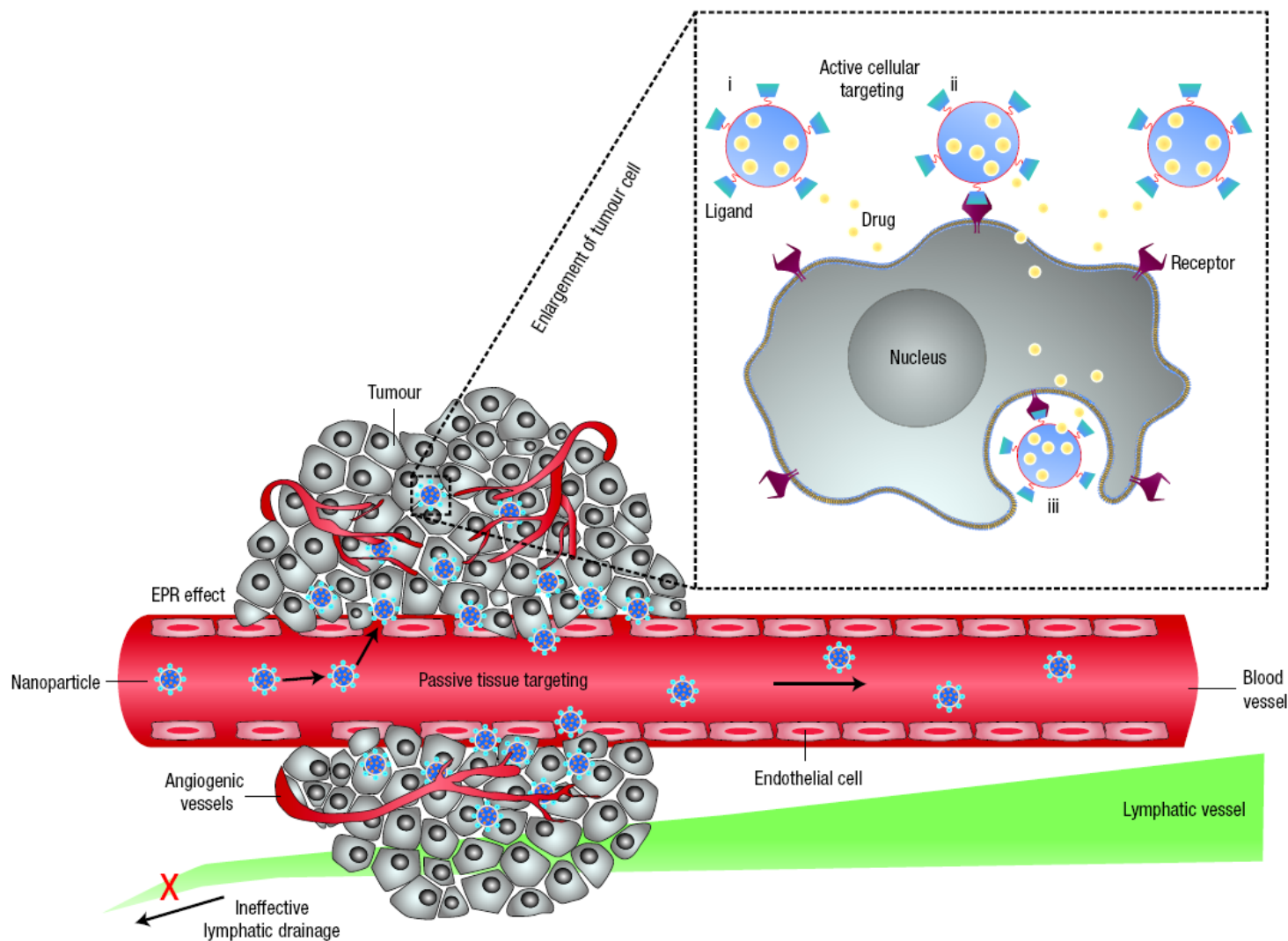


Figure 1 Schematic representation of different mechanisms by which nanocarriers can deliver drugs to tumours. Polymeric nanoparticles are shown as representative nanocarriers (circles). Passive tissue targeting is achieved by extravasation of nanoparticles through increased permeability of the tumour vasculature and ineffective lymphatic drainage (EPR effect). Active cellular targeting (inset) can be achieved by functionalizing the surface of nanoparticles with ligands that promote cell-specific recognition and binding. The nanoparticles can (i) release their contents in close proximity to the target cells; (ii) attach to the membrane of the cell and act as an extracellular sustained-release drug depot; or (iii) internalize into the cell.

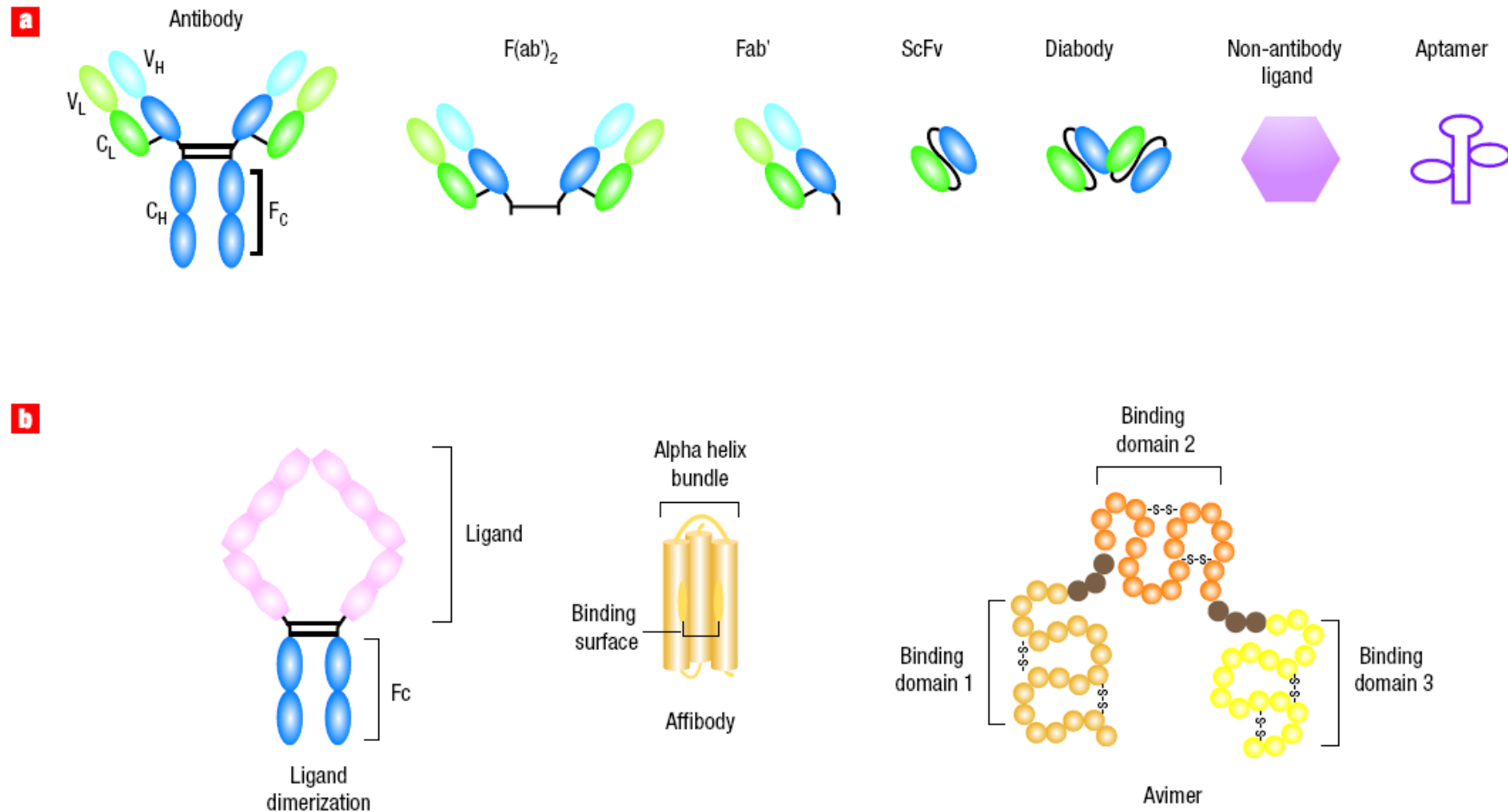


Figure 2 Common targeting agents and ways to improve their affinity and selectivity. **a**, The panel shows a variety of targeting molecules such as a monoclonal antibody or antibodies' fragments, non-antibody ligands, and aptamers. The antibody fragments $F(ab)_2$ and Fab are generated by enzymatic cleavage whereas the Fab', scFv, and bivalent scFv (diabody) fragments are created by molecular biology techniques. V_H : variable heavy chain; V_L : variable light chain; C_H : constant heavy chain; C_L : constant light chain. Non-antibody ligands include vitamins, carbohydrates, peptides, and other proteins. Aptamers can be composed of either DNA or RNA. **b**, Affinity and selectivity can be increased through ligand dimerization or by screening for conformational-sensitive targeting agents such as affibodies, avimers and nanobodies, as well as intact antibodies and their fragments.

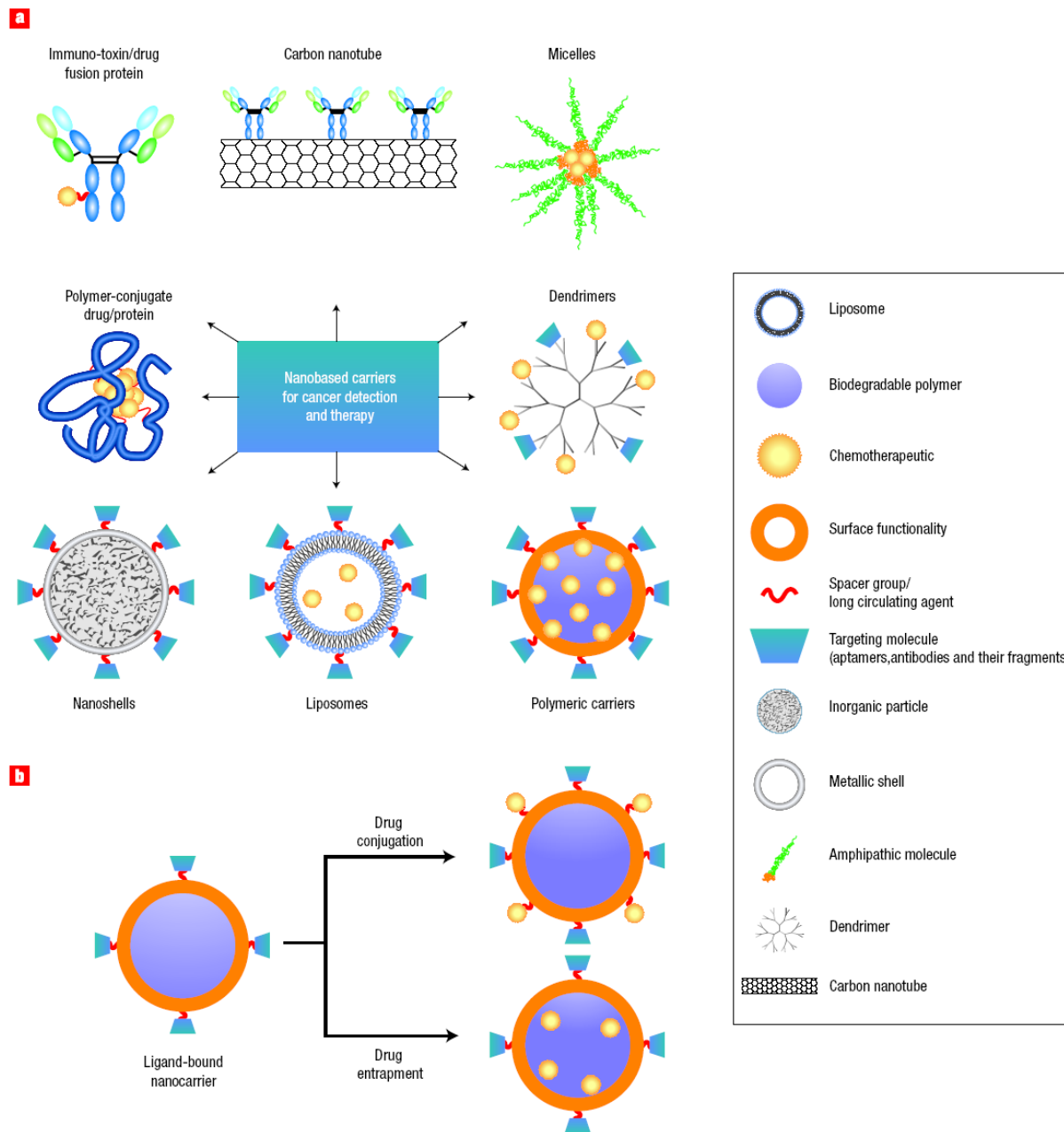


Figure 3 Examples of nanocarriers for targeting cancer. **a**, A whole range of delivery agents are possible but the main components typically include a nanocarrier, a targeting moiety conjugated to the nanocarrier, and a cargo (such as the desired chemotherapeutic drugs). **b**, Schematic diagram of the drug conjugation and entrapment processes. The chemotherapeutics could be bound to the nanocarrier, as in the use of polymer–drug conjugates, dendrimers and some particulate carriers, or they could be entrapped inside the nanocarrier.

Nanomedicine Technology Development Pipeline

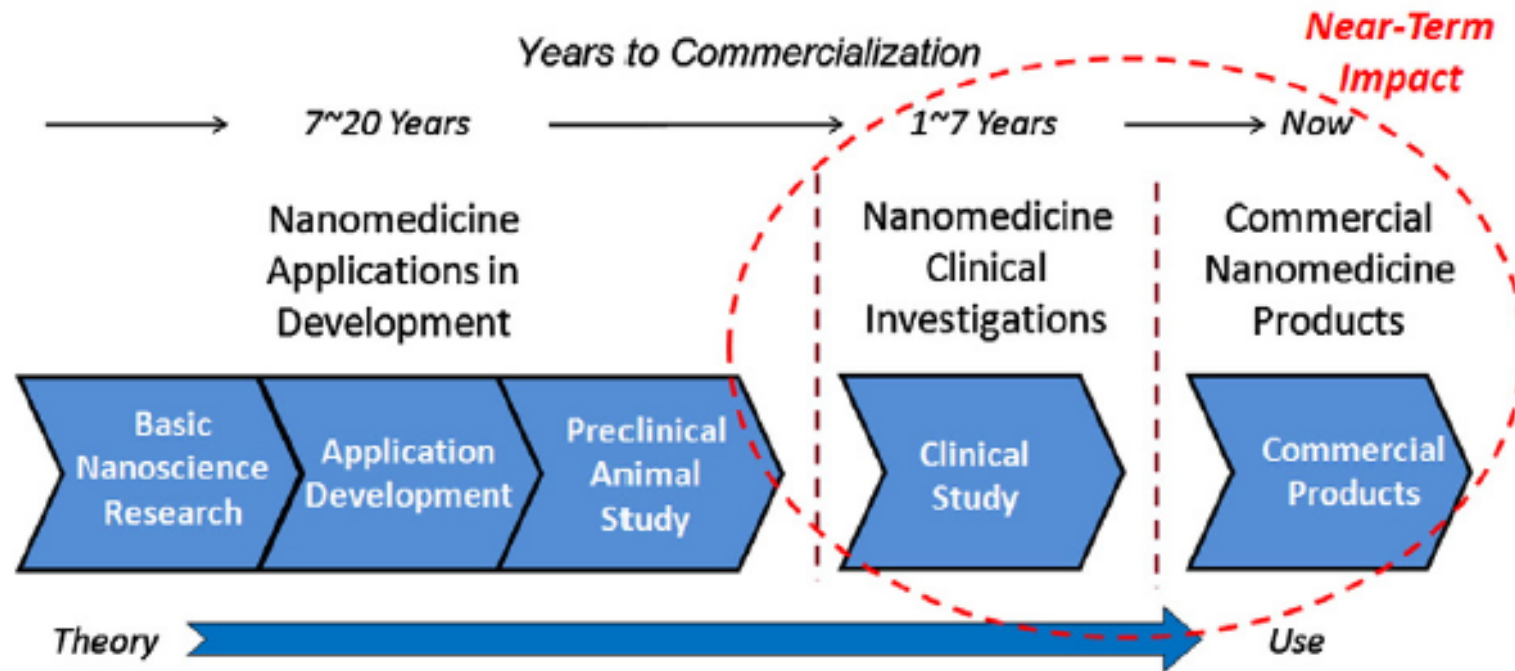


Table 5

Confirmed and likely nanomedicine applications and products identified that utilize active targeting

Application(s)/Product(s)	Company	Status	Condition	Nanocomponent	Targeting Mechanism
Ontak ^[45,46]	Seragen, Inc.	Approved (1999)	T-Cell Lymphoma	Protein NP	IL-2 Protein
MBP-Y003, MBP-Y004, MBP-Y005 ^[47]	Mebiopharm Co., Ltd	Preclinical	Lymphoma	Liposome	Transferrin
MBP-426 ^[47-49]	Mebiopharm Co., Ltd	Phase I/II	Solid Tumors	Liposome	Transferrin
CALAA-01 ^[19,50]	Calando Pharmaceuticals	Phase I	Solid Tumors	NP	Transferrin
SGT-53 ^[19,51]	SynerGene Therapeutics, Inc.	Phase I	Solid Tumors	Liposome	Transferrin
MCC-465 ^[48,52]	Mitsubishi Tanabe Pharma Corp	Phase I	Stomach Cancer	Liposome	GAH Antibody
Actinium-225-HuM195 ^[53]	National Cancer Institute	Phase I	Leukemia	NP	HuM195 Antibody
AS15 ^[54]	GlaxoSmithKline Biologicals	Phase I/II	Metastatic Breast Cancer	Liposome	dHER2 Antibody
PK2 ^[48,55]	Pharmacia & Upjohn Inc.	Phase I	Liver Cancer	Polymeric NP	Galactose
Rexin-G, Reximmune-C ^[56,57]	Epeius Biotechnologies	Phase I/II	Solid Tumors	NP	von Willebrand factor (Collagen-Binding)
Aurimune (CYT-6091) ^[19,58] Auritol (CYT-21001) ^[59]	CytImmune Sciences, Inc.	Phase II Preclinical	Solid Tumors	Colloid Gold	TNF- α
SapC-DOPS ^[60,61]	Bexion Pharmaceuticals, Inc.	Preclinical	Solid Tumors	Liposome	Saposin C
Targeted Emulsions ^[62,63]	Kereos, Inc.	Preclinical	<i>In Vivo</i> Imaging	Emulsion	"Ligands"
Opaxio ^[42,64]	Cell Therapeutics, Inc.	Phase III	Solid Tumors	Polymeric NP	Enzyme-Activated
ThermoDox ^[43]	Celsion Corporation	Phase II/III	Solid Tumors	Liposome	Thermosensitive
DM-CHOC-PEN ^[44,65]	DEKK-TEC, Inc.	Phase I	Brain Neoplasms	Emulsion	Penetrate Blood- Brain-Barrier

Table 7

Confirmed and likely nanomedicine products that exhibit active behavior, beyond active targeting, identified

Use	Application(s)/Product(s)	Company	Status	Nanocomponent	Active Mechanism
Solid Tumor Hyperthermia	NanoTherm [77]	MagForce Nanotechnologies AG	Approved	Iron Oxide NPs	AC Magnetic Heating
	Targeted Nano-Therapeutics [105]	Aspen Medisys, LLC. (Formerly Triton BioSystems, Inc.)	Pre-Clinical	Iron Oxide NPs	AC Magnetic Heating
	AuroShell [83]	Nanospectra Biosciences	Phase I	Gold Nanoshell	IR Laser Heating
Solid Tumor Treatment	NanoXray [77]	Nanobiotix	Phase I	Proprietary NP	X-Ray-Induced Electron Emission
In Vivo Imaging	Feridex IV, GastromarkCombidex (Ferumoxtran-10) [79,106]	Advanced Magnetix	Approved (1996)Phase III	Iron Oxide NPs	Enhanced MRI Contrast
	Endorem, Lumirem, Sinerem [79,106]	Guebert	Approved / Investigational	Iron Oxide NPs	Enhanced MRI Contrast
	FeraSpin [107]	Miltenyi Biotec	Research Use Only	Iron Oxide NPs	Enhanced MRI Contrast
In Vitro Imaging	Clariscan [79]	Nycomed	Phase III	Iron Oxide NPs	Enhanced MRI Contrast
	Resovist [79,106] Supravist [80]	Schering	Approved (2001)Phase III	Iron Oxide NPs	Enhanced MRI Contrast
	Qdot Nanocrystals [108]	Invitrogen Corporation	Research Use Only	Quantum Dot	Fluorescent Emission
	Nanodots [109]	Nanoco Group PLC	Research Use Only	Quantum Dot	Fluorescent Emission
	TriLite™ Nanocrystals [110]	Crystalplex Corporation	Research Use Only	Quantum Dot	Fluorescent Emission
	eFluor Nanocrystals [111]	eBiosciences	Research Use Only	Quantum Dot	Fluorescent Emission
	NanoHC [112]	DiagNano	Investigational (Research Only)	Quantum Dot	Fluorescent Emission
In Vitro Cell Separation	CellSearch® EpithelialCell Kit [99]	Veridex, LLC (Johnson & Johnson)	Approved (2004)	Iron Oxide NPs	Magnetic Separation
	NanoDX [113]	T2 Biosystems	Research Use Only	Iron Oxide NPs	Magnetic Separation

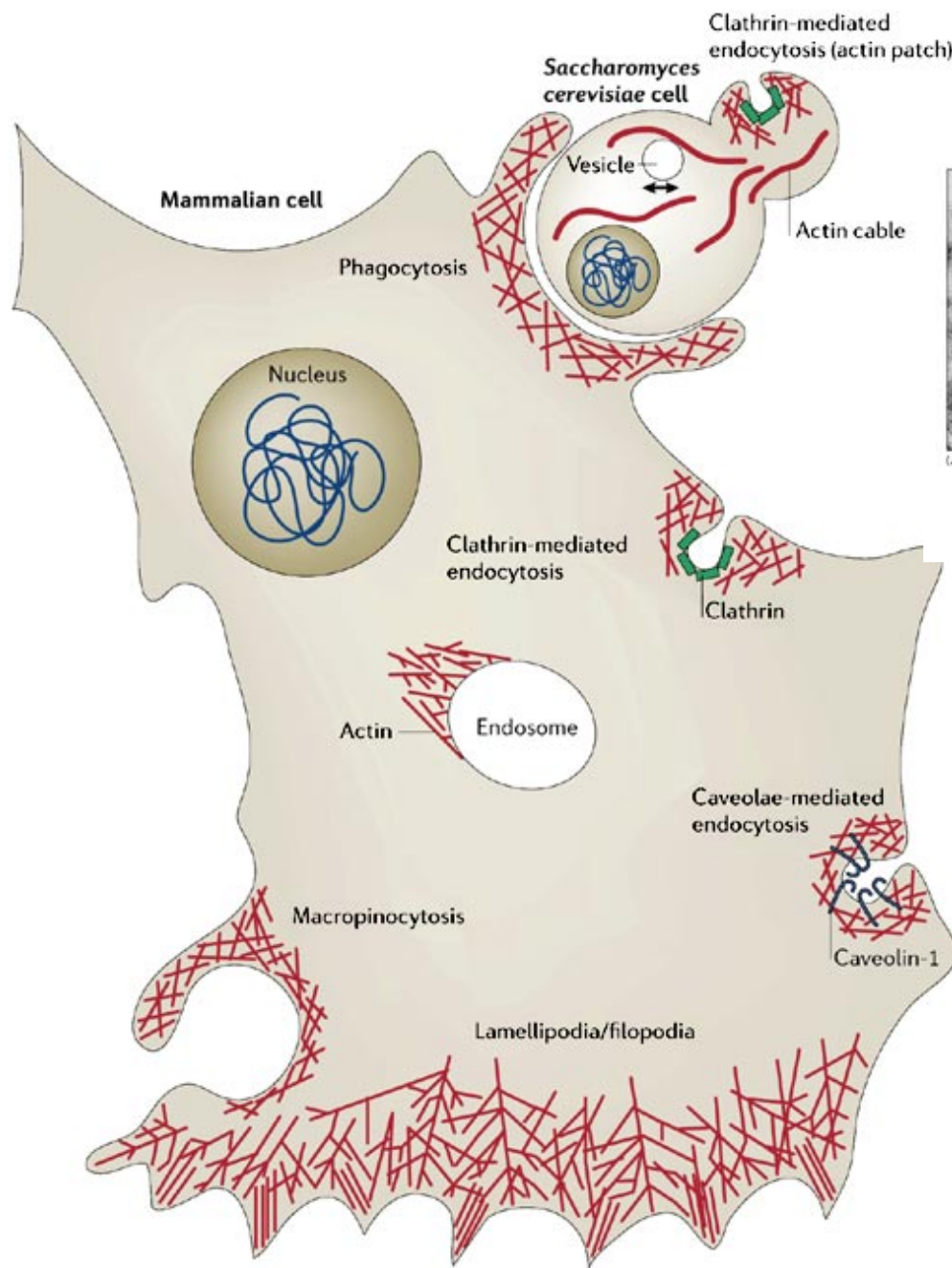
Table 6

Confirmed and likely nanomedicine products that have been approved by the FDA through the 510(k) process identified

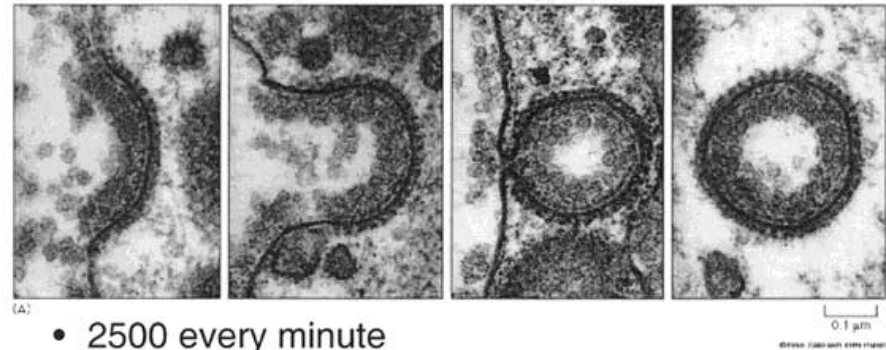
Use	Application(s)/Product(s)	Company	Approval Year	Nanocomponent Description
Bone Substitute	Vitoss [¹⁴]	Orthovita	2003	100-nm Calcium-Phosphate Nanocrystals
	Ostim [⁸⁷]	Osartis	2004	20-nm Hydroxapatite Nanocrystals
	OsSatura [⁶²]	Isotis Orthobiologicals US	2003	Hydroxapatite Nanocrystals
	NanOss [⁷⁷]	Angstrom Medica, Inc.	2005	Hydroxapatite Nanocrystals
	Alpha-bsm, Beta-bsm, Gamma-bsm, EquivaBone, CarriGen [⁹³]	ETEX Corporation	2009	Hydroxapatite Nanocrystals
Dental Composite	Ceram X Duo [⁹⁴]	Dentsply	2005	Ceramic NPs
	Filtek [⁹⁵]	3M Company	2008	Silica and Zirconium NPs
	Premise [¹⁴]	Sybron Dental Specialties	2003	"Nanoparticles"
	Nano-Bond [⁹⁶]	Pentron® Clinical Technologies, LLC	2007	"Nanoparticles"
Device Coating	ON-Q SilverSoaker / SilvaGard™ [⁹⁷]	I-Flow Corporation / AcryMed, Inc.	2005	Antimicrobial Nanosilver
In Vitro Assay	EnSeal Laparoscopic Vessel Fusion [³⁹]	Ethicon Endo-Surgery, Inc.	2005	NP-Coated Electrode
	NanoTite Implant [⁹⁸]	Biomet	2008	Calcium Phosphate Nanocrystal Coating
	CellTracks® [¹⁴]	Immunicon Corporation	2003	Magnetic NPs
	NicAlert [¹⁴]	Nymox	2002	Colloidal Gold
	Stratus CS [⁶²]	Dade Behring	2003	Dendrimers
	CellSearch® Epithelial Cell Kit [⁹⁹]	Veridex, LLC (Johnson & Johnson)	2004	Iron Oxide NPs
Medical Dressing	Verigene [^{100,101}]	Nanosphere, Inc.	2007	Colloidal Gold
	MyCare™ Assays [¹⁰²]	Saladax Biomedical	2008	"Nanoparticles"
	Acticoat® [^{97,103}]	Smith & Nephew, Inc.	2005	Antimicrobial Nanosilver
Dialysis Filter	Fresenius Polysulfone® Helixone® [¹⁰⁴]	NephroCare	1998	Nanoporous Membrane
Tissue Scaffold	TiMESH [³⁹]	GfE Medizintechnik GmbH	2004	30-nm Titanium Coating

Endocytosis

- Phagocytosis is the process by which cells ingest large objects, such as cells which have undergone apoptosis, bacteria, or viruses. The membrane folds around the object, and the object is sealed off into a large vacuole known as a phagosome.
- Pinocytosis is a synonym for endocytosis. This process is concerned with the uptake of solutes and single molecules such as proteins.
- Receptor-mediated endocytosis is a more specific active event where the cytoplasm membrane folds inward to form coated pits. These inward budding vesicles bud to form cytoplasmic vesicles.



Formation of Clathrin-Coated Vesicles



- 2500 every minute
- CCV uncoat within seconds

Porous metal-organic-framework nanoscale carriers as a potential platform for drug delivery and imaging

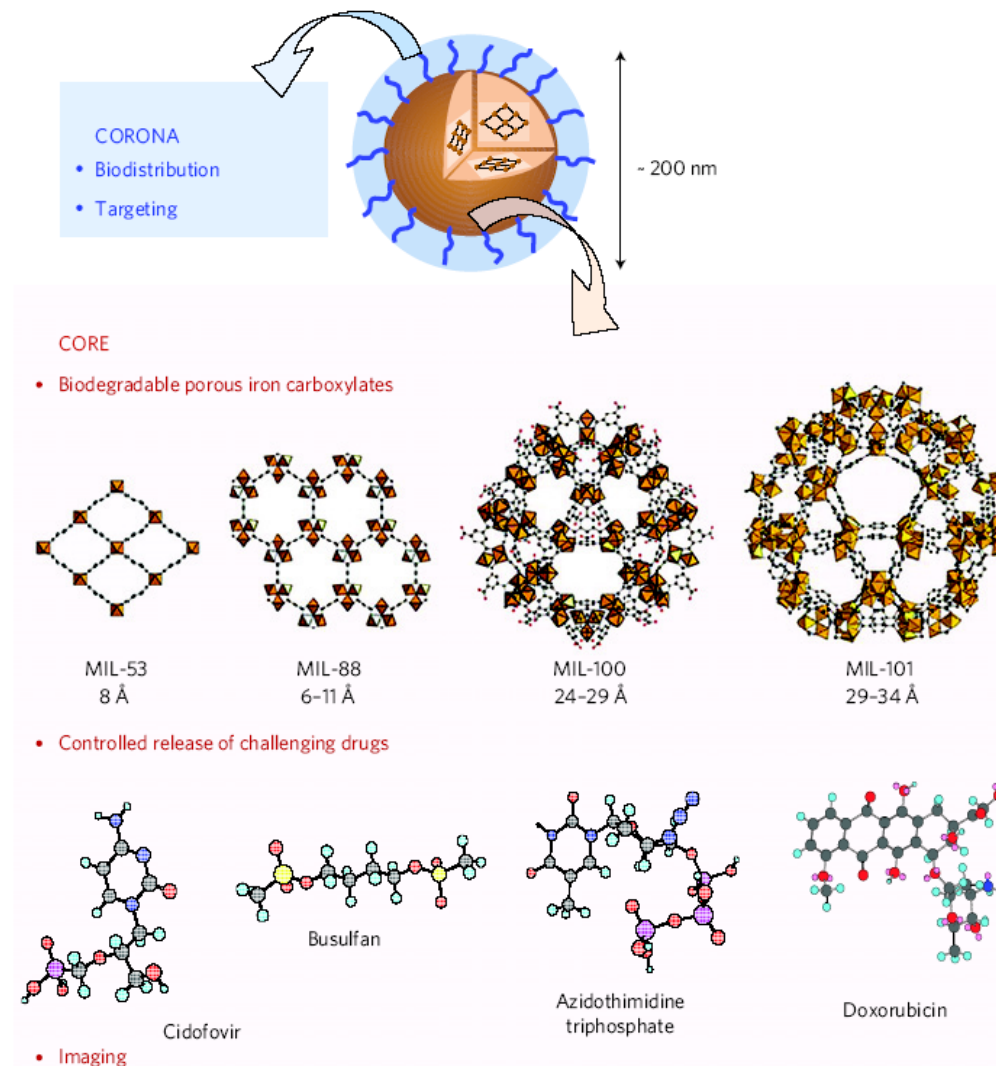


Figure 1 | Scheme of engineered core-corona porous iron carboxylates for drug delivery and imaging.

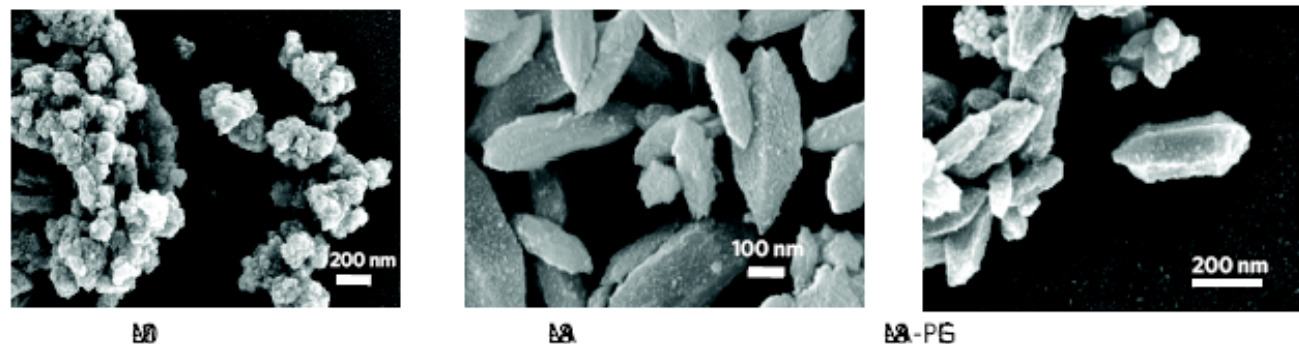


Figure 2 | Scanning electron micrographs of MIL-100 (left), MIL-88A (centre) and PEGylated MIL-88A nanoparticles (right).

Table 1 | Structure description, particle size, drug loading (wt%) and entrapment efficiency (below the drug loading values in parentheses, wt%) in several porous iron(III) carboxylate nanoparticles.

	MIL-89	MIL-88A	MIL-100	MIL-101_NH ₂	MIL-53
Organic linker	dicarboxylic acid <chem>OC(=O)CCCC(=O)O</chem>	dicarboxylic acid <chem>OC(=O)CC(=O)CC(=O)O</chem>	dicarboxylic acid <chem>OC(=O)c1cc(C(=O)O)c(C(=O)O)c1C(=O)O</chem>	dicarboxylic acid <chem>NC1=CC(=C(C(=O)O)C(=O)O)C=C1</chem>	dicarboxylic acid <chem>OC(=O)c1ccc(cc1)C(=O)O</chem>
Crystalline structure					
Flexibility	Yes	Yes	No	No	Yes
Pore size (Å)	11	6	25 (5.6) 29 (8.6)	29 (12) 34 (16)	8.6